Design and Optimization of Conformal Slot Array Antennas for X-band Applications

by

Hisham Khalil

A thesis submitted in partial fulfillment for the
degree of Doctor of Philosophy

in the

Faculty of Engineering
Department of Electrical Engineering

2020

Design and Optimization of Conformal Slot Array Antennas for X-band Applications

By

Hisham Khalil

(PE133005)

Dr. Nasimuddin, Scientist III

Institute for Infocomm Research, ASTAR, Singapore

(Foreign Evaluator 1)

Dr. Qunsheng Cao, Professor

Nanjing University of Aeronautics and Astronautics, Nanjing, China

(Foreign Evaluator 2)

Dr. Muhammad Mansoor Ahmed

(Thesis Supervisor)

Dr. Noor Muhammad Khan

(Head, Department of Electrical Engineering)

Dr. Imtiaz Ahmad Taj

(Dean, Faculty of Engineering)

DEPARTMENT OF ELECTRICAL ENGINEERING

CAPITAL UNIVERSITY OF SCIENCE AND TECHNOLOGY

ISLAMABAD

2020

Dedicated to my beloved mother (late), and my beloved wife who mean the whole world to me

CERTIFICATE OF APPROVAL

This is to certify that the research work presented in the thesis, entitled "**Design and Optimization of Conformal Slot Array Antennas for X-band Applications**" was conducted under the supervision of **Dr. Muhammad Mansoor Ahmed**. No part of this thesis has been submitted anywhere else for any other degree. This thesis is submitted to the **Department of Electrical Engineering, Capital University of Science and Technology** in partial fulfillment of the requirements for the degree of Doctor in Philosophy in the field of **Electrical Engineering.** The open defence of the thesis was conducted on **December 11, 2020.**

Student Name :   Hisham Khalil (PE-133005)

The Examination Committee unanimously agrees to award PhD degree in the mentioned field.

Examination Committee :

(a)   External Examiner 1:   Dr. Junaid Mughal,
                               Professor
                               COMSATS University, Islamabad

(b)   External Examiner 2:   Dr. Mojeeb bin Ihsan,
                               Professor
                               CEME, NUST, Islamabad

(c)   Internal Examiner :   Dr. Muhammad Ashraf
                               Professor
                               CUST, Islamabad

Supervisor Name :   Dr. Muhammad Mansoor Ahmed
                               Professor
                               CUST, Islamabad

Name of HoD :   Dr. Noor Muhammad Khan
                               Professor
                               CUST, Islamabad

Name of Dean :   Dr. Imtiaz Ahmad Taj
                               Professor
                               CUST, Islamabad

AUTHOR'S DECLARATION

I, **Hisham Khalil (Registration No. PE-133005)**, hereby state that my PhD thesis titled, '**Design and Optimization of Conformal Slot Array Antennas for X-band Applications**" is my own work and has not been submitted previously by me for taking any degree from Capital University of Science and Technology, Islamabad or anywhere else in the country/ world.

At any time, if my statement is found to be incorrect even after my graduation, the University has the right to withdraw my PhD Degree.

(Hisham Khalil)

Dated: **11** December, 2020

Registration No : PE-133005

PLAGIARISM UNDERTAKING

I solemnly declare that research work presented in the thesis titled "**Design and Optimization of Conformal Slot Array Antennas for X-band Applications**" is solely my research work with no significant contribution from any other person. Small contribution/ help wherever taken has been duly acknowledged and that complete thesis has been written by me.

I understand the zero tolerance policy of the HEC and Capital University of Science and Technology towards plagiarism. Therefore, I as an author of the above titled thesis declare that no portion of my thesis has been plagiarized and any material used as reference is properly referred/ cited.

I undertake that if I am found guilty of any formal plagiarism in the above titled thesis even after award of PhD Degree, the University reserves the right to withdraw/ revoke my PhD degree and that HEC and the University have the right to publish my name on the HEC/ University Website on which names of students are placed who submitted plagiarized thesis.

(Hisham Khalil)

Dated: 11 December, 2020   Registration No : PE-133005

List of Publications

It is certified that following publication(s) have been made out of the research work that has been carried out for this thesis:-

Journal Papers

1. **H. Kahlil**, M. M. Ahmed, and U. Rafique, "Nose-cone conformal substrate-integrated waveguide slot array antenna for X-band radar applications," *International Journal of Antennas and Propagation*, vol. 2019, pp. 1-11, 2019. **(IF: 1.347)**

Conference Proceedings

1. **H. Khalil**, U. Rafique, M. M. Ahmed, S. Rahman, and W. Nazar, "A comparative study of conformal antenna arrays for aerodynamic applications," *2019 Photonics & Electromagnetics Research Symposium-Fall (PIERS-Fall)*, pp. 3211-3217, 2019.

2. **H. Khalil**, M. M. Ahmed, and U. Rafique, "X-band conformal antenna array For low cost CubeSats," *2018 International Conference on Innovation and Intelligence for Informatics, Computing, and Technologies (3ICT)*, pp. 1-4, 2018.

3. **H. Khalil**, M. M. Ahmed, S. Rahman, and U. Rafique, "Nose cone conformal antenna array design for X-band radar applications," *2018 Progress in Electromagnetics Research Symposium (PIERS-Toyama)*, pp. 2350-2352, 2018.

4. **H. Khalil**, M. M. Ahmed, U. Rafique, M. Latif, and W. Nazar "Design of X-band cylindrical conformal substrate integrated waveguide slot antenna array," *2018 21st Saudi Computer Society National Computer Conference (NCC)*, pp. 1-4, 2018.

5. **H. Khalil**, S. Rahman, U. Rafique, and M. M. Ahmed, "Design of slot antenna array for tracking radar using particle swarm optimization," *2017 Progress in Electromagnetics Research Symposium-Fall (PIERS-FALL)*, pp. 2985-2987, 2017.

6. **H. Khalil**, S. Rahman, M. M. Ahmed, Q. Cao, and I. Hussain "Design of waveguide slot array to generate sum and difference pattern for synthetic aperture radar," *2017 Progress In Electromagnetics Research Symposium-Spring (PIERS)*, pp. 3632-3636, 2017.

(Hisham Khalil)

Registration No: PE133005

Acknowledgement

Abstract

In 1st part of this thesis, the design of the waveguide fed slot array antenna is presented with Bayliss Δ and Taylor $\sum$ pattern to meet the requirements of a tracking radar system, as well as the high power efficiency. The standard X-band waveguide is used for the design purpose at a center frequency of 9.375 GHz. The proposed design is simulated in full-wave EM simulator with opposite excitation to realize the Δ pattern. It is observed that the simulated results are well in agreement with theoretical data. For both arrays, VSWR $\leq$ 2, while SLLs for Δ and $\sum$ patterns are -20 dB and -8 dB, respectively.

In 2nd part, the design of the slot array antenna is presented for tracking radar applications. To meet the requirements, $\sum$ pattern array of 3×6 is optimized using PSO, while the Δ pattern array of 2×5 is synthesis using Bayliss current distribution technique. The $\sum$ pattern array has a feeding structure based on three inclined slot elements, while Δ pattern array has opposite excitation. From full-wave simulation, the gain for $\sum$ pattern is noted to be 16.84 dBi with an SLL of -18.59 dB. The depth of principal null for Δ pattern is equal to -27.2 dB. It is also observed from simulations that for both the cases, VSWR $\leq$ 2. Furthermore, the overall difference between $\sum$ and Δ patterns is 43.9 dB at $\theta = 0°$.

In 3rd part, the design of an X-band conformal slot array antenna is presented for cube satellites. The proposed antenna array consists of 1×6 elements, which are center inclined on the surface of a dielectric substrate. A dumbbell-shaped slot is etched from the bottom side of the radiating structure, and a SIW feeding structure is utilized to feed the proposed array. The feeding structure is also has a dumbbell-shaped broadband feeding slot on its upper part to couple the energy to the radiating structure. The simulations of the proposed design are done in Ansys HFSS and it is observed that the proposed antenna array offers a gain of 11.15 dBi with SLL of -19.62 dB at a center frequency of 10 GHz.

In 4th part, the design of an X-band cylindrical conformal SIW slot array antenna is presented. The wave propagation characteristics on the cylinder are investigated to

verify fundamental propagation mode and the MLS algorithm is used to synthesize the array. To avoid spurious radiations, RWG to SIW feeding structure is utilized to feed the array elements. A flexible substrate is used for the design of 1×6 slot elements array. From simulation results, SLL of -21.72 dB and gain of 9.8 dBi have been achieved with VSWR $\leq$ 2 at a center frequency of 10 GHz.

In 5th part, the design of the nose-cone conformal SIW slot array antenna is presented for modern radar applications. Firstly, the wave propagation characteristics are investigated in doubly curved SIW, and it is observed that they are non-uniform along the longitudinal direction of nose-cone conformal SIW. To ensure the constant wave propagation along the length of conformal SIW, the conventional design of SIW is reformulated for nose-cone conformal SIW and circuit model modification is demonstrated. Secondly, the procedure for designing a SIW-based array on curved surfaces has been developed. In the proposed design, RWG to SIW feeding structure has been used to avoid spurious radiations. Finally, 1×6 element-based nose-cone conformal slotted array has been designed and compared with planar and cylindrical conformal arrays. It has been observed from the results that the nose-cone conformal slot array offers low SLLs and high gain. For the validation of the proposed design, the conformal slotted array has been fabricated and measured, which exhibited a reasonable agreement between the measured and the simulated data.

Finally, the last part of the thesis presents the design of SIW based dual-beam conical conformal slot array antenna for X-band applications. The proposed design consists of two SIW arrays of 1×6 slot radiators located at $\phi = 0°$ and 180°. The sub-arrays are fed using an RWG to SIW 1×2 balanced T-junction power divider. The arrays are projected in the longitudinal direction on a conical surface having a lower and upper radius of $1.66\lambda_0$ and $1.33\lambda_0$, respectively. The power divider and SIW arrays are designed and simulated in full-wave EM simulation software. It is observed from the results that the proposed array has two main beams in H-plane located at $\theta = \pm90°$, and have SLLs of -22.80 dB and -20.12 dB, respectively. For the validation of simulation results, the proposed antenna system is fabricated and measured, and a reasonable agreement is observed between both results.

Contents

List of Figures

List of Tables

Abbreviations

AF	Array Factor
AR	Axial Ratio
AVA	Antipodal Vivaldi Antenna
BBO	Biogeography-based Optimization
CCMBA	Cylindrical Conformal Microstrip Bow-tie Antenna
CFDTD	Conformal Finite Difference Time Domain
CoDE	Composite Differential Evaluation
CubeSat	Cube Satellite
DC	Direct Current
EM	Electromagnetic
EMC	Electromagnetic Compatibility
FEM	Finite Element Method
FFT	Fast Fourier Transform
GA	Genetic Algorithm
GDE3	Generalized Differential Evaluation
GPS	Global Positioning System
HF	High Frequency
HFSS	High Frequency Structure Simulator
HPBW	Half Power Beam Width
LHCP	Left Hand Circular Polarization
LO	Local Oscillator
MGDE3	Memetic Generalized Differential Evaluation
MIMO	Multiple-Input Multiple-Output
MoM	Method of Moment

MLS	Method of Least Square
NATO	North Atlantic Treaty Organization
PSO	Partical Swarm Optimization
RCS	Radar Cross Section
RHCP	Right Hand Circular Polarization
RWG	Rectangular Waveguide
SAR	Synthetic Aperture Radar
SIW	Substrate Integrated Waveguide
SLL	Side Lobe Level
SWB	Super Wideband
UAVs	Unmanned Aerial Vehicles
VNA	Vector Network Analyzer
VSWR	Voltage Standing Wave Ratio
Wi-Fi	Wireless Fidelity

Symbols

a	Broad side of waveguide
b	Narrow side of waveguide
d	Conducting via's diameter
dS_1	Cylindrical surface
G_0	Normalized conductance
h	Dielectric height
h_m^{upper}, h_m^{lower}	Upper and lower limits of SLL
h_c	Height of cylindrical post
l	Slot length
I_n	Element current
L_c, L_{CoSIW}	Lenght of cone
L_{CSIW}	Length of cylinder
L_f	Feeding SIW length
L_{SIW}	Length of SIW
L_n	Total length of cone
L_r	Resonant length of slot
n, N	Number of array elements
P_r	Power receive
P_t	Power transmit
Q_n	Mutual couplings
R_{slot}	Slot resistance
R_D	Dipole resistance
r_1, r_2	Lower and upper radii of cone

r_n	Radii of cone
r_c	Radius of cylindrical post
r_p	Top to center distance of cylindrical post
S	Via's pitch
S_{11}	Input reflection coefficient
u_{up}	Zeros of Bessel function
V_n	Slot normalized voltage
w	Width of SIW
W_{sf}	Feeding slot width
W_f	Feeding SIW width
W_{eq}	Weighting function
$W(\phi)$	Modified width of cone
x	Slot off-set
x_c	Off-set of cylindrical post
Y	Slot admittance
z_c	Length of cylinder
$Z_{TE_{10}}$	Impedance of TE_{10} mode
Z_{in}	Input impedance
Z_0	Characteristics impedance
$\delta_t, \varepsilon_{sync}$	Total error function
ε_r	Relative permittivity
β	Propagation constant
Δ	Difference pattern
ψ	Angle of root on unit circle
$\sum$	Sum pattern
θ	Feeding slot angle
ϕ_s	Cylindrical slot offset
ϕ_1, ϕ_2	Angle at lower and upper sides of cone
ϕ_t	Tilt angle of modified SIW
λ_0	Free space wavelength
λ_g	Guided wavelength

Chapter 1

Introduction

1.1 Background

Conformal antenna arrays are considered to be the best choice for airborne and defense applications. They can easily be designed, fabricated, and implemented using a low profile flexible substrate such as microstrip technology or multifaceted surfaces. Unlike planar arrays, the development of conformal arrays needs Electromagnetic (EM) modeling, which changes with respect to the application.

In the 1930s, the foundation of a conformal array started with the development of a dipole array arranged in a circular manner [1]. After that, in 1936, Chireix [2] conducted experimental research on conformal antennas, which can be used for military applications. Later on, in 1953, a conformal circular array had been designed and got attraction due to its symmetrical arrangement and proper phasing of element [3]. Furthermore, the designed array can generate a unidirectional radiation pattern, which can be used for scanning applications.

During World War II, a High Frequency (HF) circular array was developed in Germany for intelligent single gathering and direction-finding. Moreover, the array was as large as 100 m. In addition to this, the fundamental work on aperture radiation from the metallic cylinder was presented by Gething [4] in the late 1960s and HF diffraction was discussed by Hessel [5] in 1970s. In 1974, Christopher

[6] designed an electronically scanned array named TACAN. In addition, many similar sets of projects had been built during the cold war. In 1996, the trend had shifted towards conformal radar applications, e.g. Colin [7] developed a circular array for experimental radar systems.

The designs presented above are related to the circular array, and their main focus was for ground-based applications. In the last 10 years, many researchers presented conformal antenna arrays for aerodynamic applications. In [8], Bearse designed a conformal array for an aircraft, and the array was protected using a dielectric name as a radome. For experimental purposes, $90°$ scanning had been achieved by using four planar arrays. In addition, a passive lens was placed at the nose of the aircraft to control the polarization, which consequently degrades the bandwidth. Later on, in 1998, Fowler discouraged its practical usage and after that Kinsey, in 2000, showed a detailed analysis of the cost-effectiveness or the benefits of the nose-mounted lens array.

1.2 Conformal Antenna

The basic definition of a conformal antenna is stated as *"an antenna that conforms to a surface whose shape is determined by considerations other than electromagnetics, e.g. aerodynamics or hydrodynamics"* [1]. In other words, the definition also includes planar antennas if a planar shape is determined other than an EM consideration as shown in Fig. 1.1(a). In the figure, the parameters L and W represent patch radiator length and width, respectively; and h denotes the thickness of the dielectric substrate. These types of antennas are not used in common practices.

Usually, the conformed shapes are cylindrical, conical, or spherical and even any shape depends on the application. The radiating elements have to mount on or perfectly attached to smoothly curved shapes. One of the examples of conformed antennas is shown in Fig. 1.1(b), where a conventional microstrip patch antenna is bent to some angle. Furthermore, many approximation methods exist such
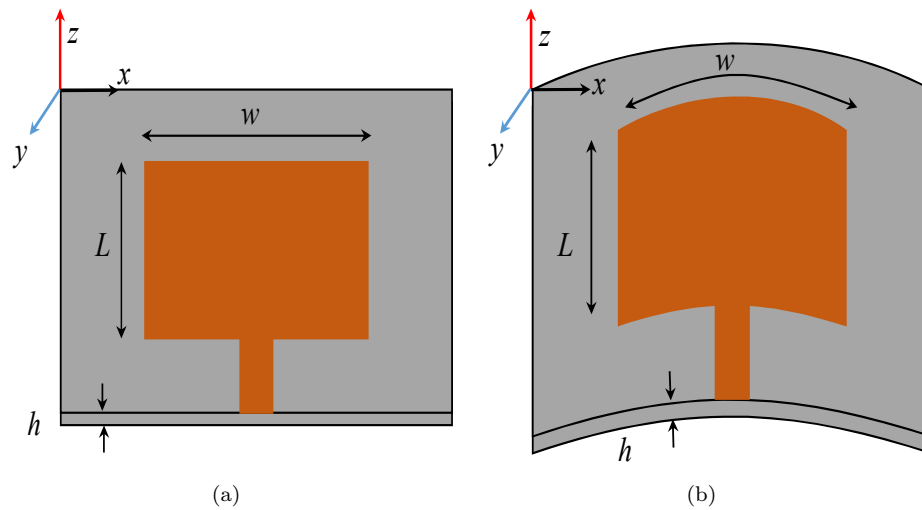
FIGURE 1.1: Schematic of a (a) planar antenna and (b) conformal antenna.

as smooth curve by several planar facets, which is used to simplify the complex radiating part [1].

In Table 1.1, a comparison is presented between planar and conformal antennas. From the table, it can be noted that the design of the conformal array is complicated compared to planar arrays. The bandwidth of conformal arrays is limited, while wide impedance bandwidth is common in planar arrays. Similarly, the gain of the conformal array is less than planar antenna arrays. The issue of gain can be overcome by increasing the number of elements in the array whereas, the conformal array does not add an extra payload for aircraft or high-speed vehicles. Additionally, the radiation characteristics can easily be controlled in conformal antennas. One major benefit of a conformal array is the larger angular coverage area, e.g. a conformal radar has wider coverage with less Radar Cross Section (RCS) however, the planar array suffers less coverage with larger RCS. Moreover, the radome is not needed in conformal arrays with adaptive surface integrity.

1.2.1 Need of Conformal Antenna

In modern aircraft, a number of antenna systems are required for different applications ranging from navigation to communication, detection radars, and instrumentation landing systems, etc. These antenna systems must integrate on the curved

TABLE 1.1: Comparison between conformal and planar antenna arrays.

Parameters	Planar Array	Conformal Array
Design	Simple	Complicated
Bandwidth	Wideband	Narrowband (< 400 MHz)
Gain	≥ 20 dBi	≤ 15 dBi
Polarization	Linear and circular	Linear and circular
Beam and null control	Use of fixed excitation phase and amplitude	Complicated
Angular coverage	$\leq \pm 60°$	$\geq \pm 60°$
RCS	Large	Less than planar
Surface integrity	Limited to planar surface	Adaptive
Radome	Abberation effects	Not needed
Packaging	Multi-layer	Single-layer

surface of an aircraft to decrease the drag and fuel consumption. Usually, broadband antennas are needed to combine the functions of more than one antenna system. Therefore, the demand of conformal antenna is increasing day-by-day for satellite and airborne applications.

According to the definition of conformal antenna that the antenna array can be conformed on the cylinder, conical shape or any other physically designed part of an aircraft or missile so, for this purpose, the conformed shape can be changed with respect to application such as high-speed jets, airborne surveillance radars, and high-speed trains.

In the case of cylindrical distributed elements, the radiation characteristics can be realized for different patterns such as omni-directional, 360° steerable pencil beam, and multiple beams. As an example, a 360° coverage needs in mobile base station applications. Accordingly, the use of a 120° sector antenna would be a better option instead of the cylindrical conformal antenna. On the other hand, the use of a conformal array in satellite-borne applications significantly reduces the drag problem.

1.3   Basic Conformal Shapes

There are three basic conformal shapes that have been used in multiple applications such as cylindrical, conical, and radome. First, the cylindrical shape has widely been used for aircraft applications whereas, the fuselage is taken as a conformal platform in order to reduce the fuel cost and payload. As long as the conformal structure remains the same, the characteristics of the array remain unchanged.

Secondly, the conical surface is another type of conformal surface. This type differs from the cylindrical shape in terms of its doubly curve surface nature. The conical shape has some advantages over the cylinder that provides better angular coverage in radar detection. Figure 1.2 shows a schematic view of the conformal antenna conformed on an aircraft. From the figure, it can be seen that the aircraft body has different transitions, which can ultimately change the behavior of antenna array [9].
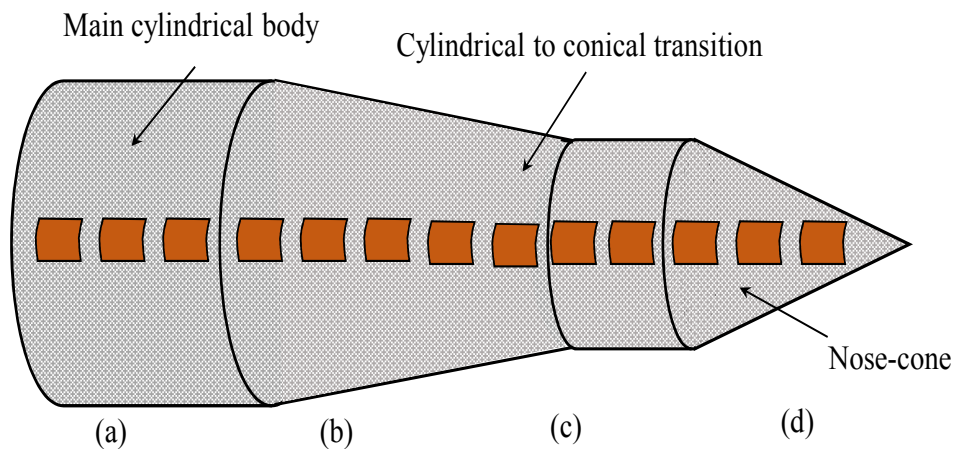
FIGURE 1.2: Design of an antenna array conformed onto (a) cylinder (b) cylinder to conical transition (c) add on cylinder and (d) nose-cone.

Thirdly, the term radome is a portmanteau of two words radar and dome. Usually, the radome is considered as a dielectric shell structure to shield an antenna structure installed on any aircraft. In Fig. 1.3, a basic structure of a radome is shown for aircraft or missile applications. Radome can be constructed according to the shape of a particular application. Radome can also be used to streamline the antenna system. For example, a planar antenna for radar applications is installed on
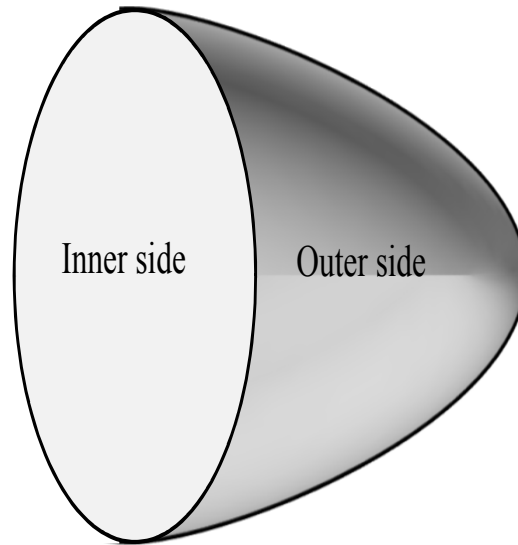
FIGURE 1.3: Nose-cone radome for aircraft or missile.

an aircraft therefore, it is necessary to protect antenna structure through radome. Although, it protects the antenna surface from atmospheric damages, but it will degrade radiation characteristics of the array due to dielectric losses. In contrast, the conformal antenna does not need any radome so, the conformal array has the advantage over conventional aerodynamic antenna array configuration. In literature, metal-based radome had been used with slot openings that allow the wave to propagate. This type of solution has been adopted to install planar arrays at high-speed aerial vehicles and missiles.

1.4 Motivation

The planar antenna array technology is mature in various aspects, while the conformal antenna technology is under development. Some conformal antenna designs are available in the literature for commercial applications but there is a need to investigate conformal antenna arrays for military and medical applications. In planar arrays, the performance parameters like beam and null position have been controlled by optimizing phase and amplitudes of the input signal but these factors are difficult to handle in the designing of conformal antenna arrays. Additionally, the polarization is also considered as a function of th doubly curved surface in the

case of conformal antennas. Similarly, the bandwidth of an antenna is also a function of singly and doubly curved surface. In general, the impedance bandwidth is dependent on the conformal platform as long as the curvature remains unchanged. Furthermore, fuel efficiency and payload reduction for aircraft applications attract researchers to adopt these antenna types. In addition, the higher integration capability of the conformal antenna also increased its worth. One major advantage of conformal antennas over planar antennas is its angular coverage, which is an important factor for defense-related applications.

1.5   Research Questions

Keeping in view the future requirements of conformal antenna arrays for aircraft and Unmanned Aerial Vehicles (UAVs), there is a need to develop an **optimized antenna array that can generate sum ($\sum$) pattern with −30 dB Side Lobe Level (SLL) and difference (Δ) pattern with −25 dB principle null depth.** So that it can be utilized for radar applications. For this purpose, array parameters such as excitation current need to be optimized while keeping inter-element spacing constant.

In the modern era, Cube Satellites (CubeSats) have become a new approach to explore space. CubeSats are a more affordable solution for deep space and remote sensing applications but path loss is their main problem. To overcome path loss issues, the antenna system of CubeSats needs to be efficient. So, there is a need to **design a low-cost and flexible antenna system for CubeSats**.

There is a need to develop a low profile antenna array that can be fabricated using a flexible substrate in order to conform on a cylindrical surfaces. For this purpose, **a design of cylindrical conformal Substrate Integrated Waveguide (SIW) slotted array is needed with SIW to Rectangular Waveguide (RWG) feeding structure**. One basic reason to utilize SIW to RWG feeding network to achieve suppressed spurious radiations.

In the current state of conformal arrays, there is a need to investigate the integration of antenna arrays on the surface of high-speed jets. Owing to this, **a nose-cone conformal SIW slotted array design is needed for high-speed jets, missiles, and aircrafts**. Owing to this, there is also a need to design an antenna system, which can track multiple targets at the same time. For this purpose, a novel design of a feeding network is also needed so that the arrays can be excited with equal amplitude and phase.

1.6   Thesis Outline

This chapter presents details pertaining to conformal antennas. The chapter starts with the historical background on conformal antennas. After that, a discussion is provided that why conformal antennas are considered to be a good candidate for airborne applications. Different conformal shapes are discussed, and it is observed that in most of the airborne applications, cylindrical and conical shapes are being utilized, and there is a need to design such antenna system, which can easily be integrated with the mentioned shapes. The remaining organization of the thesis is given below:

Chapter 2 presents a detailed overview of previously presented conformal antennas for various applications. The chapter starts with the discussion of previously reported planar SIW based slot array antenna designs. The second section describes the cylindrical conformal antenna arrays designed by researchers for commercial and military applications. In the end, a detailed discussion is presented on conical conformal antenna arrays designed to the date.

Chapter 3 presents the design and simulation of the planar slotted array to generate $\sum$ and Δ radiation pattern. The presented array follows the design principle developed by Elliot for the synthesis of $\sum$ pattern, while Bayliss's current distribution has been used to generate Δ pattern. The simulation of the proposed array has been carried out in HFSS, a commercially available electromagnetic software,

which is based on the Finite Element Method (FEM). From the presented results, a good agreement between theoretical and simulated results has been achieved.

Chapter 4 describes the design of a slotted array with an aim to improve the SLL. The antenna parameters such as inter-element spacing, d, number of elements, N, and element excitation amplitude has been optimized using the PSO algorithm. A linear array has been synthesized and optimized to find the ultimate result of minimum SLL and finally, optimized element excitation has been generated. The second part of this chapter consists of two design examples for -20 dB and -30 dB SLL design goals.

Chapter 5 presents an SIW based conformal slotted array with broadband feeding slot for CubeSat applications. The designed array is fed through another SIW placed on the lower side of the radiating part. The simulation results show that the designed array has a wide impedance bandwidth compared to the conventional slotted array.

Chapter 6 discusses the design of cylindrical conformal SIW slot array antenna with minimum SLL. A RWG is used to excite the designed array through a coupling slot of the same dimensions. The feeding slot is off-set to suppress the spurious radiations generated from the feed structure.

Chapter 7 demonstrates the design and implementation of a nose-cone conformal SIW based slot array antenna for X-band applications. It has been investigated through EM simulation that the propagation constant, β will increase with the increase in the length of SIW along the direction of nose-cone. Therefore, the modification in SIW has been proposed to propagate a constant β. A design process is also described for a doubly curved surface. Finally, the simulated array is also validated through fabrication and it is observed that the simulated and measured results are well in agreement.

Chapter 8 presents the design of the conical conformal sub-array antenna system for X-band multi-target tracking applications. To the author's best knowledge, no work has been presented previously regarding the nose-cone conformal multi-beam

system. An array factor is derived for two unit vectors pointed to two arbitrary target locations. In order to feed the arrays, a balanced RWG to SIW 1×2 T-junction power divider is also designed. The proposed antenna system is also fabricated and measured to validate the simulation results.

Chapter 9 discusses the conclusion drawn from this research and its extension as future work.

Chapter 2

Literature Review

2.1 Introduction

In this chapter, a review has been presented of conformal antenna arrays, which include planar, cylindrical, and conical conformal arrays. In the first part, a detailed overview of SIW based planar antenna arrays has been presented along with their potential use in several communication applications. The second part presents the development of cylindrical conformal antenna arrays to the date. Finally, the arrays developed on doubly curved surfaces known as conical surfaces are also discussed.

2.2 Planar SIW-based Antenna Arrays

SIW is considered as a replacement of conventional RGW due to its non-planar structure. However, the design of SIW has three main parameters such as the width of SIW, A_e, the diameter of conducting vias, d, and spacing, s between them as shown in Fig. 2.1.

SIW has two basic types: firstly, a two-port network and the other is a standing wave uni-port network. These two types have a different set of characteristics
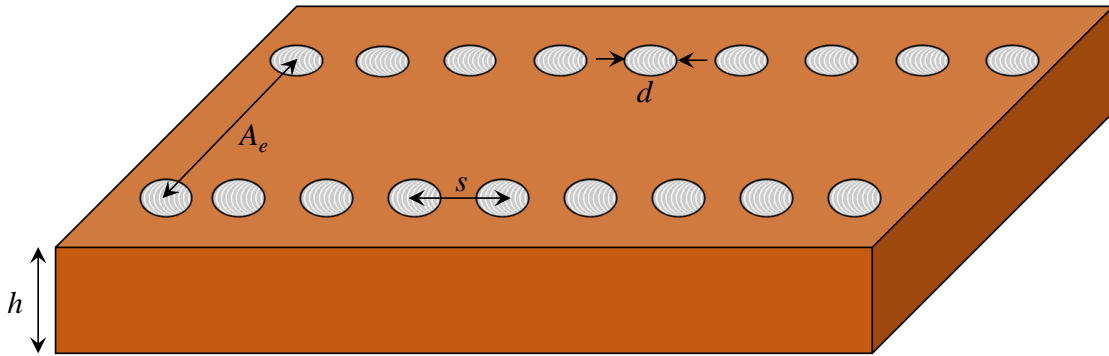
FIGURE 2.1: Cross-sectional view of planar SIW.

such as traveling wave suffers due to radiating power loss but it provides wide impedance bandwidth. In contrast, the standing wave SIW has higher radiating efficiency at the cost of narrower impedance bandwidth.

In [10], a design of 16×16 slot array had been implemented for X-band applications. The array was synthesized with a uniform slot off-sets and achieved a gain of 24.4 dB at 10 GHz with SLL of -30 dB. In [11], the authors utilized RWG to SIW feeding structure to excite the slot array antenna designed at 35 GHz. This technique provides a return loss of -15 dB over the range of 800 MHz. In aircraft applications, a fundamental reason to select the slot array is that it provides reduced SLL in H-plane. In [12], a wideband SIW based slot array antenna was presented for 60 GHz applications. To achieve wide impedance bandwidth, a multi-sector antenna was introduced whereas, the array elements were closely placed. For gain enhancement and to achieve unidirectional radiation characteristics, the authors utilized radiators and reflectors. In [13], a 16×8 slotted array with 45° inclined linearly polarization was presented for Ka-band applications as shown in Fig. 2.2. The designed array also consisted of an alternating reactance slot pairs that lead to achieve better impedance matching and uniform field excitation. From the presented configuration, the authors achieved 990 MHz bandwidth with a peak gain and efficiency of 24.3 dBi and 53.7%, respectively.

In [14], a dual-layer pillbox antenna was designed for mechanical beam-scanning applications at millimeter-wave frequencies. The designed antenna system consisted of three main subsystems: input part, multislot quasi-optical transition,
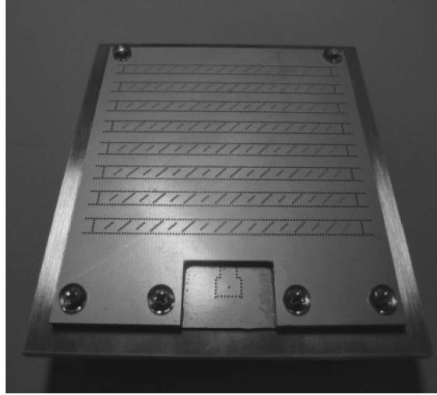
FIGURE 2.2: Fabricated prototype of slotted array for 45°-inclined linear polarization [13].

and radiating part. The radiating and input parts were placed on two different layers of the dielectric substrate, and the quasi-optical transition placed on another layer, which behaves like a 180° E-plane coupler-type bent. By using this technique, a scan range of ±35° was achieved with a Half Power Beamwidth (HPBW) of 15° in H-plane. For airborne applications, with improved radiation characteristics, there is a need to solve the problem of unwanted back lobes. For this purpose, a simple design technique was reported in Ref. [15] to minimize back lobe levels of an antenna array. According to the presented work, the back lobe levels were minimized using a quarter-wavelength choke fabricated on the bottom side of the SIW-based slot array. The same kind of technique was used by Karami et al. [16] where the authors constructed a combination of planar choke, microstrip lines, and short-ended stubs. The spill-over currents and edge diffractions were removed by adjusting the position of the choke structure.

In [17], the design of the traveling wave antenna array was reported for X-band applications. The authors introduced an error function to improve the radiation properties of the array and achieved a maximum measured gain was 12.26 dBi in the presence of 10 radiating slots. The SIW array was terminated with the matched load and accordingly, the main beam was off-set and located at $\theta = 63.5°$. In [18], the authors reported a SIW based slotted array for automotive radar applications. A slot array with 32×4 elements had been designed using a coplanar waveguide (CPW) fed technique. From the presented results, it was observed that the designed array had SLL of -23 dB in H-plane, while for E-plane,

the SLL increased up to -12 dB. In [19], basic formulas for designing SIW at X-band (8-12 GHz) were presented with microstrip to SIW transition.

In [20], an antenna array was reported for low cross-polarization. A slotted ridged SIW had been proposed along with the effects of mutual coupling. The slot elements were placed on the centerline of the broad wall of the SIW to achieve reduced cross-polarization. In [21], an X-band traveling wave SIW slot array antenna was presented to achieve a shaped beam. The array element was composed of a dual-layer SIW longitudinal slot-coupled cavity. By utilizing the presented slot structure, an improved impedance bandwidth was achieved with reduced cross-polarization.

In [22], a higher-order cavity mode feeding network was designed for an H-shaped 2×2 slotted array as shown in Fig. 2.3. For enhanced bandwidth, the slot elements were arranged asymmetrically with different sizes and locations. But the radiation characteristics of the designed array are not stable over the reported frequency range due to the variations in surface current. On the other hand, Mohamed et al. [23] proposed a sable antenna array that was simulated at 54, 60, and 66 GHz. A tapered slot geometry was utilized to achieve the required array characteristics such as gain of 21 dBi, SLL of -15 dB, and main beam positioning.

In [24], a planar phased array was presented for wide-angle scanning applications. The center off-set 1×8 SIW based slot array was designed, which can operate in the frequency range of 5.4-6.2 GHz. The results show that the main beam can steer from -71° to 73° in the whole operating band. In [25], a single-layer planar SIW based monopulse slotted array was designed that can generate both $\sum$ and Δ patterns. The proposed array was resonating at 5.83 GHz and provides an SLL of -27 dB for sum pattern, while the principle null had a depth of -40 dB. For improved broadside radiation characteristics, Nasimuddin et al. [26] designed a leaky-wave SIW antenna for the frequency range of 8.8-9.2 GHz. Their measured result showed that the array had a gain of 10.6 dBi at the operating frequency range. Furthermore, a trapper transmission line had been introduced for the feeding of the array. Finally, the broadside radiation pattern was achieved at 0°.
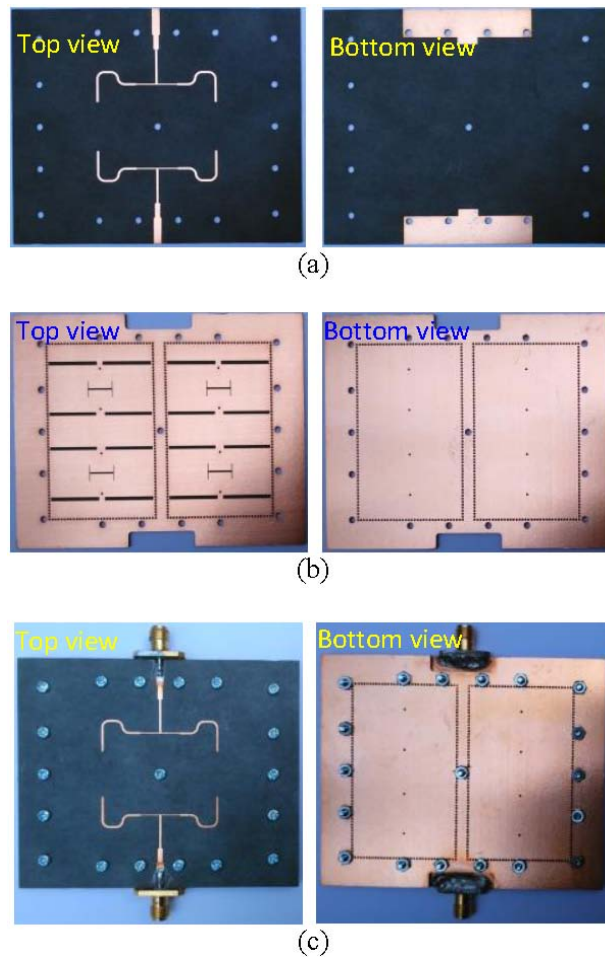
FIGURE 2.3:   Fabricated prototype of differential-fed slot antenna array (a)
Layer I (b) Layer II (c) Designed antenna [22].

Yang et al. [27] also presented a single-layer shared-aperture slotted array for
dual-frequency applications. A cavity resonator principle was used to a distinctive
SIW antenna array cavity to obtain dual-frequency at 5.7 GHz and 5.88 GHz on
two separate ports. In [28], a SIW ring-slot antenna array was designed for beam
and polarization-reconfigurable applications. A 2×2 ring-slot antenna array was
designed, shown in Fig. 2.4, that can generate four beams in different directions
with two orthogonal linear polarizations. The four beams were achieved by using
a feeding network, which consisted of four 90° SIW based 3-dB couplers. The
reconfiguration characteristics were achieved through PIN diodes, switched by a
DC bias network.

In [29], a SIW slot array was presented with beam scanning capabilities. Seven
and eight elements arrays were fed through phase-shifters backed by 1×8 power
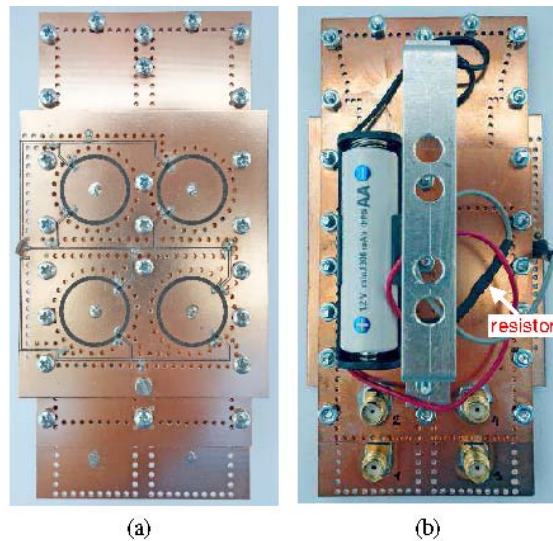
FIGURE 2.4: Fabricated prototype of beam and polarization reconfigurable ring-slot antenna array (a) front view (b) back view [28].

dividers. Through this technique, a beam scanning in the range of $\pm15°$ was achieved with an SLL of less than -10 dB. In [30], a 3×2 slot antenna array was developed for tri-beam characteristics. The beamforming network was a buttler matrix of 3×3, which consisted of four phase shifters and three 90° couplers. Three beams in a direction of $\pm30°$ and 0° were obtained when different ports were excited, respectively. A brief overview of above-presented antenna arrays is also given in Table 2.1.

TABLE 2.1: Brief summary of previously presented planar SIW slot array antennas.

Author	Year	Development	Ref.
Xu et al.	2009	Design and development of SIW longitudinal slot array antenna for low SLL.	[10]
Li et al.	2009	Development of RWG to SIW feeding structure for slotted arrays.	[11]
Ohira et al.	2010	Design of a wideband SIW based slot array antenna for 60 GHz applications.	[12]
Kim et al.	2012	Design of a 16×8 slotted array with 45°-inclined linearly polarization for Ka-band applications.	[13]
Gandini et al.	2012	Development of a SIW slotted array for beam scanning applications.	[14]

Wei et al.	2013	Design of a compact SIW slot array antenna for reduced back lobe levels.	[15]
Hosseininejad et al.	2013	Design of optimum traveling wave SIW slot array antenna.	[17]
Xu et al.	2014	Design of a 32×4 SIW based slotted array for automotive radar applications.	[18]
Nawaz et al.	2014	Analytical approach for designing SIW.	[19]
Mallahzadeh et al.	2015	Design of a slotted ridged SIW array antenna for low cross-polarization.	[20]
Karami et al.	2015	Design of a SIW slot array antenna with suppressed back lobe levels for X-band applications.	[16]
Qiu et al.	2016	An X-band traveling wave SIW slot array antenna design for shaped beam.	[21]
Wu et al.	2016	A wideband 2×2 slotted array design with higher-order cavity mode feeding network.	[22]
Mohamed et al.	2016	A tapered slot array antenna design for high gain, reduced SLL , and beam steering.	[23]
Wen et al.	2016	A planar phased array design for wide angle scanning applications.	[24]
Cao et al.	2017	A single-layer planar SIW based monopulse slotted array design for both $\sum$ and Δ patterns.	[25]
Nasimuddin et al.	2017	Design of a slotted leaky-wave SIW antenna for high gain and backward beam scanning.	[26]
Yang et al.	2018	A single-layer shared-aperture slotted array for dual-frequency applications.	[27]
Vasina et al.	2018	Beam and polarization-reconfigurable 2×2 SIW ring-slot antenna array.	[28]
Li et al.	2019	Design of an SIW slotted array with beam scanning capabilities.	[29]
Wang et al.	2019	A 3×2 slot antenna array deign for tri-beam characteristics.	[30]

2.3   Cylindrical Conformal Arrays

Cylindrical conformal antenna arrays are widely used in aerodynamic applications. A basic requirement that enforced to employ the conformal antenna is the less drag, which consequently leads to a reduction in fuel cost or battery requirement. In this section, a brief description of previously presented antenna arrays is provided, which are conformed on the cylindrical platform.

In [31], the authors presented an analytical approach to model patch antennas on a cylindrical platform. In [32], the designs of 4-element cylindrical conformal microstrip bow-tie antenna (CCMBA) and 2-element array were presented for large bandwidth. It was shown that even with a small curvature radius, CCMBA was able to achieve wide impedance bandwidth. In [33], a cylindrical conformal 2×2 microstrip antenna sub-array was designed for millimeter-wave bands. For enhanced bandwidth and better radiation performance, an H-shaped slot was etched from the radiating element. It was also demonstrated that the designed array had less spurious radiations interference from the feed network compared to the conventional design.

In [34], a non-planar cylindrical conformal antenna design was presented for 360° azimuth coverage. For antenna design, a rectangular waveguide structure was used due to its high power handling capability. A 1×8 slot elements were etched from the narrow wall of the waveguide and observed an SLL of -25 dB. In [35], a cylindrical conformal Yagi-Uda antenna composed of five conformal dipoles was designed to realize the radiations toward the axis of the cylinder. Furthermore, a symmetrical antenna structure was mounted on the other side of the cylinder to form a mono-pulse antenna. In [36], a dual-polarized X-band cylindrical conformal array antenna was presented for UAVs with polarimetric radars/sensors. The designed array antenna consisted of sixteen 2×2 sub-arrays conformed on a cylinder of various curvature radii to reduce the payload. In [37], a cylindrical conformal switchable array antenna was designed for 2.4 GHz band. From the results, it was observed that the antenna system provides a quasi-isotropic pattern with suppressed nulls. It was also described that by using three tri-polarization

antennas and switching among them, complete spherical coverage can be achieved with a gain >2.5 dBi.

In [9], a study on conformal antenna element design was carried by the NATO research group. This work demonstrated the statics deformation due to the vibration effects on the antenna system. The antenna had two resonant bands at 1.25 GHz and 1.575 GHz and reported gains were 5 dBi and 6.5 dBi, respectively. In [38], a design of a traveling-wave slotted array conformed on cylindrical objects was presented. The designed antenna system can offer a maximum gain in the range of 10.9-11.8 dBi, but it suffered due to increased SLLs. In [39], a cylindrical conformal array of 1×12 circular patch elements was reported on the missile platform. The presented array operates at 2.4 GHz and provides SLL of -20 dB. In [40], a SIW based traveling wave slot array antenna was reported at 25 GHz for scanning applications. The array consists of four antenna elements fed using a conformed SIW 1×4 power divider and measured a maximum gain of 14 dBi with beam scanning capability up to 10°.

A conformal leaky-wave antenna design was reported in Ref. [41] for automotive radar applications. The measured results show that the array had a gain of 11.5 dBi and the main beam was positioned at 45°. In [42], a cylindrical conformal slot array at 35 GHz was presented using a traveling wave topology. The array consisted of 6×35 elements excited using Taylor distribution as shown in Fig. 2.5. As the array consisted of a large number of elements therefore, the simulated gain of 25.59 dBi had been achieved with SLL of -17 dB in H-plane. The main beam was off-set due to the traveling wave effects of the slot array. It was described that in traveling wave configuration, the array must be terminated with a matched load. To feed multiple conformal arrays, there is a need for an external circuitry such as power divider. The power divider is a passive component that is used for power division as well as the power combiner. In [42], a 1×8 power divider was used to divide the input signal into eight outputs to excite respective arrays. However, in receiving mode, the eight inputs combined into one output. In general, the output of power divider considered to be in-phase with equally divided outputs.
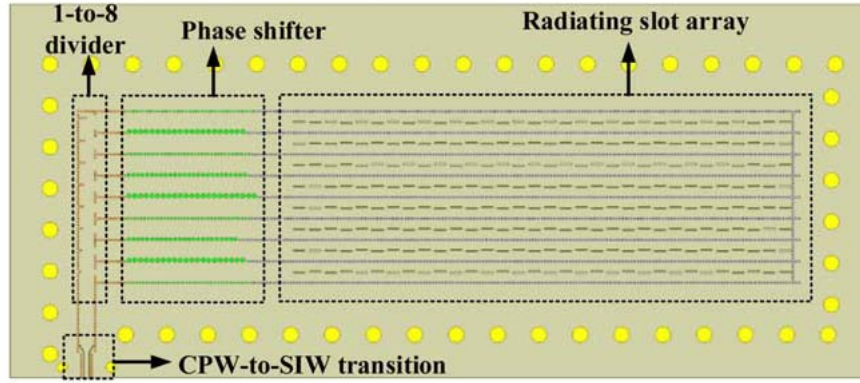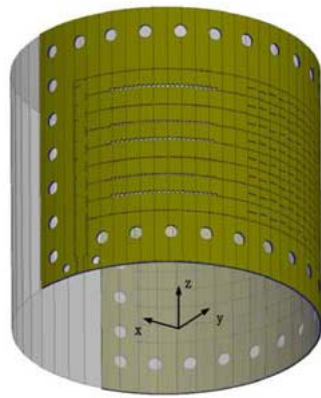
FIGURE 2.5: (a) Design of planar SIW slotted array ; (b) 3D view of cylindrical conformal; (c) Fabricated prototype [42].

In [43], a cylindrical conformal array antenna was reported for millimeter-wave applications. An 8×32 elements based longitudinal slotted array was fabricated and measured, and it was observed that it provides a gain of 11.5 dBi with 0.5 dB variation along with the range of 41.7-42.5 GHz. Moreover, a 1.4 dB and 1.6 dB variation in SLL was noted at 42.6 GHz and 42.2 GHz, respectively. Also, a 4.5° deviation was observed in the tilt angle over the operating frequency range. In [44], the design equations for cylindrical conformal slot arrays were developed. The basic topology was similar to Elliott design procedure however, the expression for admittance Y_n/G_0 was derived in this work. Furthermore, the mutual admittance of $n+1$ slot elements was also mentioned. The array consisted of 10×10 elements in order to achieve a shaped beam in E- and H- planes. It has been observed from the measured results that the SLL was <-25 dB in H-plane and it was below -15 dB

in E-plane. It has been noted that the analytical model developed for slot arrays conformed on cylindrical surface converge with the measured results. In [45], a circularly bent Antipodal Vivaldi Antenna (AVA) was presented for X-band (8-12 GHz) satellite applications. The results showed that the array had a maximum gain of 17.6 dBi whereas the main beam located at 90°. It had also been observed that the back lobe has a significant level positioned at 270°. Furthermore, the array can only be used in the applications where omni-directional radiation characteristics are required. A cylindrical conformal antenna for Wireless Fidelity (Wi-Fi) application was presented in Ref. [46]. A four-element symmetrical circular slot antenna structure was wrapped on the cylinder. The designed array had a gain of 5.4 dBi at 2.4 GHz. Moreover, the presented array has stable radiation characteristics.

In [47], a design of super wideband (SWB) conformal wideband antenna array was presented on the cylindrical platform. A three-element array with a modified ground plane was used to increase the impedance bandwidth. But the designed array suffered from poor radiation characteristics due to the presence of nulls. In [48], a design of a conformal array was presented for gain prediction for two different applications. One array designed on the leading wing of an aircraft, while the second one related to mobile communication. The STL file of the complete 3D model of the fighter jet was simulated to find the estimated gain for a conformal array. Similarly, a 3D design of a building having the conformal base station antenna was also simulated. Moreover, the gain of the antenna compared to physically developed arrays and good approximation was observed.

In [49], a conformal antenna array design was reported for air traffic control applications. The array was composed of 128 radiating elements conformed onto a cylindrical surface. It was observed that the array can generate both $\sum$ and Δ patterns, which is helpful for tracking applications. Recently, the design of a cylindrical conformal slot array antenna was presented in Ref. [50] for multiple beam-forming. The size of the array was 10×10 and fed through a modified Rotman Lens as shown in Fig. 2.6. It was noted from the presented that the multiple

beam-forming was achieved through modified Rotman Lens with SLLs and a scanning range of <-20 dB and ±46°, respectively. In [51], a design of a planar SIW based slotted array was presented for millimeter-wave applications. Ten L-shaped slots were etched from the broad wall of SIW array to achieve wide impedance bandwidth, while PIN diodes were used with each radiating slot to ensure beam steering in a specified direction. Table 2.2 summarizes the cylindrical conformal antenna's development history so far.
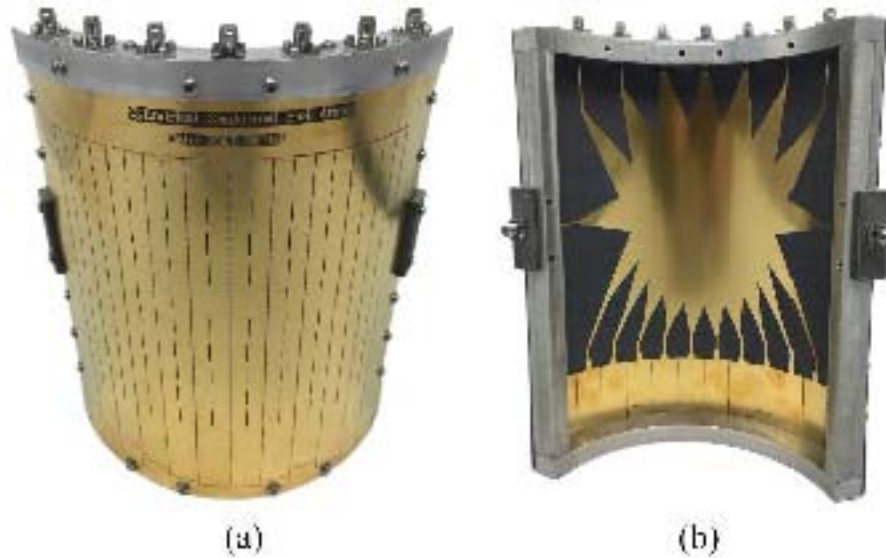
FIGURE 2.6: Fabricated prototype of multi-beam conformal array (a) front view (b) back view [50].

TABLE 2.2: Brief summary of cylindrical conformal antenna array's development history so far.

Author	Year	Development	Ref.
Herschlein et al.	1996	An analytical approach to model patch antennas on cylindrical platform.	[31]
June-Wei et al.	2003	Designs of 4-elements CCMBA and 2-element array for large bandwidth.	[32]
Wu et al.	2007	A cylindrical conformal 2×2 microstrip antenna sub-array for millimeter-wave bands.	[33]
Traille et al.	2007	A non-planar cylindrical conformal antenna design for 360° azimuth coverage.	[34]

Song et al.	2008	A cylindrical conformal Yagi-Uda antenna for broadside radition characteristics.	[35]
Ahn et al.	2010	A dual-polarized X-band cylindrical conformal array antenna for UAVs with polarimetric radars/sensors.	[36]
Zhang et al.	2011	A cynlidrical conformal switchable array antenna design for 2.4 GHz band.	[37]
Knott et al.	2011	A study on conformal antenna element design to demonstrate the statics deformation due to the vibration effects on antenna system.	[9]
Liu et al.	2012	A design of traveling-wave slotted array conformed on cylindrical objects.	[38]
Labowski et al.	2013	A cylindrical conformal array of 1×12 circular patch elements designed on the missile platform.	[39]
Bayraktar et al.	2014	An SIW based traveling wave slot array antenna at 25 GHz for scanning applications.	[40]
Martinez-Ros et al.	2014	A conformal leaky-wave antenna design for automotive radar applications.	[41]
Wang et al.	2015	A design of cylindrical conformal slot array at 35 GHz using a traveling wave topology.	[42]
Fan et al.	2016	A cylindrical conformal array antenna for millimeter-wave applications.	[43]
Yang et al.	2016	Development of design equations for cylindrical conformal slot arrays.	[44]
Tao et al.	2016	A circularly bent antipodal Vivaldi antenna for X-band satellite applications.	[45]
Chen et al.	2016	A cylindrical conformal antenna for Wi-Fi applications	[46].

Agnihotri et al.	2016	A design of SWB conformal antenna array on cylindrical platform.	[47]
Pelham et al.	2016	A design of conformal array for gain prediction for two different applications.	[48]
Angelilli et al.	2017	A conformal antenna array design for air traffic control applications.	[49]
Liu et al.	2018	A design of cylindrical conformal slot array antenna for multiple beam-forming.	[50]
Serhsouh et al.	2018	Design of a planar SIW based slotted array for millimeter-wave applications.	[51]

2.4 Conical Conformal Arrays

The development towards the conformal antennas specifically on the conical shape is of very much significance due to its use in aerodynamics applications. However, the utilization of conical conformal array has three major advantages over the cylindrical conformal array. First, it covers a more angular range compared to cylindrical conformal arrays. Second, it does not contribute the drag because the speed of aircraft is very much high. Third, there is no need to install radome or dielectric shell at the nose of an aircraft or UAVs in order to protect the array. Moreover, a radome suffers from dielectric losses, while the nose-cone conformal array does not require any radome protection. In short, the use of conical conformal antenna array has significance in aircraft tracking applications.

In [52], the authors designed arrays of dipoles on the conical surface. A projected distribution was used to observe array characteristics, e.g. SLL, polarization, and beamwidth. They also compared the similar arrays on a cylindrical platform and observed that the conical arrays offered better performance compared to cylindrical arrays. In [53], a theoretical analysis of the conical conformal microstrip patch antenna was presented. The authors showed that the radiation characteristics of

patch antenna change with the change in phase. In [54], a 4×4 microstrip antenna array was designed on a conical platform for millimeter-wave applications. The Conformal Finite Difference Time Domain (CFDTD) method was used for the analysis of the designed array. In [55], the authors presented an analytical approach to analyze the performance of conical conformal arrays for airborne applications. The analysis was done for a number of antennas in terms of SLLs, beamwidth, directivity, grating lobes, scan volume, and cross-polarization.

In [56], a slot array was designed on conducting cone. However, the basic analytical model for the conical structure was reported with greens function for the elliptic cone. Also, the coupling between slot radiators had been discussed in detail. Finally, the presented mathematical model was simulated using numerical expressions. In [57], design of a 1×8 microstrip patch antenna array was presented for millimeter-wave applications. For array feeding, a conventional corporate feeding network was utilized, and it was described that this kind of feed can lead to achieve low SLLs. Therefore, from the presented results, it was observed that the designed array offers SLL of -30.5 dB. In [58], the authors designed two different kinds of conical conformal antenna arrays for Global Position System (GPS). One array consisted of a quadrifilar helix antenna and the other one is a microtrip patch antenna array. Through theory and simulation results, they observed that both the arrays can provide omni-directional radiation characteristics normal to the axis of the chosen platform.

In [59], the design of a low frequency conical conformal antenna array was presented for missile applications. As the array was designed for missile applications therefore, the radiation pattern along the direction of the conical surface was required. However, two design considerations have been fulfilled: first, the radiation pattern was off-set, and secondly, the low-frequency band had been adopted (1.257-1.276 GHz). In [60], the authors designed a conical conformal phased array for modern Multi-input Multi-output (MIMO) radar applications. The antenna array can steer electronically in order to improve the mechanically scanning technology. Moreover, the SLL had also been minimized using the Genetic Algorithm (GA),
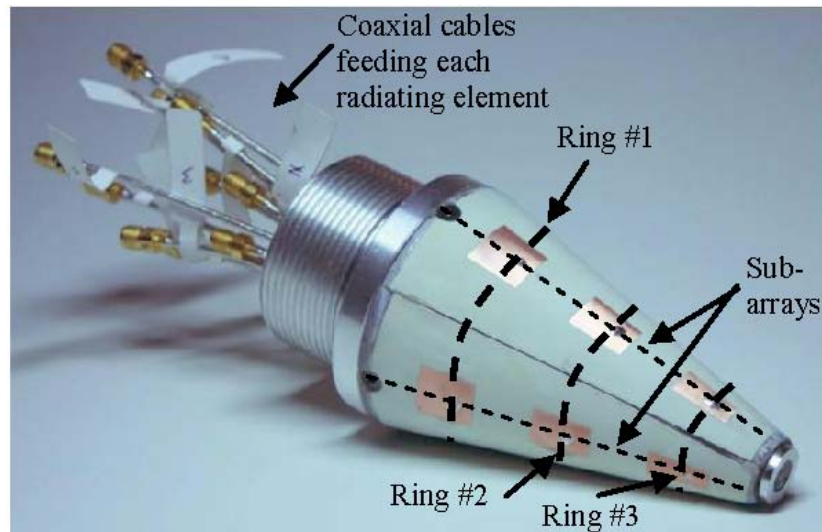
FIGURE 2.7: Fabricated prototype of 12-element patch antenna array on a conical platform with individual feeding [61].

while the array elements were radially distributed. Furthermore, the gain of 11.8 dBi was achieved from the presented configuration.

In [61], a 12-element conical conformal patch antenna array was designed and presented for a 5.2 GHz frequency band. Four sub-arrays were designed and each array consisted of three probe-fed patch antennas linearly placed on the conical platform as shown in Fig. 2.7. According to the authors, the designed array can provide a promising solution to steer and rotate the beam for point-to-point communication. In [62], a low-profile cavity-backed slot array antenna was designed into a conical platform for end-fire radiation characteristics. Three closely spaced radiating slots of different lengths were etched from the cavity to achieve high gain and broad bandwidth. The simulation results show that the presented conformal antenna can provide an impedance bandwidth in the frequency range of 9.3-10.81 GHz with a peak gain of 9.5 dBi.

In [63], a conical conformal SIW slot array antenna was presented for millimeter-wave applications. A flexible SIW transition from conical-to-cylindrical was designed for improved impedance matching. The presented configuration provides better return loss in the band of interest, but conical-to-cylindrical SIW transition can increase the size of the antenna structure, which limits its use in many aerodynamic applications. In [64], the design of conical conformal linear eight-element

patch antenna arrays was presented. A 1 to 8 power divider was used to feed the arrays. From the eight arrays, one array was excited individually by the RF switch to achieve the requirements of beam-switching. From the presented results it was observed that the designed array offers almost wide solid scanning from 0° to 218° in H-plane and >16° HPBW in E-plane. Furthermore, each linear array antenna provides a gain of over 10 dBi, while the peak gain of the final antenna was >15 dBi with an average radiation efficiency of 59.5%.

In [65], a high-gain conical conformal double rhombus antenna was presented with axial radiation and Right Hand Circular Polarization (RHCP). A nine director strips with double rhombus antenna was used to achieve high-gain and end-fire radiation pattern. A 1-to-4 Wilkinson power divider with a 90° phase difference was used as a feeding network to obtain RHCP radiation. The results showed that the designed antenna operated from 8.85 GHz to 10.57 GHz with a gain of >9.33 dBi and an axial ratio of <1.85 dB. Table 2.3 also provides a brief summary of previously presented conical conformal antenna arrays.

TABLE 2.3: Brief summary of previously presented conical confromal array antennas.

Author	Year	Development	Ref.
Munger et al.	1974	Design of dipole arrays on conical surface.	[52]
Augustin et al.	1995	A theoretical analysis of patch antennas on conical surface.	[53]
Yu et al.	2006	A 4×4 microstrip antenna array design on a conical platform for millimeter-wave applications.	[54]
Morton et al.	2006	An analytical approach to analysis the performance of conical conformal arrays for airborne applications.	[55]
Kaifas et al.	2006	A mathematical model for slotted array on conducting cone.	[56]
Liu et al.	2008	Design of a 1×8 microstrip patch antenna array for millimeter-wave applications to achieve low SLLs.	[57]

Xiangjun et al.	2009	Design of two different kinds of conical conformal antenna arrays for GPS application.	[58]
Li et al.	2014	Design of a low frequency conical conformal antenna array for missile applications.	[59]
Aboul-Seoud et al.	2014	A conical conformal phased array design for modern MIMO radar applications.	[60]
Jaeck et al.	2016	A 12-element conical conformal patch antenna array design for 5.2 GHz frequency band beam steering applications.	[61]
Chen et al.	2017	A low-profile cavity-backed slot array antenna into a conical platform for end-fire radiation characteristics.	[62]
Wu et al.	2017	A conical conformal SIW slot array antenna with conical-to-cylindrical transition for millimeter-wave applications.	[63]
Xu et al.	2018	Design of conical conformal linear eigth element patch antenna array for wide scanning applications.	[64]
Gao et al.	2019	A high-gain conical conformal double rhombus antenna design with axial radiation and RHCP.	[65]

From the above-presented literature, it has been identified that a conformal antenna array, which provides broadband impedance bandwidth, low SLLs, and high gain could be a good candidate for aerodynamic applications such as CubeSats. Additionally, in the current state of technology, most of the antenna arrays discussed above used mechanically to electrical beam scanning capabilities. Such antenna arrays offer large RCS, which limits the stealth characteristics of an aircraft. For this purpose, there is a need to design a conformal antenna array with low RCS for missile and airborne applications. Moreover, the developed arrays should provide beam scanning capabilities for the desired application.

2.5   Summary

In this chapter, a detailed overview of conformal antenna arrays is given. The performance of antenna arrays on different platforms (planar, cylindrical, and conical surfaces) is reported. The antenna performance against the design requirements has been compared. It has been noted that the conical conformal arrays have lower SLLs compared to the planar and cylindrical arrays. Moreover, the conical conformal antenna arrays are considered the most suitable antenna type for target tracking applications.

Chapter 3

Waveguide Slotted Array to Generate Sum and Difference Patterns

3.1 Introduction

Space and airborne Synthetic Aperture Radar (SAR) delivers an enormously useful surveillance system for both military and civil applications [66]. On the other hand, from the last 10 years, the demand of domestic purpose UAVs has been increasing exponentially and the issue for accuracy of instrumentation landing system needs to be improved to ensure the safety during landing. For this purpose, a slot array is widely used, which was initially introduced by Elliot [67]. Elliot, for the first time, introduced the procedure to calculate design parameters of a slot element. Furthermore, he also provided a guideline to generate required radiation pattern in H-plane [68].

There also generates a concern that the designed slotted array should provide $\sum$ and Δ radiation patterns for RADAR tracking applications. The main beam of the $\sum$ pattern is pointed at $\theta = 0°$, while Δ pattern has two main beams having principle null located at $\theta = 0°$ as shown in Fig. 3.1. It can be seen from the
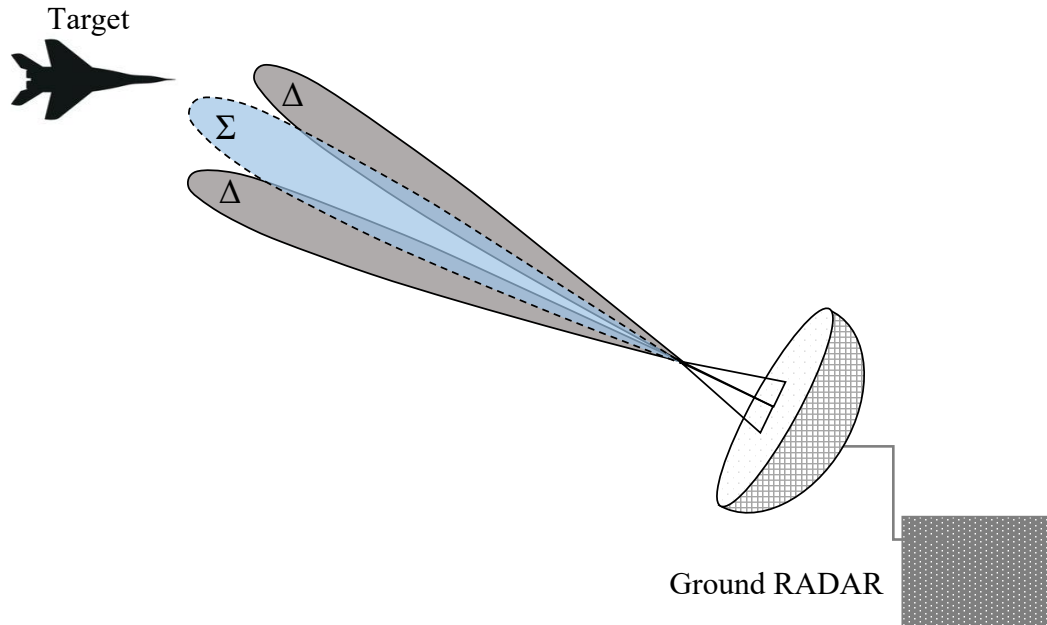
FIGURE 3.1: Ground RADAR with $\sum$ and Δ radiation patterns.

figure that the ground RADAR main beam is referred to as $\sum$ pattern, while the other two beams are called Δ patterns. For particular application, the target is considered to be locked when received signal from $\sum$ is maximum and from Δ is minimum.

For this purpose, in [69], a time-modulation based sub-array system was presented for $\sum$ and Δ pattern generation which has been controlled through radio frequency switches. In [70], a non-uniform antenna array design was presented for tracking applications. The authors utilized Fast Fourier Transform (FFT) to get non-uniform element's distribution. It was observed from the analytical results that the designed array can offer low SLLs with high gain. In [71], a cosine distribution was used to model 10 slot elements based antenna array. By using the proposed distribution function, deep principle null had been achieved. In [72], a slot array antenna for X-band SAR applications was presented. It was reported that the designed slotted array provides good radiation characteristics for $\sum$ pattern.

This chapter presents the design of $\sum$ and Δ pattern arrays for X-band tracking applications. Two sub-arrays have been designed by using Taylor $\sum$ and Bayliss current distributions. The $\sum$ pattern array consists of 2×4 slot elements, while Δ pattern is composed of 2×5 slot elements. In order to generate a Δ pattern,

two opposite excitation parts have been used. The proposed design is simulated in HFSS and it has been observed that the H-plane $\sum$ patter has a gain of 11.75 dBi with SLL of -8 dB whereas, the Δ pattern array has -25 dB depth of principle null with SLL of -23 dB.

3.2 Theory of a Slot Element

Elliott [67], for the first time, explained the theory of a slot element and described the design procedure for a longitudinal slot in the broad wall of the planar waveguide. A slot of length $\lambda_0/2$ at a center of a rectangular waveguide of length $\lambda_g/2$ was used to find the slot resonant length as shown in Fig. 3.2. Figure 3.3 shows the equivalent circuit model of a slot element. Two design equations were developed for shunt slot array by considering mutual coupling between slot elements. The theory of dielectric-filled waveguide was also incorporated to improve the design [73]. Elliott also reported a modified slot element design in Ref. [74] by including higher-order modes. The longitudinal slot has half-sine E-field variation whereas, the slot offsets from the center will disturb the surface currents, which results in the generation of slot voltages V_n.

Consider a rectangular waveguide of dimensions a and b. The inclined slot is considered on the broad wall at a distance of x_1 from the axis (x, y, z) of the waveguide. The inclination of slot is ψ at a distance of $a/2$ (center of waveguide). So, the waveguide axes can be re-defined as $(x'y', z')$. To meet the requirements defined by Elliot, slot axis at ψ can be represented as $(x''y'', z'')$. Now, from Fig. 3.2, the coordinate systems can be represented as

$$z = z' \tag{3.1}$$

and

$$x' = x - x_1 \tag{3.2}$$

If z' is transferred to z'' then,
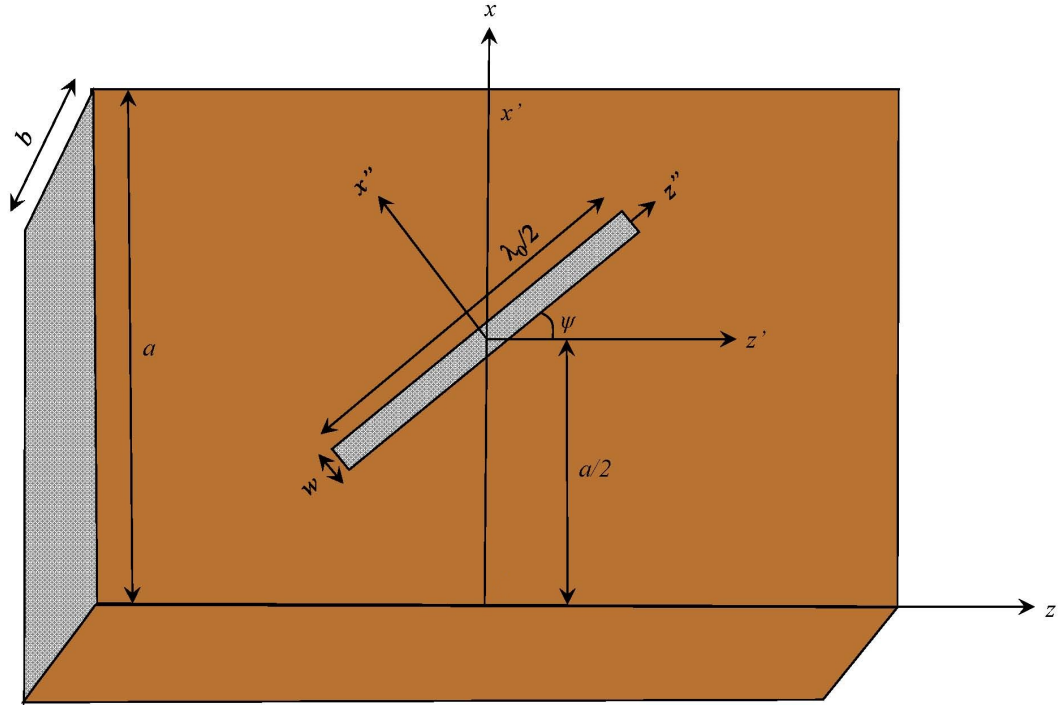
FIGURE 3.2: Schematic of a center inclined slot on a rectangular waveguide.
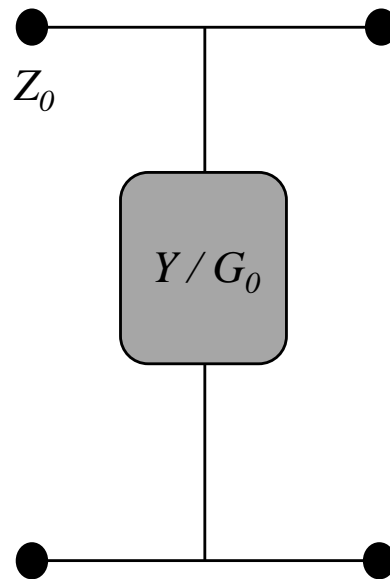
FIGURE 3.3: Equivalent circuit model of a slot element designed on a rectangular waveguide [40].

$$z' = z'' \cos(\psi) - x'' \cos(90 - \psi) \tag{3.3}$$

The above equation can also be written as

$$z' = z'' \cos(\psi) - x'' \sin(\psi) \tag{3.4}$$

Similarly

$$x' = z'' \sin(\psi) - x'' \cos(\psi) \tag{3.5}$$

The projection on the (x', z') are

$$z'' = z' \cos(\psi) + x' \sin(\psi) \tag{3.6}$$

and

$$x'' = z' \sin(\psi) - x' \cos(\psi) \tag{3.7}$$

The narrowness of the inclined slot element permits the assumption E-field as

$$\vec{E} = E(z'')\widehat{a}_z \tag{3.8}$$

The E-field can be write as

$$\vec{E}_1 = (\cos(\psi)\widehat{a}_z - \sin(\psi)\widehat{a}_z)\frac{V_m}{w} \sin[k(l - z'')] \tag{3.9}$$

where $V_m \sin[k(l - z'')]$ is the orientation of E-field and w is the width of slot. The H-field in the waveguide must have both $\vec{H}_x$ and $\vec{H}_z$ components. Keeping this in mind, $\vec{H}_2$ can be written as

$$\vec{H}_2 = \vec{H}_z + \vec{H}_x \tag{3.10}$$

The Poynting vector for slot can be written as

$$\int_{slot} (\vec{E}_1 \times \vec{H}_2)ds \tag{3.11}$$

where $ds = dx''dz''$. Here, one more condition is imposed that at $t = 0$, waveguide has only fundamental propagation mode TE_{10}. So, $\vec{H}_2$ can be writte as

$$\frac{V_m}{w} \int_{-l}^{l} \int_{-w/2}^{w/2} e^{-j\beta_{10}z} V_m \sin\left[k\left(l - z''\right)\right] \left[\frac{\beta_{10}}{\frac{\pi}{a}} \sin\left(\psi\right) \sin\left(\pi\frac{x}{a}\right)\right]$$
$$- j\cos(\psi)\cos\left(\pi\frac{x}{a}\right) dx'' \, dy'' \tag{3.12}$$

The solution of the above mentioned equation is given as

$$\frac{V_m}{jw} \int_{-l}^{l} \int_{-w/2}^{w/2} e^{-j\beta_{10}z} V_m \sin\left[k\left(l - z''\right)\right] \left[\frac{\beta_{10}}{\frac{\pi}{a}} \sin\left(\psi\right) \left(e^{j\pi\frac{x}{a}} - e^{-j\pi\frac{x}{a}}\right)\right]$$
$$+ \cos(\psi) \left[e^{j\pi\frac{x}{a}} - e^{-j\pi\frac{x}{a}}\right] dx'' \, dy'' \tag{3.13}$$

By transforming relative coordinate system to fundamental coordinate system (x, y, z)

$$x = z'' \sin(\psi) + x'' \cos(\psi) + x_1 \text{ and } z = z'' \cos(\psi) + x'' \sin(\psi) \tag{3.14}$$

Substituting Eq. (3.14) in Eq. (3.13) and simplifying

$$\frac{V_m}{2jw} \int_{-l}^{l} \int_{-w/2}^{w/2} e^{-j\beta_{10}z} V_m \sin[k(l - z'')] \left[\frac{\beta_{10}}{\frac{\pi}{a}} \sin(\psi) j \left(e^{jz''C}.e^{jx''A} + e^{jz''D}.e^{jx''B}\right)\right]$$
$$+ \cos(\psi) j \left[e^{jz''C}.e^{jx''A} - e^{jz''C}.e^{jx''A}\right] dx'' \, dy''$$
$$\tag{3.15}$$

where

$$A = \frac{\pi}{a} \sin(\psi) - \beta_{10} \cos(\psi) \tag{3.16}$$

$$B = \frac{\pi}{a} \cos(\psi) + \beta_{10} \sin(\psi) \tag{3.17}$$

$$C = \frac{\pi}{a} \sin(\psi) + \beta_{10} \cos(\psi) \tag{3.18}$$

and

$$A = \frac{\pi}{a} \sin(\psi) + \beta_{10} \cos(\psi) \tag{3.19}$$

3.3 Introduction to Array Synthesis

Before designing a slot array for $\sum$ and Δ pattern characterization, there is a need to synthesize it. For this purpose, the design is divided into two parts: the first synthesis is done by using Bayliss distribution to generate Δ pattern of a 2×5 slot array antenna [68], while the second synthesis is done for $\sum$ pattern of 2×4 center inclined slot array antenna using Taylor distribution. Two side by side X-band waveguides are used for both the cases with top plate thickness
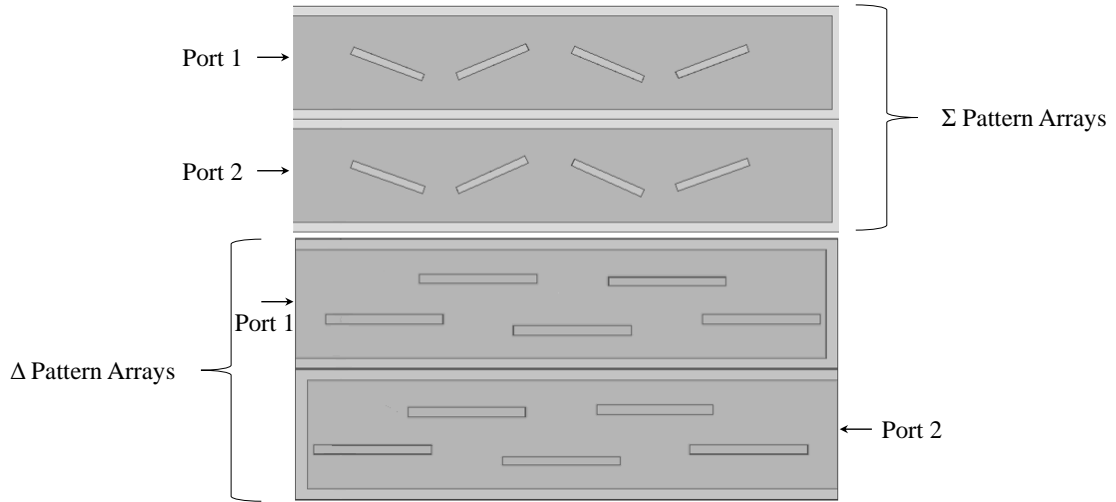
FIGURE 3.4: Design of the proposed waveguide slotted array.

of 2 mm as shown in Fig. 3.4. The Δ pattern array is synthesized with 10 number of elements for 30/30 dB SLL criteria. To find the slot off-sets form the center, line source distribution is used. For simulation purposes, Δ pattern linear array is decomposed into two parallel X-band waveguides with opposite excitation polarities. In $\sum$ pattern linear array, 8 slot elements are considered with in-phase excitation for both parallel waveguides as shown in Fig. 3.4.

The synthesis process starts with the generation of Δ pattern array. One can find the continuous line source distribution that will generate symmetric pattern by placing the null at $u = 0(|u| < 1)$ and main beam on either sides. The generic expression for the calculation of Δ pattern is given as [68]

$$D(u) = \pi u \cos(\pi u) \frac{\prod_{n=1}^{n^*=1} \left(1 - \frac{u^2}{u_n{}^2} \right)}{\prod_{n=1}^{n^*=1} \left(1 - \frac{u^2}{\left(n + \frac{1}{2} \right)^2} \right)} \tag{3.20}$$

where u is the range variable and it must be less. In order to achieve desired radiation characteristics, below mentioned equation can be utilized.

$$f(w) = (w - 1) \prod_{n=1}^{n=4} (w^2 + 2w \cos(\psi_n) + 1) \tag{3.21}$$

where ψ is the angle of roots on the Shelkunoff unit circle.

The corresponding current distributions for Δ pattern can be found by multiplying a constant factor with Eq. (3.21). The current distribution for positive and negative excitations are found and second order curve fitting is applied as shown in Fig. 3.5. It has been described that for $\sum$ pattern, Taylor distribution was used [68]. Equation (3.22) shows a general array factor expression for $\sum$ pattern.

$$S(\theta) = \int_{-a}^{a} g(\zeta)e^{jk\zeta\cos(\theta)}d\zeta \tag{3.22}$$

where $g(\zeta)$ is the aperture distribution with uniform amplitude and progressive phase. By considering $g(\zeta) = ke^{-j\beta\zeta}$ where k and β are constants, then the pattern Eq. (3.22) can be written as [68].

$$S(\theta) = 2ka\frac{\sin\left(ka(\cos(\theta) - \beta/k)\right)}{ka(\cos(\theta) - \beta/k)} \tag{3.23}$$

The universal power pattern can be generated using relation Eq. (3.23). By applying the conditions for discretization of linear array, one can write range variable as

$$u = \frac{2a}{\lambda}\left[\cos(\theta) - \frac{\beta}{k}\right] \tag{3.24}$$

By using Eq. (3.23) and (3.24), one can have the relation for controllable null positions. So, the $\sum$ pattern can be expressed as

$$S(u) = \frac{\sin\pi u}{\pi u}\frac{\prod_{n=1}^{n^*}\left(1 - \frac{u^2}{u_n{}^2}\right)}{\prod_{n=1}^{n^*}\left(1 - \frac{u^2}{u_n}\right)} \tag{3.25}$$

The current distribution for positive and negative excitations can be calculated as [68]

$$\frac{1}{2R_{slot}}v_n^2 = \frac{1}{2}I_nR_D \tag{3.26}$$

where R_{slot} and R_D represent radiation resistance of slot in ground plane and short dipole, respectively; v_n is the slot voltage, and may change with the slot off-set as
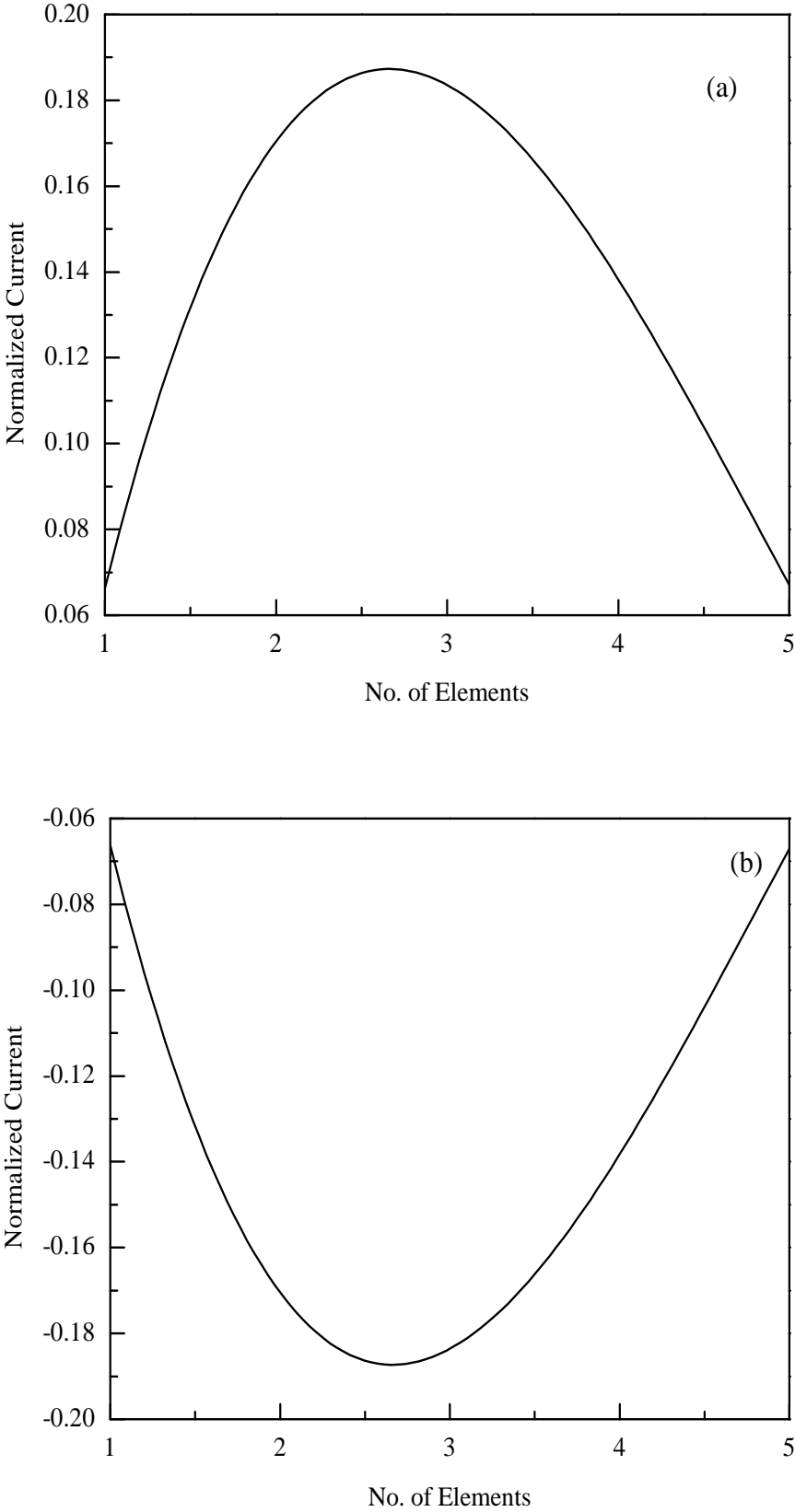
FIGURE 3.5: Δ pattern element current distribution for (a) positive and (b) negative excitations.

fields in waveguide changes. The relation for conductance of nth element related to corresponding n^{th} normalized current is given as

$$G_n = KI_{nd} \qquad (3.27)$$

To find constant K, one can need normalized conductance of slot, which can be calculated from below mentioned expression.

$$G_0 = \frac{1}{Z_{TE_{10}}} \qquad (3.28)$$

From the Stevenson theory of slot, the normalized conductance can also be written as

$$\frac{G}{G_0} = \left[2.09 \frac{(a/b)}{\beta_{10}/k} \cos^2 \left(\frac{\beta_{10}\pi}{2k} \right) \right] \sin^2 \left(\frac{\pi x}{a} \right) \qquad (3.29)$$

one can write Eq. (3.28) and (3.29) as

$$\frac{G_n}{G_0} = a \sin^2 \left(\frac{\pi x_n}{a} \right) \qquad (3.30)$$

It can be observed from the Eq. (3.30) that normalized conduction of slot must be proportional to constant times the square of sin function. The off-set from the center of waveguide can be calculated as [68]

$$x_n = \frac{a \sin^{-1} \left(\sqrt{\frac{G_n}{aG_0}} \right)}{\pi} \qquad (3.31)$$

The off-sets from the center of a waveguide are being modeled with shunt resistance and tilted slot elements are modeled as series elements [17].

3.4 Design Procedure

An air filled X-band rectangular waveguide of dimensions a and b are used with N number of slots. The slots are uniformly spaced at $\lambda_g/2$ in both the cases, where λ_g is the guided wavelength for TE_{10} mode. The first slot element for Δ pattern

array is at $\lambda_g/4$, while for $\sum$ pattern array, it is located at $1.5\lambda_g$ distance from stating edge of waveguide. For $\sum$ pattern array, 4 center off-set slots are designed on the top side of each waveguide as shown in Fig. 3.4. For Δ pattern array, five number of center inclined slots are designed on each waveguide.

The non-resonant length of slot radiators for Δ pattern array is 16 mm. The slot off-sets for Δ pattern array are shown in Fig. 3.6 for both positive and negative excitations, respectively. The side-by-side Δ pattern arrays are excited with phase $1\angle 0°$ and $1\angle 180°$, while $\sum$ pattern array is excited with in-phase input [68]. In Fig. 3.7, the whole design process is summarized. In general, two type of arrays have been synthesized with Taylor and Bayliss distribution, and by using these distributions, physical parameters are extracted to simulate the whole array.

3.5   Simulation Results

The proposed design, shown in Fig. 3.4, is simulated in full wave EM simulator named Ansys HFSS. The Δ and $\sum$ pattern arrays are simulated with opposite and in-phase excitations, respectively. The inter-element spacing in Δ pattern array is about $0.7\lambda_g$ [17, 75]. If inter-element spacing will increase from $0.7\lambda_g$, principle null will lose its depth, which can cause disturbance in radiation pattern and consequently, the accuracy of target tracking will be compromised. To fix the directivity of twin beams, the inter-element spacing must be greater than half of the guided wavelength $\geq \lambda_g/2$. The off-sets of slot elements in two side-by-side waveguides are inverse to each other in order to generate Δ pattern. The considered slot array can be taken as the sub part of planar array as shown in Fig. 3.6.

The VSWR of $\sum$ and Δ arrays are shown in Fig. 3.8. From the figure, one can observe that the VSWR of both the arrays falls within the acceptable range (<2) for the band of interest. From the figure, one can also observe that the impedance bandwidth of $\sum$ pattern array is $\approx$250 MHz (9.2-9.45 GHz), while for Δ pattern array, the impedance bandwidth is equal to $\approx$550 MHz (8.9-9.45 GHz).
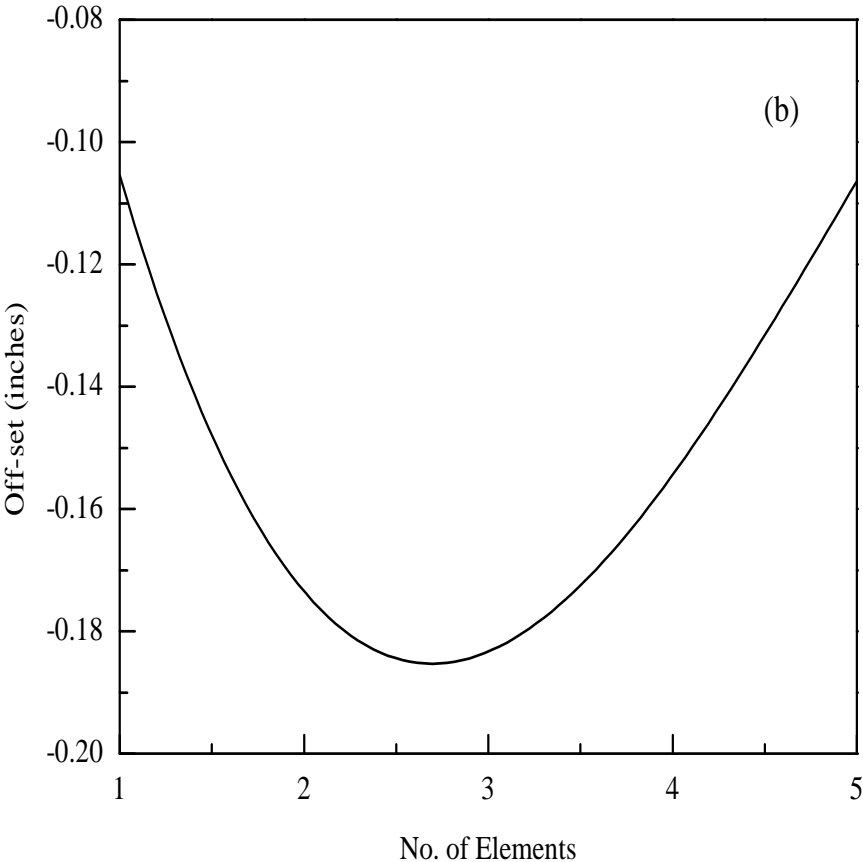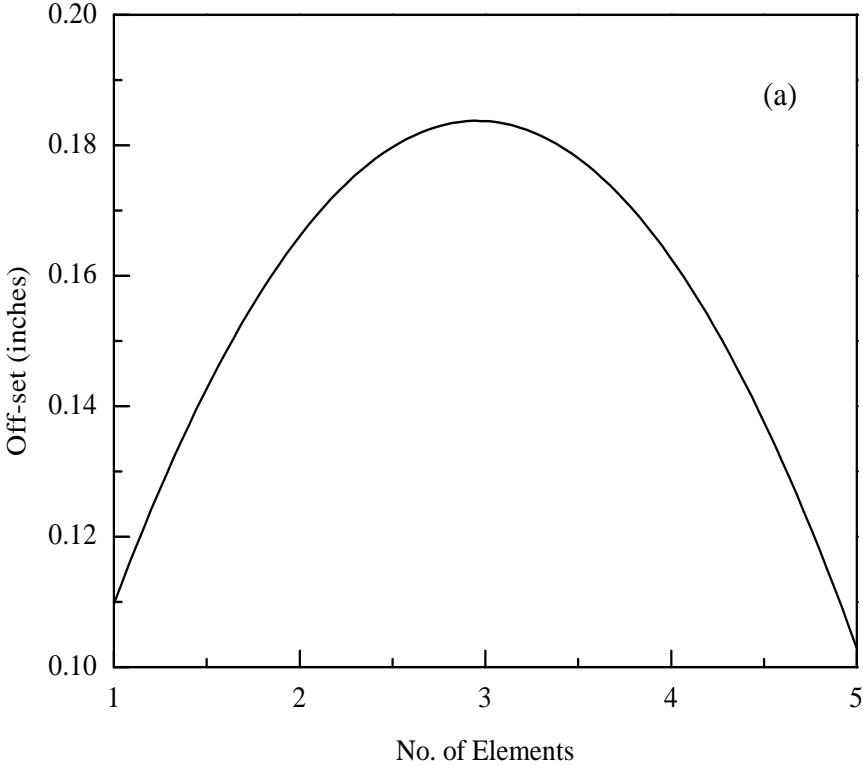
FIGURE 3.6: Δ pattern slot off-sets for (a) positive and (b) negative excitations.
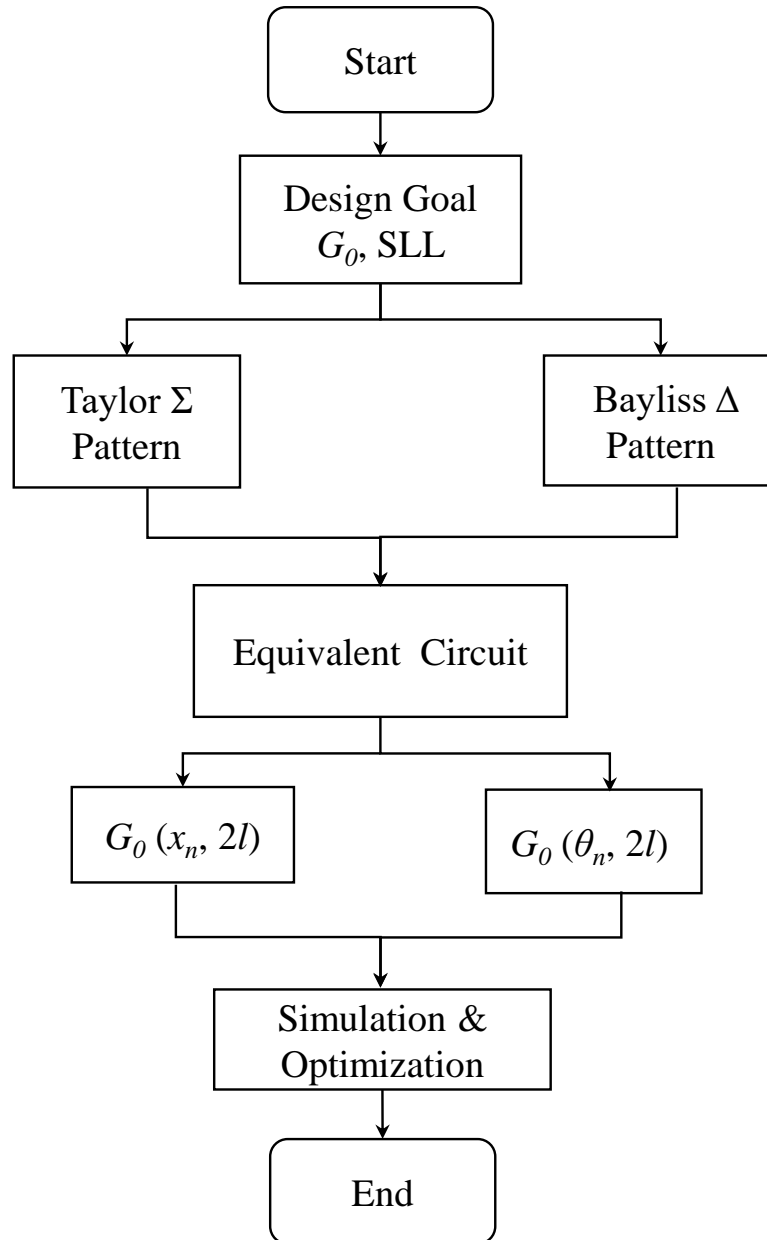
FIGURE 3.7: Flow process for the design of $\sum$ and Δ pattern arrays.

The simulated isolation, S_{21} between the ports of proposed arrays is illustrated in Fig. 3.9. From the figure it is observed that the isolation between the ports for $\sum$ and Δ pattern arrays is less than 15 dB.

The simulated H-plane radiation characteristics of proposed $\sum$ and Δ pattern arrays are shown in Fig. 3.10. A gain of 11.75 dBi with SLL of -8 dB has been observed for $\sum$ pattern array whereas, the Δ pattern array has -25 dB depth of principle null with SLL of -23 dB. The Δ pattern array has two main beams
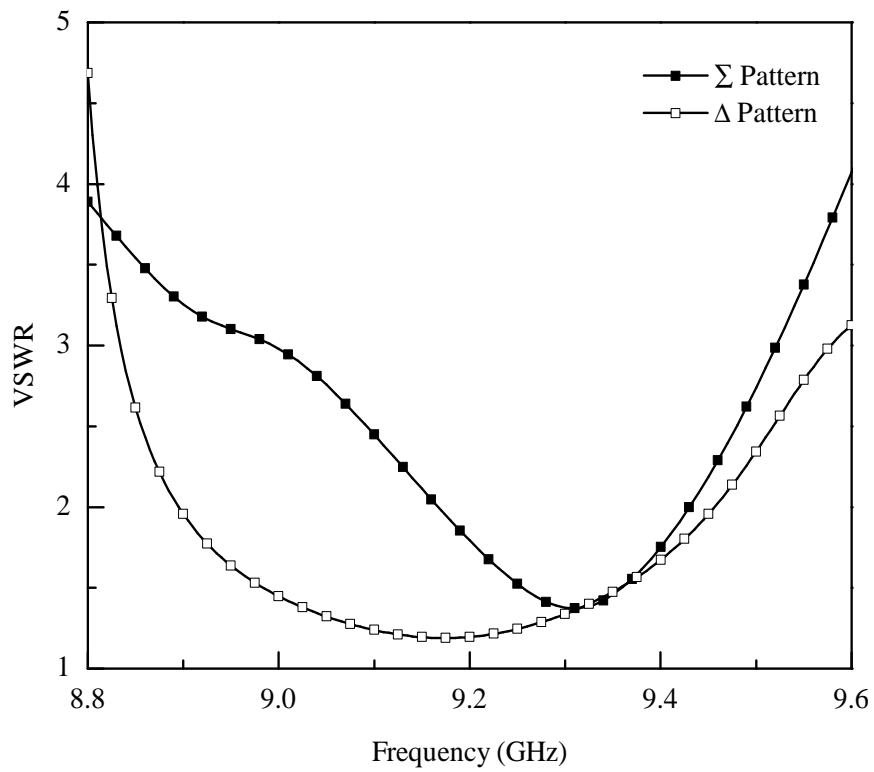
FIGURE 3.8: VSWR of $\sum$ and Δ pattern arrays.
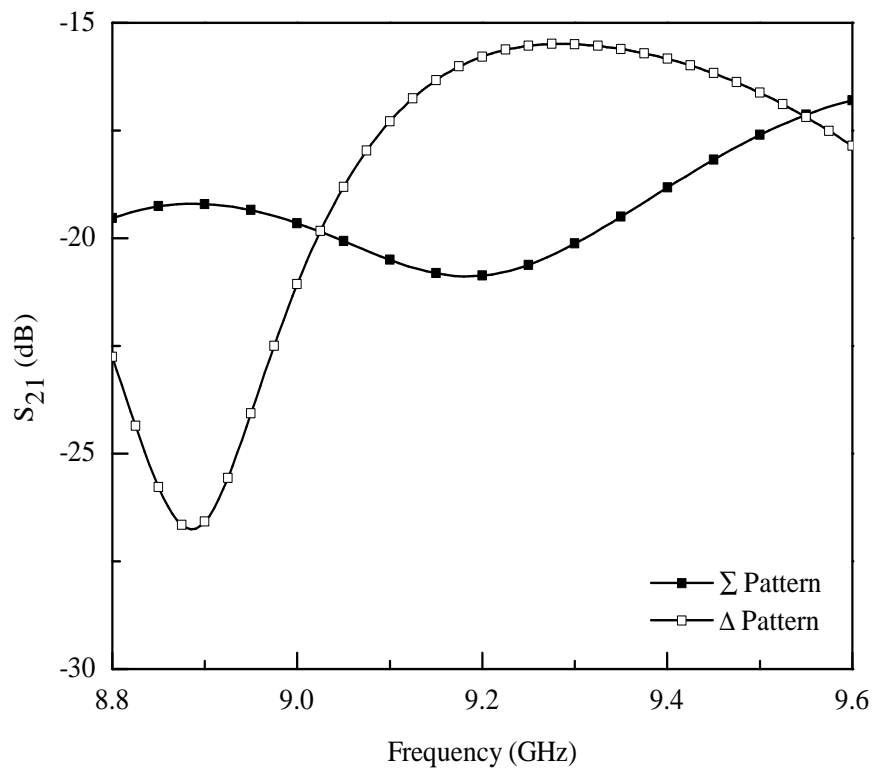
FIGURE 3.9: Isolation between ports of $\sum$ and Δ pattern arrays.

approximately at $\pm 50°$, which proves the concept of tracking applications.
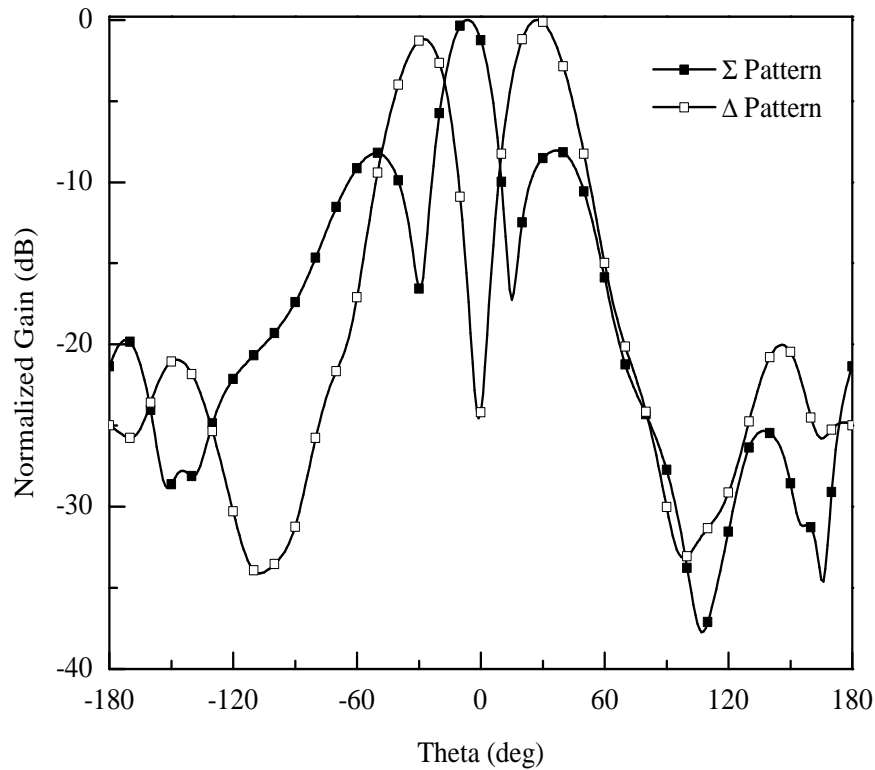
FIGURE 3.10: Normalized gain of the proposed slot array for $\sum$ and Δ patterns.

3.6   Summary

This chapter presents the design and simulation of $\sum$ and Δ pattern waveguide fed slot array antenna for tracking applications. The design process is based on classical theory of slot and each array is decomposed into two sub-arrays. The Δ pattern array is excited from alternate edges of sub-array with opposite polarities, while $\sum$ pattern array has in-phase excitation. The proposed design is simulated in Ansys HFSS and results show quite good agreement with the theory. The SLL in Δ pattern array is -23 dB and the gain of array is 8 dB. The main beams have principle null at center of power pattern. The simulated gain of $\sum$ pattern array is 11.75 dBi with SLL of -8 dB. VSWR for both the cases is 2.6 and 1.6, respectively.

Chapter 4

Design of Slot Array Antenna Using Particle Swarm Optimization

4.1 Introduction

In most of the wireless communication systems, directional antenna arrays are required with high gain, directivity, and spatial diversity. For this purpose, the synthesis of arrays has received much importance in the recent past, where various performance goals were considered. For array synthesis, different optimization algorithms, e.g. Simulated Annealing [76], Ant-Colony optimization [77] and PSO [78] have been used in the previous studies. Additionally, the optimization of linear antenna array provides a pattern that has minimum SLL and HPBW, i.e. by using PSO and GA [78–80]. In [81, 82], a Composite Differential Evaluation (CoDE) algorithm has been applied to optimize inter-element spacing between two consecutive elements to minimize SLL and to place nulls in the desired direction.

A multi-objective optimization approach has been used in Ref. [83, 84] to maximize the directivity and to minimize SLL of an antenna array. In [83], the authors introduced a new technique memetic multi-objective evolutionary algorithm called

Memetic Generalized Differential Evaluation (MGDE3) algorithm, which is the extension of Generalized Differential Evaluation (GDE3) algorithm. In [85], the authors introduced a new technique for realizing the characteristics and performance of the non-uniform linear array. The presented technique utilized multi-objective functions to optimize inter-element spacing, excitation currents, and excitation phases as well as to minimize SLL and HPBW. Real-coded genetic is employed for time modulating linear antenna array to impose nulls in the desired direction by optimizing inter-element spacing and excitation amplitude. The main purpose of optimization is to introduce an algorithm that provides maximum directivity, minimum SLL, HPBW, and have fast convergence.

In this chapter, two design examples are presented for a slot array antenna to generate $\sum$ pattern for tracking radar applications. The antenna array of 1×6 slot elements (in one branch) has been synthesized using PSO. Two fitness functions are utilized: one function is defined to place nulls in the desired direction by optimizing excitation amplitude, and another one is defined to get minimum SLL and HPBW. After that, the optimized antenna array has been designed and simulated in Ansys HFSS. Three different slot arrays are designed and fed using an RWG that has three inclined slot elements. The simulation results show that the gain for $\sum$ pattern is 16.84 dBi and SLL is -18.59 dB.

4.2   PSO Algorithm

In PSO algorithm, every individual in swarm refers to as a particle. All particles move in search of space and update their velocity according to their best position. PSO is a computational method, which iteratively optimizes the problem using a certain fitness function. Since, we are dealing with both uniform and non-uniform linear antenna arrays, so each particle is considered as a vector, which contains the information for each antenna; such as excitation amplitude, $|a|$, excitation phase, $|\phi|$ and inter-element spacing, d in the array. Therefore, PSO algorithm can be summarized as:

i. Generate random d_i , a_i and ϕ_i, where $x_i = [d_i \ |a_i| \ \phi_i]$ and range for $|a|$, $|\phi|$ and d is [0, 1], [0°, 360°], $[d_{max}, d_{min}]$, respectively

ii. Initialize individual particle velocities:

$$v_{i,d} = U(-|d_{max} - d_{min}|, |d_{max} - d_{min}|)$$
$$v_{i,|a|} = U(-|a_{max} - a_{min}|, |a_{max} - a_{min}|)$$
$$v_{i,\phi} = U(-|\phi_{max} - \phi_{min}|, |\phi_{max} - \phi_{min}|)$$

iii. Computer fitness function for each particle.

iv. Compute particles best position (p_i) and global best position (g) such that $f(p_i) < f(g)$.

After the initialization phase, the optimization steps are as follows:

i. For each particle $i = 1, \cdots, S$.

ii. Pick uniformly distributed random numbers for local best, r_p and global best position, r_g.

iii. Update the velocity for each dimension:

$$v_{i,d} = \beta v_{i,d} + \alpha_p r_p (p_{i,d} - x_{i,d}) + \alpha_g r_g (g_d - x_{i,d})$$
$$v_{i,|a|} = \beta v_{i,|a|} + \alpha_p r_p (p_{i,|a|} - x_{i,|a|}) + \alpha_g r_g (g_a - x_{i,|a|})$$
$$v_{i,\angle a} = \beta v_{i,\angle a} + \alpha_p r_p (p_{i,\angle a} - x_{i,\angle a}) + \alpha_g r_g (g_{\angle a} - x_{i,\angle a})$$

where $\beta = 1, \alpha_p = 0.9$ and $\alpha_g = 0.9$.

After updating the velocity, this algorithm will repeat till certain termination criteria.

4.3 Synthesis of Linear Antenna Array Using PSO

In this section, PSO algorithm is employed to linear antenna array to get minimum SLL and HPBW. Three design examples for $N = 10$, 12 and 16 are presented here,

where N corresponds to the number of elements, and obtained results are compared with previously published data. It is described previously that to achieve desired goals and fast convergence, PSO algorithm requires an appropriate fitness function. For our proposed application, two fitness functions are designed, which are given below

$$f_1 = \begin{cases} \min(\text{HPBW}) - \min(\text{SLL}), \\ \text{if } \min(\text{SLL}) \leq A_0 \quad \& \quad \min(\text{HPBW}) \leq B_0 \\ (\min(\text{HPBW}) - A_0) - (\max(\text{SLL}) - B_0), \quad \text{else} \end{cases} \tag{4.1}$$

$$f_2 = \max(\text{AF}_1(\theta_d)) \quad \text{where} \quad \text{AF}_1 = |\text{AF}|^2 \tag{4.2}$$

where A_0 and B_0 are the fixed values of HPBW and SLL that keep the SLL and HPBW below A_0 and B_0. θ_d is the angle at which null can be controlled.

From above mentioned expressions, it can be observed that fitness function, f_1 is employed to minimize SLL and HPBW, while second function, f_2 is used to control the nulls in the specific direction by optimizing excitation amplitude. The excitation amplitude is also known as the weighting factor, which also changes the characteristics of the antenna array.

The PSO algorithm is applied on 10, 12, and 16 elements array. The excitation amplitude is optimized, while the inter-element spacing and excitation phase is fixed. The inter-element spacing between two adjacent antenna elements is $\lambda_0/2$, and excitation phase for each element is at $90°$. The excitation amplitude assumed to be within the range $(0, 1)$. For uniform inter-element spacing and excitation phase, for $N = 10$, the proposed PSO algorithm provides a SLL of -17.26 dB with HPBW of $11°$ as shown in Fig. 4.1. For $N = 12$ and 16, shown in Fig. 4.1, the SLL is further reduced to -24.14 dB and -28.05 dB, respectively; while HPBW is minimized to $9°$ and $7°$, respectively. Table 4.1 shows a comparative analysis between proposed and previously presented antenna arrays. From the data of the table, it is observed that for $N = 10$, there is a 1.29 dB improvement in SLL using proposed algorithm compared to BBO [86, 87]. And for $N = 16$, there is a 11.98 dB improvement in SLL compared to GA [88].
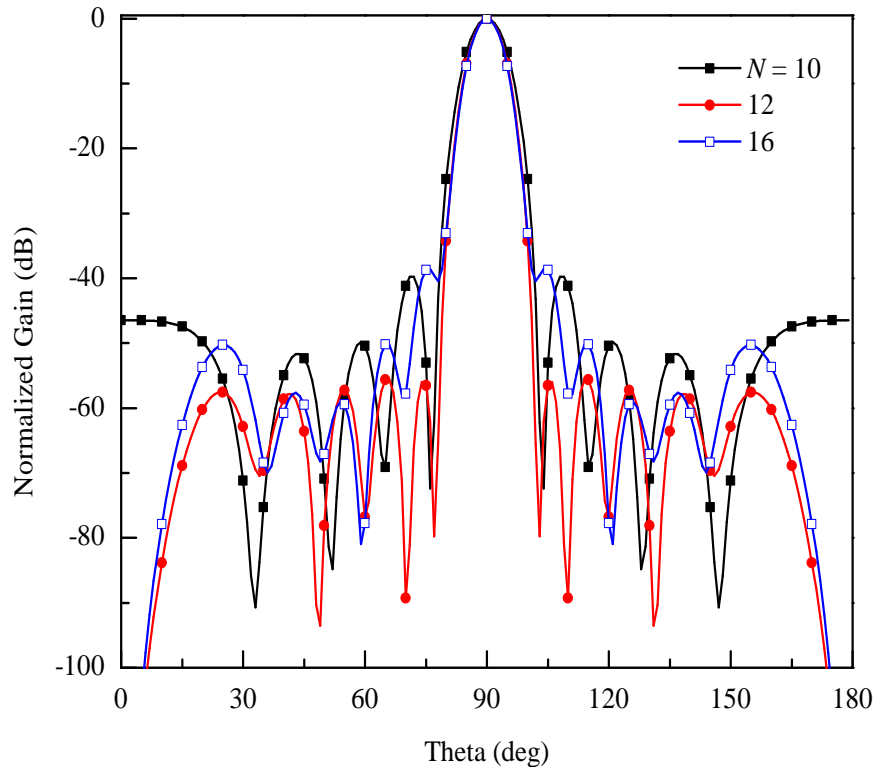
FIGURE 4.1: Array factor as a function of elevation angle (θ) and number of elements (N) in a linear array using PSO.

TABLE 4.1: Comparison of proposed and previously presented algorithms for linear antenna array optimization.

Parameters	Proposed			[86]	[87]	[88]
N	10	12	16	10	10	16
SLL (dB)	-17.26	-24.14	-28.05	-15.97	-15.93	-16.07
HPBW	11°	9°	7°	–	–	–

4.4 Slot Array Design Using PSO

In this section, the synthesis of $\sum$ pattern for 1×6 elements based slotted array has been carried using PSO. Equation (4.1) is used to find optimum antenna element's excitation amplitude, while the inter elements spacing remained fixed at $\lambda_0/2$ (in waveguide $\lambda_g/2$). On the other hand, the excitation phase is 0°, and the excitation currents are normalized to $0 < I_n < 1$.

Once the excitation amplitude of each element is optimized, then Elliot design procedure is applied to find design parameters of slot element. For this purpose, a
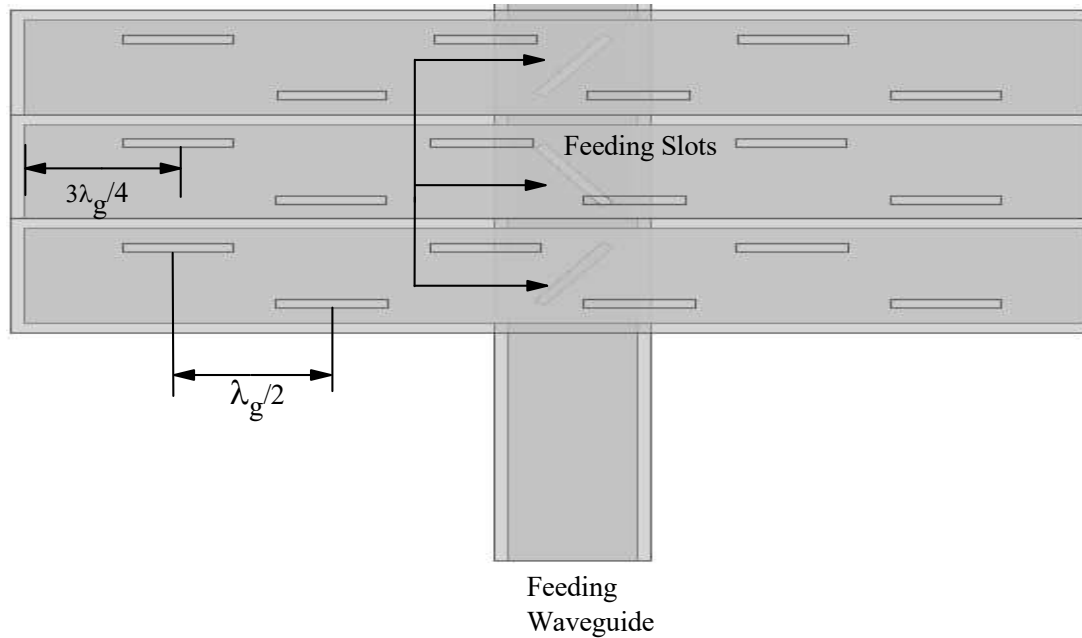
FIGURE 4.2: Design of the proposed waveguide slotted array.

MATHCAD code has been developed. First, there is a need to determine slot conductance. Equation (4.3) shows the sum of slot conductance as Elliot's standard design procedure [74].

$$G_0 = \sum_{n=1}^{N} g_n \tag{4.3}$$

In general, slot impedance has only real part, which means no phase variation therefore, Eq. (4.3) can be written as [74]

$$\sum_{n=1}^{N} \text{real}(g_n) = G_0 \tag{4.4}$$

which leads to

$$\text{real}(X_n) = \tilde{X} \tag{4.5}$$

Equation (4.5) is used to find slot off-sets during simulation process keeping in mind that the value of slot off-sets should be $< \lambda_0/4$.

In order to validate PSO based design, a rectangular waveguide is designed with dimensions a and b. For $\sum$ pattern, three different slot antenna arrays have been designed with six number of slot elements as shown in Fig. 4.2. Two design example are simulated in Ansys HFSS to verify PSO based current distribution.
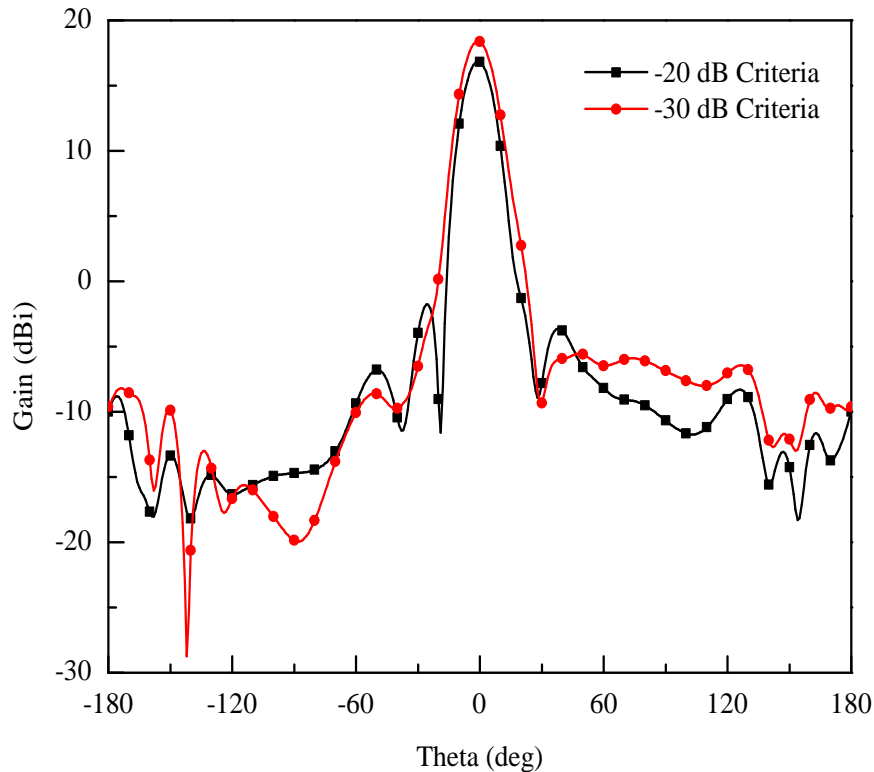
FIGURE 4.3: Simulated H-plane radiation characteristics of the proposed slot array antenna for the presented cases.

In the first case, -20 dB SLL design goal is simulated with slot off-sets obtained using Eq. 4.5. As mentioned earlier, six slot elements are employed in each array and all the arrays are fed using a waveguide. The feeding waveguide has three inclined coupling slots having length of 15.12 mm. Each array has uniform inter-element spacing ($\lambda_g/2$) and it is short circuited at $3\lambda_g/4$ as shown in Fig. 4.2. The center to center distance of arrays is 21 mm.

Figure 4.3 shows H-plane radiation characteristics for the first case (-20 dB SLL design goal). It can be observed from the result of Fig. 4.3 that a SLL of -18.61 dB has been achieved with a gain of 16.84 dBi. Moreover, the main beam is located at 0° and the nulls are located at -20° and 30°.

As a second case, the designed slotted array, shown in Fig. 4.2, has been simulated for -30 dB SLL design criteria and the results are shown in Fig. 4.3. From the figure, it is observed that for second case, the slotted array provides SLL of -26.99 dB and gain of 18.51 dBi. Furthermore, the first null is located at -41°, while the second null is located at 30°.

The comparison of both the cases is also given in Table 4.2. From the data of the table, it can be noted that the results obtained from HFSS simulation are well in agreement with the results obtained using PSO algorithm, which validates our proposed design technique.

TABLE 4.2: Comparison between PSO based design and HFSS simulation.

Parameters	PSO		HFSS	
	Case 1	Case 2	Case 1	Case 2
SLL (dB)	-20	-30	-18.61	-26.99
Gain (dBi)	–	–	16.84	18.51

4.5 Summary

In this chapter, a slot array antenna has been designed using PSO. In the first part of this chapter, linear antenna arrays having $N = 10$, 12, and 16 have been optimized by using the PSO algorithm to get minimum SLL and HPBW. Two fitness functions are used to get the desired results. It has been observed from the results that the proposed algorithm offers better results than previously published data. In the second part, a slot array antenna has been designed and simulated for two cases: (1) -20 dB SLL criteria, and (2) -30 dB SLL criteria. The slot off-sets are calculated using Elliot's design equations and the array is synthesized using PSO. From the presented results, it has been noted that the proposed slot array antenna offered an SLL of -18.61 dB and -26.99 dB for the first and second case, respectively.

Chapter 5

Conformal Slot Array Antenna for Low Cost CubeSats

5.1 Introduction

In the modern era, CubeSats have become a new approach to explore space. Normally, CubeSats are smaller in size with high stowing efficiency, and have minimum development time with lower cost compared to traditional satellites. CubeSats are widely designed and tested by academia, space agencies, and industries at lower earth orbit for applications like earth imaging, and weather forecast applications, etc. Recently, a new trend has been introduced in the applications of CubeSats for deep space exploration missions, e.g. Lunar Ice Cube [89], Lunar Flashlight [90], and NEASCout, etc [91].

CubeSats are more affordable for deep space and remote sensing applications compared to conventionally used satellites but, the path loss is the biggest problem in CubeSats. To overcome path loss issues, the antenna system of CubeSats needs to be efficient. On the other hand, in satellite communication, it is preferred to use circularly polarized antennas but, the cost of transmitter and receiver will increase up to some extent. So, to reduce transceiver cost, a compact circularly polarized antenna was demonstrated for satellite communication at X-band with a gain of

10 dBi [92]. The presented antenna was based on a microstrip feed line with cross slot structure.

In this chapter, a design of an X-band rectangular conformal SIW based slot array antenna is presented. A novel feeding structure is used to excite the proposed array. It is observed that the proposed feeding structure is able to provide high gain with reduced SLL. From our proposed design, a gain of 11.15 dBi with an SLL of -19.62 dB is achieved. To our best knowledge, the SIW based slot array has never been used for CubeSat (U2) applications. One major benefit of adopting SIW for CubeSat is that SIW has the capability to handle high power, and it is easy to install on the surface of rectangular CubeSat. By using SIW based feeding structure, the Electromagnetic Compatibility (EMC) issues can be reduced in compact CubeSats.

The remaining composition of the chapter is that Section 5.2 presents the numerical proof for Axial Ratio (AR) for CubeSat applications. Section 5.3 describes the slot array design and proposed feeding structure along with simulation results. Finally, Section 5.4 provides the conclusion of the presented work.

5.2   Effect of Station-Keeping on Received Signal

Consider a U1 CubeSat at low earth orbit as shown in Fig. 5.1. The transmitted signal from CubeSat is denoted as P_t and received signal at ground station is represented as P_r. The plane wave received from the CubeSat at the ground station can be expressed as

$$E_r = E_{r0}(\widehat{x} \pm j\widehat{y})e^{-jk_0z} \tag{5.1}$$

By considering $E_{r0} = 1$, then Eq. (5.1) will deduced to

$$E_r = \frac{\widehat{x} \pm j\widehat{y}}{\sqrt{2}} \tag{5.2}$$
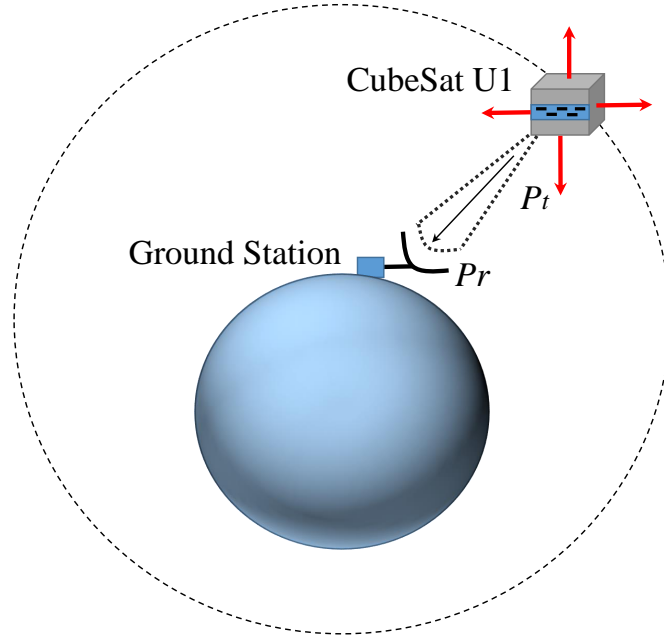
FIGURE 5.1: U1 CubeSat in lower earth orbit.

As the RHCP and Left Hand Circular Polarization (LHCP) have variations due to the station keeping effects so, it produces two unit vectors named $\widehat{a}_x$ and $\widehat{a}_y$ as shown in Fig. 5.1. Therefore, the variation in amplitude $\triangle E_0$ due to these unit vectors can be expressed as

$$E_r = \frac{E_{r0}\widehat{a}_x \pm j(E_{r0} + \triangle E_{r0})\widehat{a}_y}{\sqrt{E_{r0}^2 + (E_{r0} + \triangle E_{r0})^2}} \tag{5.3}$$

By resolving the square, Eq. (5.3) becomes

$$E_r = \frac{E_{r0}\widehat{a}_x \pm j(E_{r0} + \triangle E_{r0}/E_{r0})\widehat{a}_y}{E_{r0}\sqrt{2}} \tag{5.4}$$

It is a known fact the an elliptic polarization is a sum of RHCP and LHCP so, Eq. (5.4) becomes

$$E_r = \frac{\widehat{a}_x + j\widehat{a}_y}{\sqrt{2}}A + \frac{\widehat{a}_x - j\widehat{a}_y}{\sqrt{2}}B \tag{5.5}$$

By putting

$$A = 1 + \frac{\triangle E_{r0}}{2E_{r0}} \tag{5.6}$$

and

$$B = \frac{-\triangle E_{r0}}{2E_{r0}} \tag{5.7}$$

one can get

$$\frac{A}{B} = 1 + \frac{\left(\dfrac{\triangle E_{r0}}{2E_{ro}}\right)}{\left(\dfrac{-\triangle E_{r0}}{2E_{ro}}\right)} \tag{5.8}$$

$$\frac{A}{B} = \frac{-2E_{r0}}{\triangle E_{r0} - 1} \tag{5.9}$$

The required isolation between RHCP and LHCP is 30 dB therefore, the term on left hand side in Eq. (5.9) will be equal to 30 dB and it can be expressed as

$$30\text{dB} = 20\log\left|\frac{-2E_{r0}}{\triangle E_{r0} - 1}\right| \tag{5.10}$$

From the above equation, $E_{r0}/\triangle E_{r0} = 0.653$ and on its basis, AR can be expressed as

$$\text{AR} = \frac{E_{max}}{E_{min}} \tag{5.11}$$

$$\text{AR} = 1 + \frac{\triangle E_{r0}}{E_{r0}} \tag{5.12}$$

By putting the values in Eq. (5.12), AR = 1.653, which is the required AR for CubeSats communication.

5.3   Conformal Slot Array Antenna Design

The purpose of this work is to develop a concept of tracking array antenna conformed on the surface of U2 CubeSat. The slot array of 1×6 elements is projected on U2 CubeSat having dimensions 20×10×10 cm³. The design center frequency is 10 GHz and width of SIW, W is half of the free space wavelength ($\lambda_0/2$) to avoid grading lobes when array is conformed. The radius of metalized vias of SIW is 0.5 mm and separation between them is 0.9 mm. The array is synthesized using MLS algorithm with -20 dB SLL [93]. To design array in rectangular coordinates (x, y, z), the length of the array is increased in y-direction, width is along the x-axis and height is along z-axis as shown in Fig. 5.3. The elements are separated uniformly by a distance of $\lambda_g/2$ as shown in Fig. 5.4.
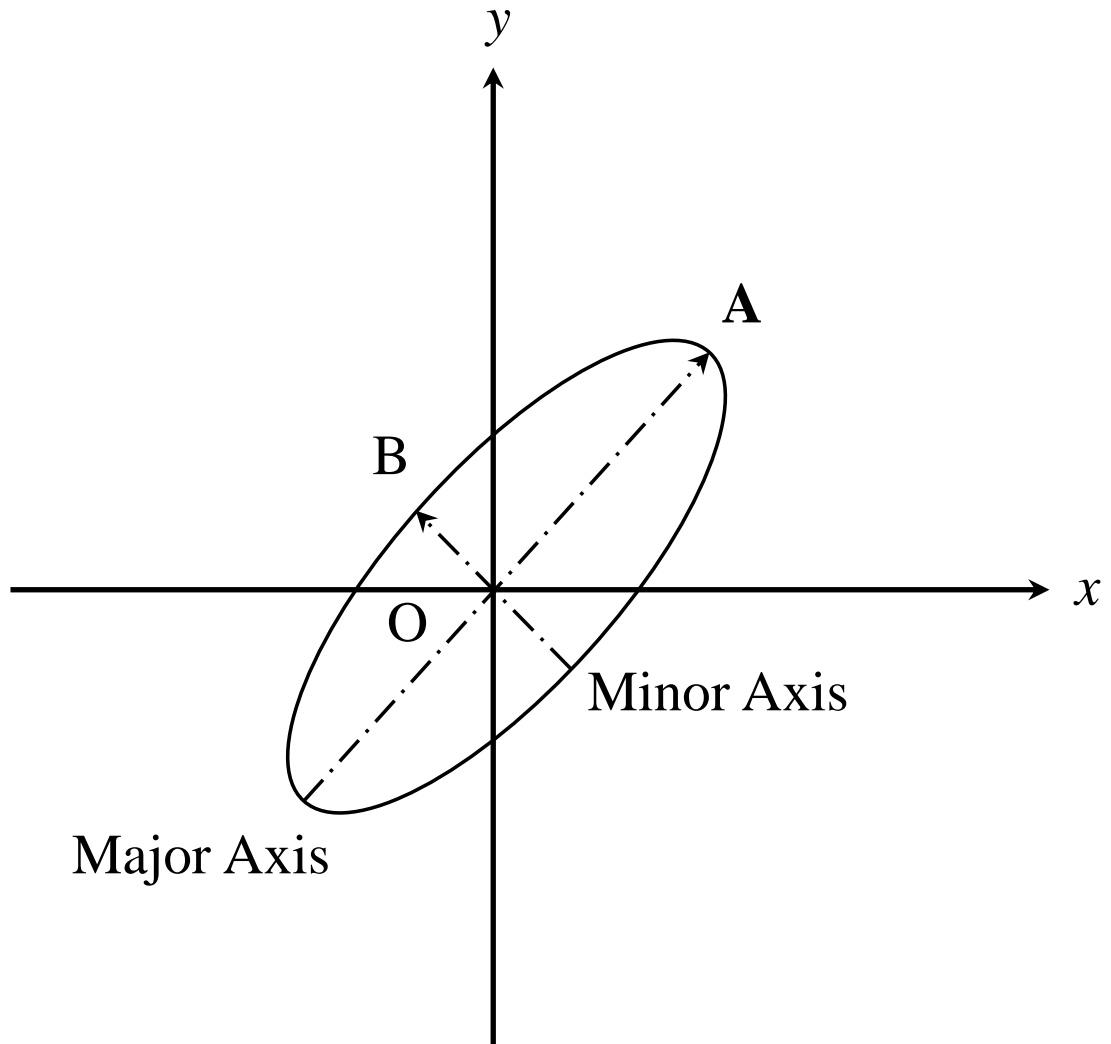
FIGURE 5.2: A graphical representation of elliptical polarization.
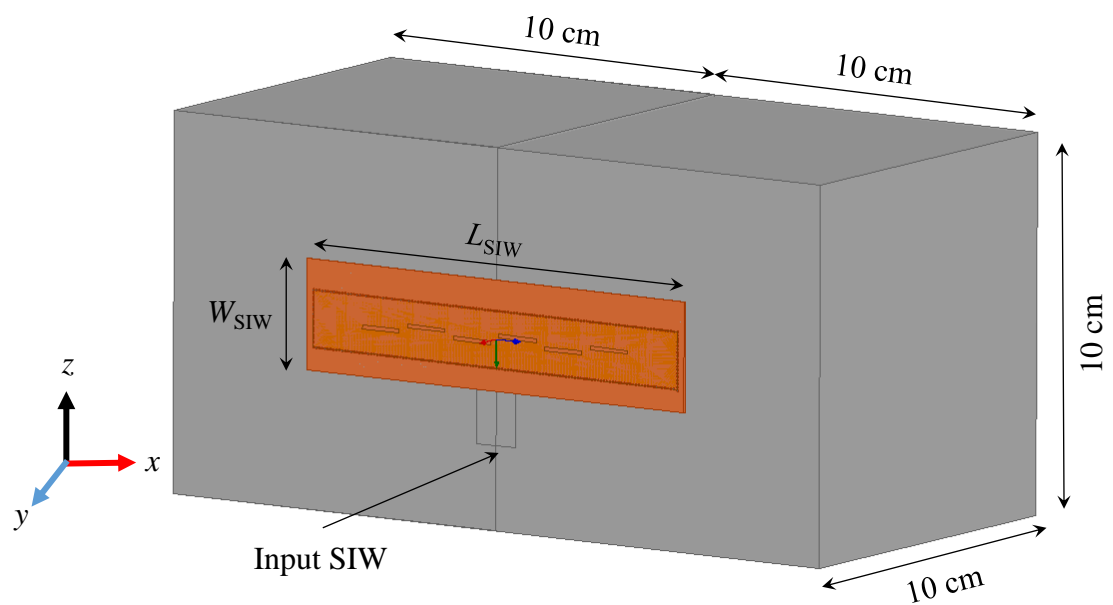
FIGURE 5.3: Geometry of U2 CubeSat with conformal slot array.
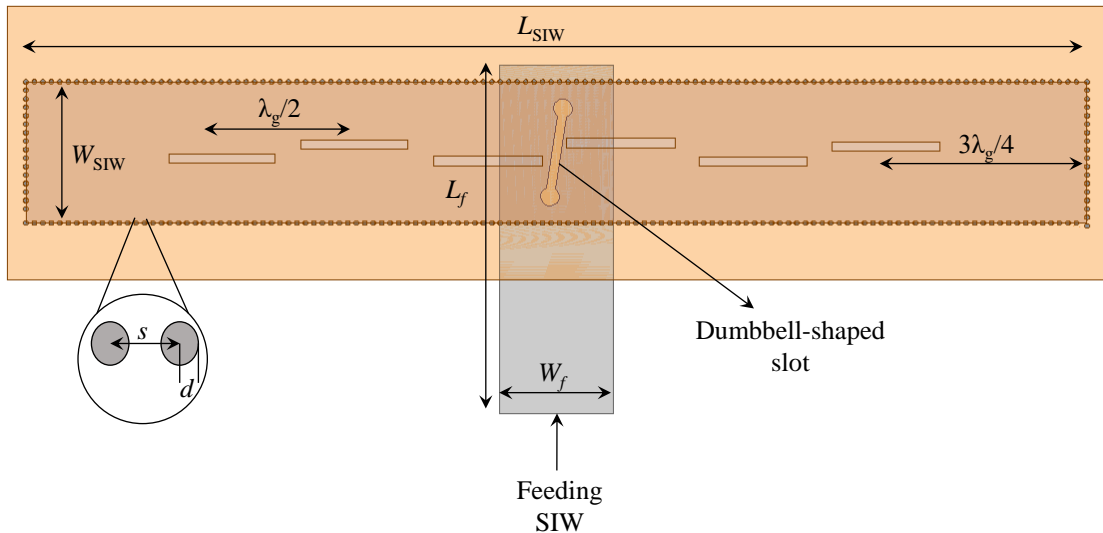
FIGURE 5.4: Proposed SIW slot array antenna with feeding structure and broadband dumbbell-shaped slot.

TABLE 5.1: Optimized design parameters of the proposed 1×6 slot array antenna.

Variables	Values
L_{SIW}	$5\lambda_g$
W_{SIW}	$\lambda_0/2$
d	0.5 mm
s	0.9 mm
W_f	12 mm
L_f	37 mm

The array is short-circuited at $3\lambda_g/4$ and fed using a dumbbell-shaped coupling slot on the lower side of slot array. The dumbbell-shaped slot has a length and width of 13.5 mm and 1 mm, respectively; and the radius of the edge circle is 2 mm. The coupling slot is rotated at an angle of 8.5° to get maximum power transfer to the radiating slots. The propagating wave of SIW feeding incidents on coupling slot that couples the energy to dielectric medium of upper SIW based slot array. It is observed that the coupling loss is not more than 0.5 dB. In Table 5.1, the complete set of variables of the proposed design is given.
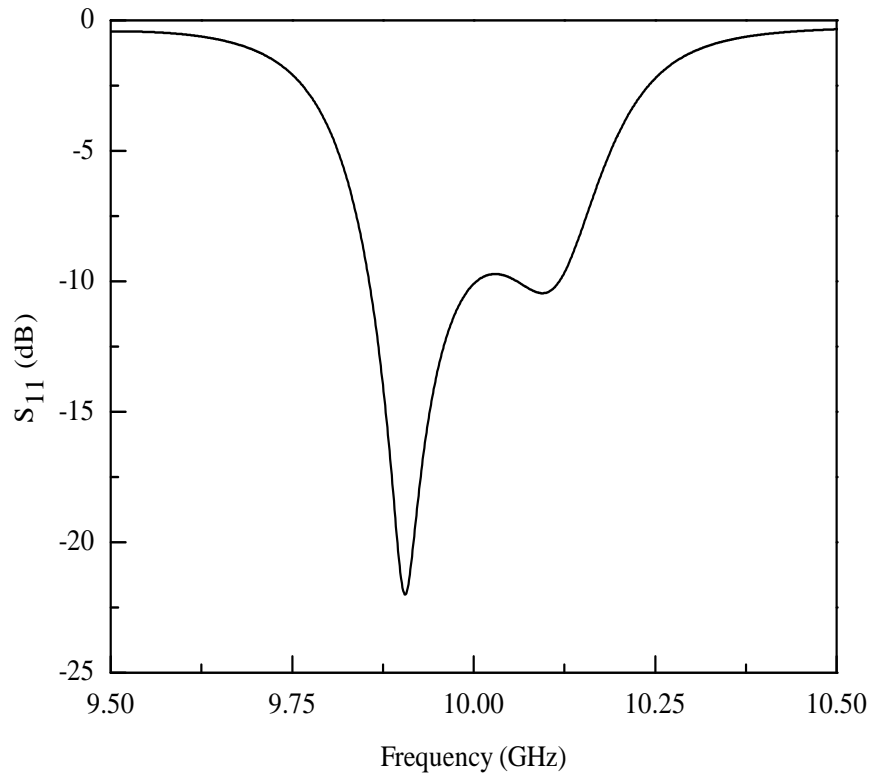
FIGURE 5.5: Simulated return loss S_{11} characteristics of the proposed slot array antenna.

5.4 Simulation Results and Discussion

The simulation of the proposed array is carried out in Ansys HFSS, a commerically available electromagnetic software. In Fig. 5.5, the return loss characteristics of the proposed array are illustrated. From the figure, it can be noted that the design array is performing well in the band of interest with an impedance 147 MHz from 9.856 to 10.003 GHz.

In Fig. 5.6, the normalized H-plane radiation pattern is illustrated. From the figure, it is observed that the proposed array offers SLL of -19.62 dB with a gain of 11.15 dBi. Furthermore, the proposed slot array antenna consists of one row of non-uniformly placed radiating slots therefore, the radiation characteristics in the E-plane are deteriorated, shown in Fig. 5.7, by the lateral size of an SIW slot array antenna.

The comparison between the proposed design and already existing antenna arrays are given in Table 5.2. From the data of the table, it is observed that the proposed
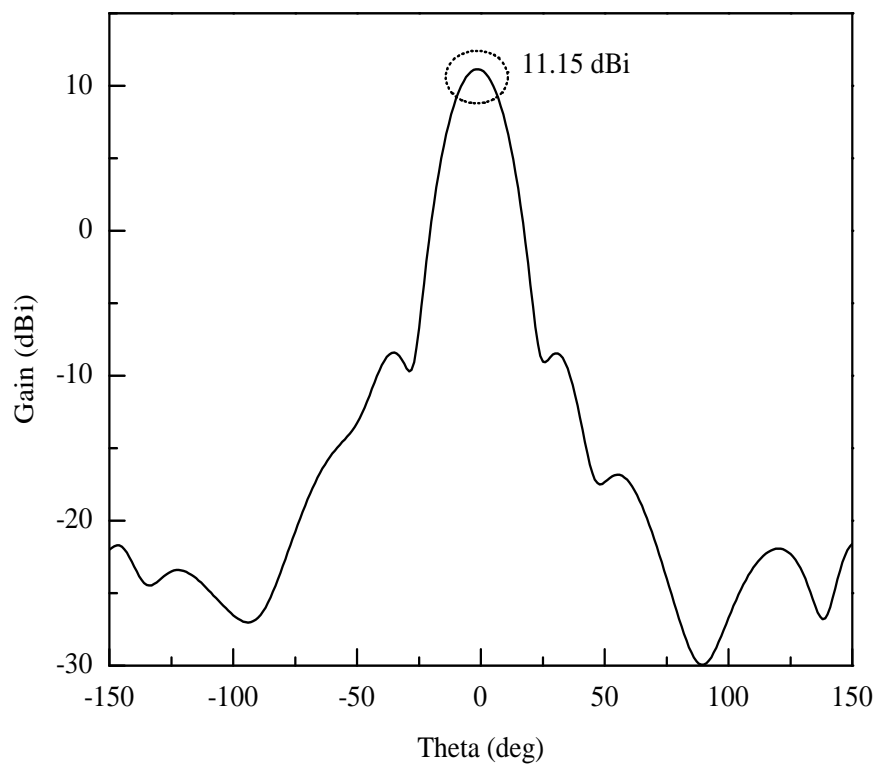
FIGURE 5.6: H-plane radiation pattern of the proposed slot array antenna.
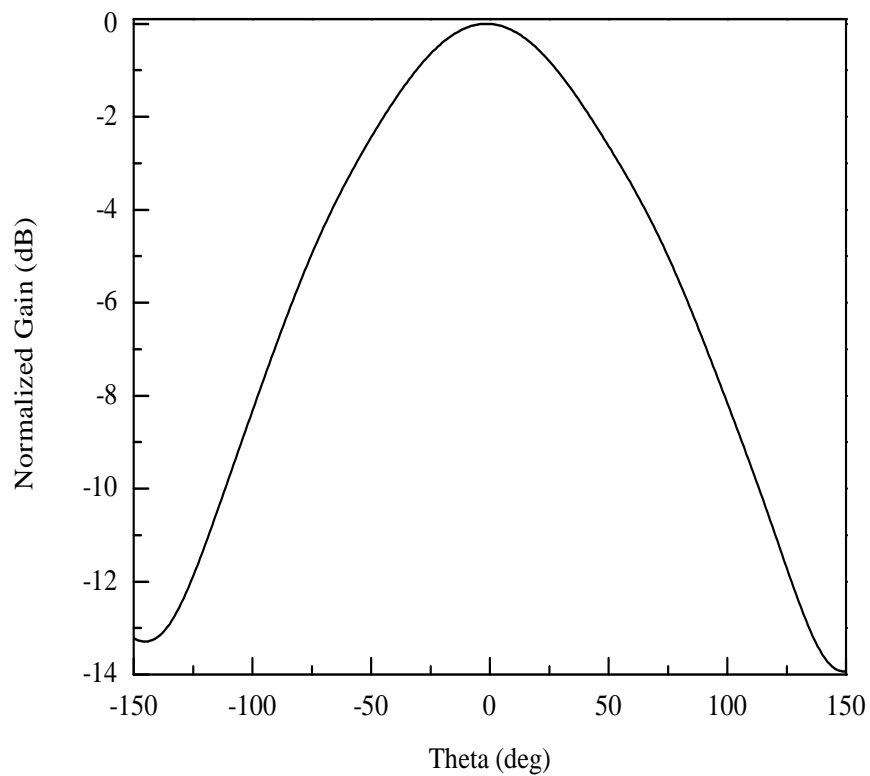
FIGURE 5.7: Normalized E-plane radiation pattern of the proposed slot array antenna.

TABLE 5.2: Comparison between proposed and previously presented antennas for CubeSat applications.

Ref.	Antenna Type	Frequency (GHz)	Gain (dBi)
[92]	Stacked patch	7.8	6.4−9.3
[94]	Patch	7.145−7.190	5
[95]	Inflatable	8.4	8
Proposed	SIW slot array	9.856−10.003	11.15

antenna array provides acceptable even with less number of slot elements. Therefore, the proposed conformal SIW slot array is a suitable candidate for CubeSat applications.

5.5 Summary

This chapter presents a design of low profile CubeSat conformal SIW slotted array with a dumbbell-shaped broadband feeding structure. To validate the propagation of a plane waves, the Axial Ratio for CubeSats is formulated. The array is synthesized using the MLS algorithm, and the design is simulated in Ansys HFSS. The observed SLL, H-plane gain, and VSWR are -19.62 dB, 11.15 dBi, and ≤ 2, respectively; at a center frequency of 10 GHz.

Chapter 6

Cylindrical Conformal Substrate Integrated Waveguide Slot Array Antenna

6.1 Introduction

Conformal antenna is an antenna that conforms to a certain predefined object or surface. A conformed shape can be a part of an aircraft, UAV or a bullet train. The perfect attachment of antenna arrays on the surface of earlier mentioned objects can be achieved by using flexible and low profile antennas [1]. In these particular applications, the printed microwave antennas with SIW technology are of ultimate choice. The reason to select SIW is to replace traditional microwave systems, which are non-planar and based on strip-lines [93, 96]. By adapting SIW technology, the waveguide structures can be synthesized in to planar structures and for this purpose, metalized via-holes are formed on dielectric substrate. One can also integrate the whole system on one substrate from passive circuits (filter, mixers and power divider) to active circuits (LO circuit and power amplifiers). Most of the conformal arrays discussed in the literature employed planar structures and few of them were based on SIW conformal slot arrays [34, 38].

In [40], traveling wave cylindrical conformal slot array was presented. The array consisted of 4×16 elements and it offered SLL of -11 dB and a gain of 14 dBi at center frequency of 25 GHz. However, SLL and gain were compromised as the array had 50Ω termination. In [97], Method of Moment (MoM) was used to determine RCS of conformal slotted array. An airborne conformal Vivaldi antenna array was reported at 400-800 MHz with Dolph-Chebyshev synthesis technique [98].

This chapter presents the design of a cylindrical conformal slot array with RWG to SIW feeding structure for X-band applications. The dimensions of the cylinder (r,R) are considered according to the desired applications such as fuselage of aircraft or missiles. The array is synthesized using the MLS algorithm and the simulations are carried out in Ansys HFSS. From simulations, an SLL of -21.72 dB and a gain of 9.8 dBi has been achieved. The center frequency of the slotted array is at 10 GHz and VSWR is ≤2.

6.2 Array Design Procedure

6.2.1 Characterization of Curved Surface

For the selection of cylinder's dimensions, a certain procedure is adopted, which is required for SIW on a curved surface as shown in the Fig. 6.1. The planar cross-section of SIW is converted into the sectoral waveguide as the substrate is conformed to a cylinder. The ultimate effect of this structural modification is expressed as the change in wave propagation constant, β. According to the fundamental slot theory [73], the excitation of TE_{10} mode in the waveguide is required and this condition must be true for SIW based slot array design [93]. A number of cylindrical SIW needs to be characterized to design slot array. One optimum selection of cylindrical radius can be chosen within the limits of $10\lambda_0$ and after ten free space wavelength, the effect of curvature is negligible. Therefore, the lower limit of $1.66\lambda_0$ is taken so that the design parameters should be extracted for worst case.
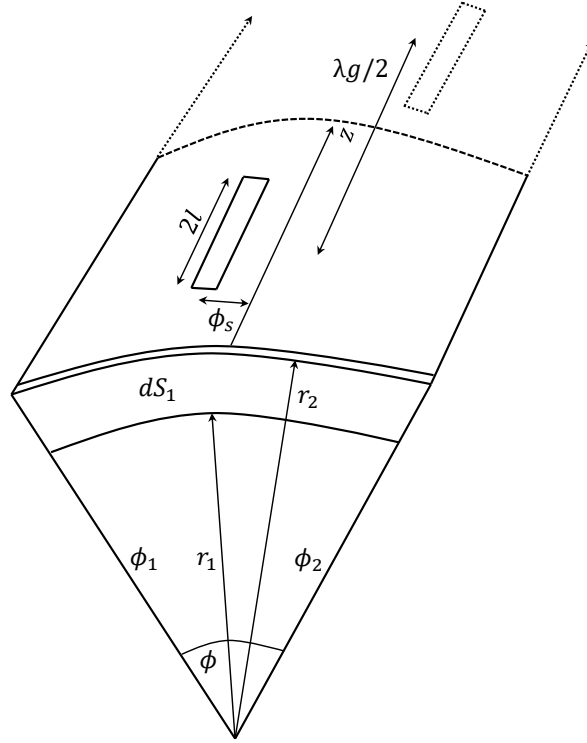
FIGURE 6.1: Representation of slot elements conformed on a cylindrical platform.

6.2.2   Design Equations

Slot array of N number of elements on SIW is considered to be projected on the cylinder of radius r. As the SIW is low profile compared to RWG therefore, the mutual coupling of the higher mode is meaningful in SIW. So, the design formulas given below can be used to characterize SIW based slot array [44, 67, 75].

$$\frac{Y_n^a}{G_0} = K_1 f_n \frac{V_n}{V_n} \tag{6.1}$$

$$\frac{Y_n^a}{G_0} = \frac{2f_n^2}{Q} \tag{6.2}$$

where Q denotes mutual coupling between slot elements and it can be expressed as

$$Q_n = \frac{2f_n^s}{\dfrac{Y}{G_0}(\phi_{sn}, l_n) + MC_n} \tag{6.3}$$

The active admittance of nth slot element is Y_n^a/G_0 and V_n^s/V_n is the mode excitation voltage. The MC_n can be segmetizes as

$$MC_n = MC_{n,intr.} + MC_{n,extr.} \tag{6.4}$$

where $MC_{n,intr.}$ and $MC_{n,extr.}$ are abbreviated as internal and external mutual couplings of nth slot on cylinder [44].

6.2.3   Error Correction Technique

The total error term in the design is related to the design parameters; such as design equations, input matching, array synthesis and cross-section of the pre-defined surface. Therefore, the total error term denoted as δ_t can be formulated as

$$\delta_t = \delta_{design} + \delta_{matching} + \delta_{synth} + \delta_r \tag{6.5}$$

The error in the design equations can be evaluated by using Eqs. (6.1) to (6.3), and it can be expressed as

$$\delta_{design} = W_{eq} \sum_{n=1}^{N} \left| \frac{|f_n| Q_{n+1}}{|f_{n+1}| Q_{n+2}} - \frac{V_n^s}{V_n} \right|^2 \tag{6.6}$$

where W_{eq} is defined as the weighting function. Equation (6.6) is formed by dividing n^{th} element with $n + 1$ element's mutual coupling and voltage. Furthermore, one assumption is undertaken in Eq. (6.6) that the elements are reasonably spaced to have the negligible mutual effect up to $n + 2$ element.

The input matching error term, $\delta_{matching}$ is obtained by using the RWG to SIW feeding structure. A coupling slot is located on the lower side of SIW as shown in Fig. 6.2, which is excited by the E-field propagation at center plane of RWG.

A single slot on the lower broad wall is considered as a receiving dipole having characteristic impedance Z_0 and the propagating mode (TE$_{10}$) in SIW having impedance R_0.

$$\frac{Z_0}{R_0} = \sum_{n=1}^{N} \kappa^2 \frac{Y_n^s}{G_0} \tag{6.7}$$

where

$$\kappa = \frac{S_{11}(\theta)}{1 - S_{11}(\theta)} \tag{6.8}$$

where S_{11} is the input reflection coefficient. It is conditional that the normalized admittance of array must be real so $Y/G_0 = 1 + j0$ [75, 93]. Applying this to Eq. (6.7), one can find $\delta_{matching}$ as

$$\delta_{matching} = W_{in} \left| \text{Re}\left(\frac{Z_0}{R_0}\right) - 1 \right|^2 + W_{in} \left| \text{Im}\left(\frac{Z_0}{R_0}\right) \right|^2 \tag{6.9}$$

The array factor, $\text{AF}(\theta, \phi)$ of conformal slot array having the element factor can be expressed as

$$\text{AF}(\theta, \phi) = \sum_{n=1}^{N} \left| \frac{V_n^s}{V_n} \right|^2 W_n e^{j(nkd\cos(\theta) + \beta_n)} \tag{6.10}$$

where $k = 2\pi/\lambda_g$ is the angular wave number and W_n represents element's weights. By using Eq. (6.10), the synthesis error, δ_{synth} can be formulated as the upper and lower limits of SLL.

$$\delta_{synth} = W_{synth} \left(\sum_{n=1}^{N} |\text{AF}(\theta, \phi) - h_n^{max}|^2 + \sum_{n=1}^{N} |\text{AF}(\theta, \phi) - h_n^{min}|^2 \right) \tag{6.11}$$

where h_n^{max} and h_n^{min} are upper and lower limits of SLL, respectively; and W_{synth} denotes the weights. The conformal behavior of SIW can also contribute in total design error because, the cross-section of SIW is changed according to the radius of cylinder therefore, it can be modeled as

$$\delta_r = W_r \beta_r \tag{6.12}$$

Equations (6.6), (6.9), (6.11), and (6.12) are based on complex functions therefore, GA or conjugate gradient optimization tool can be utilized to reduce δ_t. The synthesis procedure has an inherent error that depends upon weights W_{synth} and N. As N increases, V_n^s also increases until $N/2$ element and then decreases. Due to this, δ_{synth} also varies accordingly. If the radius of the cylindrical surface decreases, which means more conformity of SIW array therefore, δ_r increases. Once the optimum weights are achieved, then the physical parameter can be calculated.
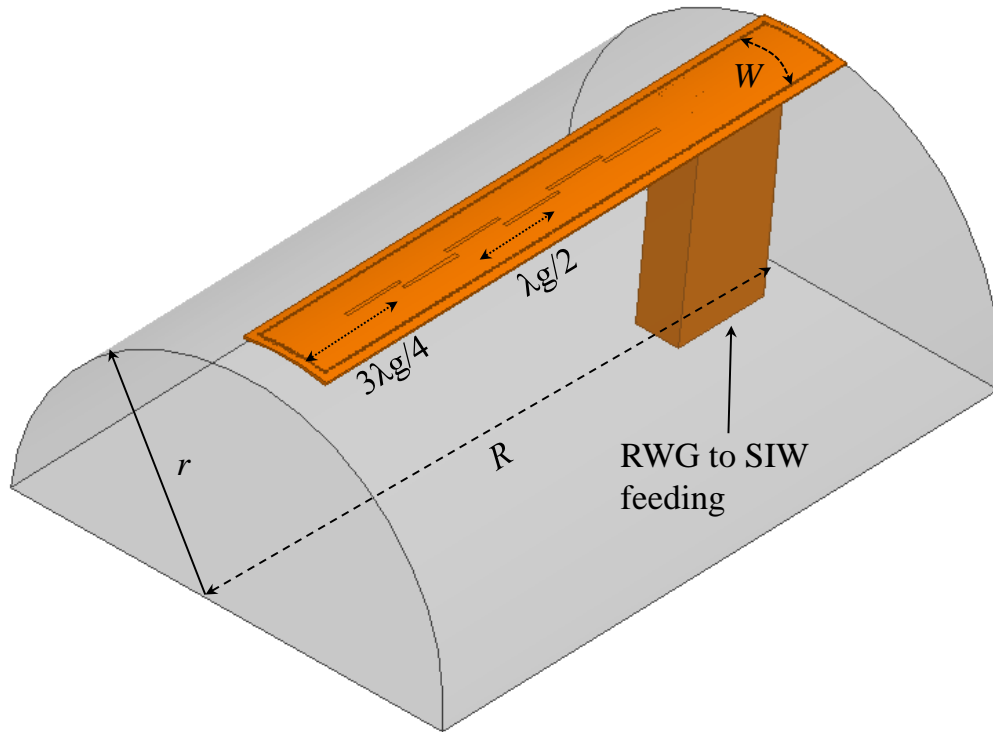
FIGURE 6.2: 3-D view of half cylindrical conformal slot array antenna with RWG to SIW feeding structure.

6.3   Simulation Results and Discussion

The slot array of 1×6 elements is projected on a cylinder of radius $r = 50$ mm. The design center frequency is 10 GHz and SIW of width W is half of the free space wavelength to avoid the grading lobe as the array is conformed. This property needs to be maintained in the design that metal vias of radius 0.25 mm and pitch 0.9 mm must lay at $(r_1, \triangle\phi, z)$. The array is synthesized using MLS algorithm with -20 dB SLL criteria [93]. To represent array in cylindrical coordinates (r, ϕ, z), the length of the array is laying along the direction z and conformed cross-sectional face along $\triangle\phi$. The elements are separated uniformly by a distance $\lambda_g/2$ as shown in Fig. 6.2, where λ_g is the guided wavelength. The array is short-circuited at $3\lambda_g/4$ and fed using a coupling slot on the lower side of SIW. The propagating wave of RWG incidents on coupling slot, which couples the energy to a dielectric medium. It has been observed that the coupling loss is not more than the 0.5 dB.

The simulation of the array is carried out in Ansys HFSS. In Fig. 6.3, the H-plane radiation pattern is shown and RWG to SIW input reflection characteristics, S_{11}
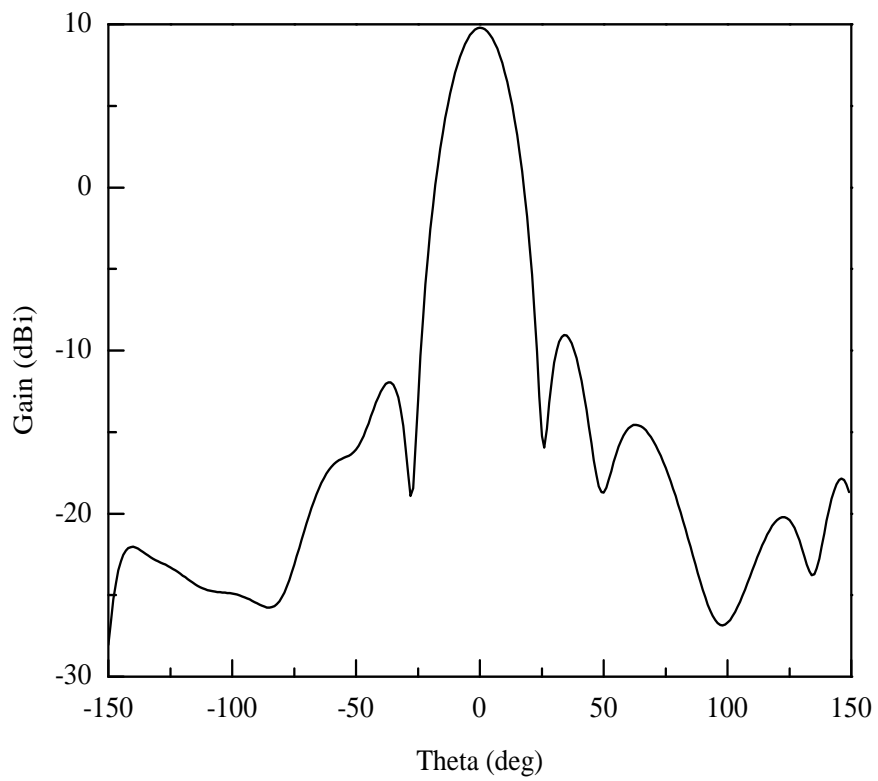
FIGURE 6.3: Simulated H-plane radiation characteristics of the proposed array.
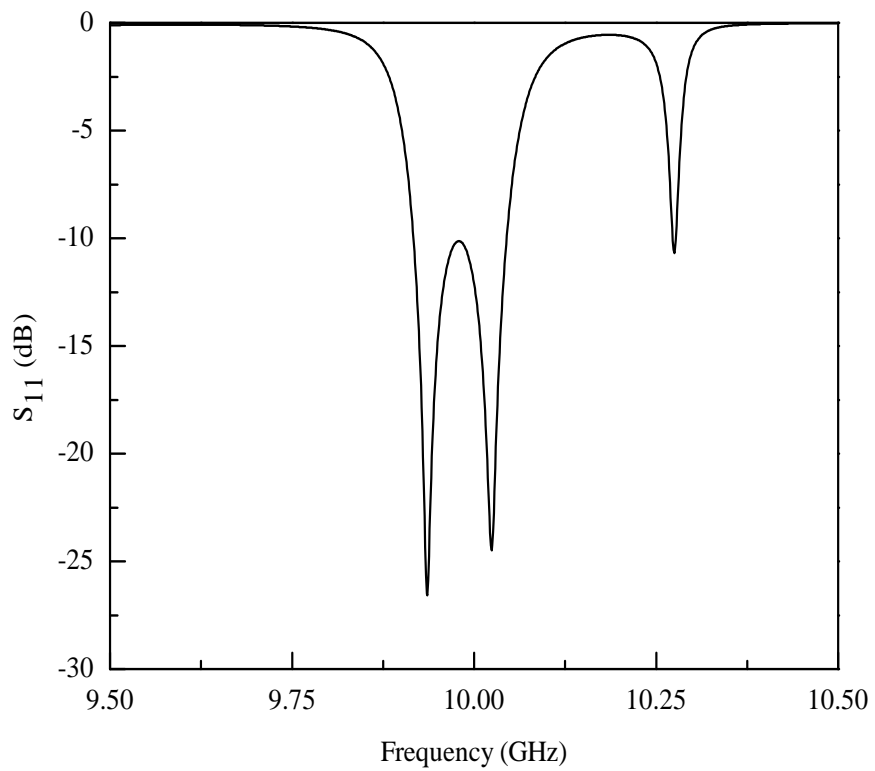
FIGURE 6.4: Simlated return loss of the proposed array.

are shown in Fig. 6.4. From Fig. 6.3, it has been observed that the gain of the proposed array is 9.8 dBi with SLL of -21.72 dB and -17.50 dB, respectively. The variation in HPBW of the conformal array $\approx 21.24°$.

The comparison between proposed design and already existing antenna arrays are shown in Table 6.1. From the data of the table, it can be noted that minimum SLL and acceptable antenna gain have been achieved with less number of slot elements. Therefore, the proposed cylindrical conformal SIW slot array antenna is a suitable candidate for X-band RADAR applications.

TABLE 6.1: Comparison between proposed and previously presented cylindrical conformal arrays.

Ref.	No. of Elements	Frequency (GHz)	Gain (dBi)	SLL (dB)
[40]	4×16	25	14	-13
[99]	1×12	2.4	14	-19
[100]	8×32	40.25-44	12	-22
Proposed array	1×6	10	9.8	-21.72

6.4 Summary

This chapter presents cylindrical conformal SIW slot array antenna design with RWG to SIW feeding structure. The design equations in cylindrical coordinates are presented along with the design tolerance such as synthesis and impedance. The array is synthesized using the MLS algorithm and it is simulated in Ansys HFSS. From simulation results, it is observed that the proposed array offer SLL and H-plane gain of -21.72 dB and 9.8 dBi, respectively; with VSWR ≤ 2 at a center frequency of 10 GHz.

Chapter 7

Nose-Cone Conformal Substrate Integrated Waveguide Slot Array Antenna

7.1 Introduction

In modern aircraft and UAVs, most of the communication systems depend on antennas. Generally, planar antenna arrays are utilized in these systems, which could potentially increase the payload and thus, make the system inefficient [101]. To overcome these problems, now-a-days, conformal antennas are being used on the surface of aircraft and UAVs [1, 102]. Also, SIW based conformal antennas are considered good candidates for airborne applications. SIW has the inherent property of the microstrip line with an added advantage of a waveguide. Moreover, it is compact in size, cost-effective, offers low insertion loss and better integration capability for microwave circuits compared to conventional waveguides [17, 19, 96, 103–105]. The closed configuration of SIW suppresses the spurious radiations from feeding structure, which otherwise, could lead to narrow beamwidth [17, 93].

In the literature, many conformal antenna arrays have been presented for multiple applications. In [98], a conformal Vivaldi antenna array with high gain and

low SLL is presented for airborne applications. The array elements are synthesized using the Dolph-Chebyshev technique, and the presented array operates in the frequency range of 400-800 MHz. In [34], a conformal RWG is presented for aircraft applications. It covered 360° azimuth angle for scanning purpose in the frequency range of 16-16.6 GHz. However, the presented array is non-planar, which is considered a negative feature from the design perspective. In [40], a cylindrical conformal SIW based traveling wave slot array is designed and implemented. The array consisted of 4×16 elements, and employed microstrip to SIW type feeding structure conformed on a cylindrical surface. It was noted that this kind of configuration degrades radiation characteristics especially SLL. Another cylindrical conformal slotted array with large beam tilt (84°) is presented in Ref. [38]. The reported array had -13 dB SLL, but the design compromised over the beam scanning. A microstrip fed circular patch antenna array conformed on a cylinder for C-band applications is discussed in Ref. [106].

It is worth mentioning that the designs presented in [34, 38, 40, 98, 106] are simulation based, and their experimental or analytical validation is not available. In [44], an analytical design approach is adopted and equations are presented for a cylindrical curved slot array. In [9], an experimental study for conformal antennas on aircraft surface is presented; wherein, suitable material for array fabrication and their mechanical aspects are reported. In [48], the authors estimated the gain of the conformal array on the wings of an aircraft and compared it to the gain of the conventional planar array. In [60], a conformal antenna array factor is simulated and optimized using a MATLAB program for radar scanning applications. The authors reported a peak SLL of -20 dB.

In the current state of conformal arrays, there is a need to investigate the integration of antenna arrays on the surface of high-speed jets. Owing to this, in this work, a nose-cone conformal SIW slotted array is designed, fabricated and characterized at X-band. Since, the conical surface is an essential part of aerodynamic applications such as space rockets, supersonic aircraft, and missiles [1] therefore, design consideration of nose-cone conformal SIW is emphasized in this work. In cylindrical conformal SIW, the cross-section of SIW remains the same

along longitudinal and circumferential directions therefore, the wave propagation characteristics have to be uniform in the conformed structure. Thus, a standard slot array design procedure can be implemented on cylindrical surface [67, 68, 73–75]. The same design strategy of a slot array cannot be implemented directly on doubly curved surfaces due to the involvement of θ and ϕ in the conformed SIW. Because of the variation in both θ and ϕ, the uniform wave propagation along the direction of nose-cone would be the first design challenge, while keeping the SLL at the desired level would be the second major consideration. In [63], a conical conformal SIW slot array antenna is presented for millimeter-wave applications. A flexible SIW transition from conical-to-cylindrical is designed for improved impedance matching. The presented configuration provides better return loss in the band of interest, but it has no effect on gain compared to its counterpart, i.e. conical surface. Furthermore, conical-to-cylindrical SIW transition can increase the size of the antenna structure, which limits its use in many aerodynamic applications.

In this chapter, a design of the nose-cone conformal slot array antenna is presented for X-band radar applications. The problems in the wave propagation characteristics for such a medium are identified and to overcome this issue, a generalized solution is proposed. It has also been demonstrated that the proposed design offers better performance compared to the design reported in [63]. Moreover, the proposed array is cost-effective, lightweight and offers enhanced radar coverage without involving mechanical steering. Furthermore, the conventional planar slot array needs protective radome for aircraft applications that implies dielectric losses [1], which are not there in the proposed design hence, making it a good candidate for such applications.

7.2   Characterization of SIW on Curved Surface

This section describes the wave propagation characteristics of conformal SIW on curved surfaces. Two curved surfaces are under consideration: cylindrical and

conical. A planar SIW of width, W and length, L is conformed onto the cylinder of radius, r along the longitudinal direction z as shown in Fig. 7.1(a). The planar cross-sectional face of SIW is converted into a curved surface and due to this change, the propagation constant, β and input impedance, Z_{in} will change. Since, the curvature of a cylindrical surface remains unchanged therefore, β will remain the same.

When planar SIW is conformed to the doubly curved surface such as nose-cone defined by spherical coordinates (r, ϕ, θ) as shown in Fig. 7.1(b), to maintain the conformity, the cross-section of SIW will not remain the same along the height of the cone. In other words, the cross-sectional face of SIW is more conforming on the vertex of the cone as shown in Fig. 7.1(b). This continuous structural variation causes a change in β. In this situation, the design of the slot array on SIW is not feasible as there could be n^{th} β propagations on the surface of SIW. It means that every element on SIW will resonate at different β and due to this phenomenon, the array cannot be analyzed practically.

To represent nose-cone conformal SIW in spherical coordinates, the base of excitation of SIW is at (r_1, ϕ_1, θ) and short circuit end is at (r_2, ϕ_2, θ) as shown in Fig. 7.1(b). The cross-section at base has a radius r_1 at ϕ_1 and cross-section at vertex has a radius r_2 at ϕ_2. For wave propagation in conical SIW, below mentioned condition must be validated [63, 107].

$$r_1\phi_2 = r_2\phi_1 \tag{7.1}$$

On the other hand, the analytical expression for the change in β can be written as [107],

$$\beta = \frac{u_{np}}{r_n} \tag{7.2}$$

where u_{np} represents the zeros of Bessel's function and r_n represents radii of the cone from base to vertex. If r_n changes, β also changes accordingly, and if r_n of a cone decreases or approaches towards zero, the corresponding ϕ increases according to Eq. (7.1), consequently β increases as described in [63].
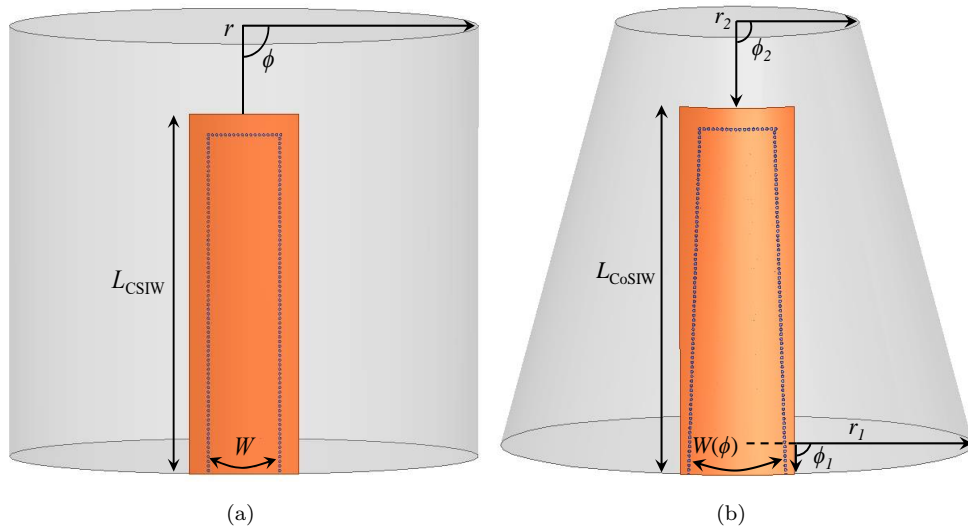
FIGURE 7.1: Conformal substrate integrated waveguide on (a) cylindrical and (b) conical surface.

For slot array, it is assumed that n^{th} element is laying on any radius r_n. The mutual coupling between the array elements is difficult to establish and practically, the design is invalid for N number of elements. To overcome this problem, a design technique has been proposed whose explanation is provided in the next section.

7.3 Modified Nose-Cone Conformal SIW

Two design topologies are presented for β regulation along the conformed surface: one is the cylindrical equivalent and other is the conical equivalent modification. Here an assumption is made that at any location on the cone (L_n) as shown in Fig. 7.2(a), one can consider that specific portion as a cylinder having radius according to the conical radius at that specific location defined by n. For this purpose, it is required to find the radius at the corresponding length L_C, which can be calculated using below mentioned expression.

$$r_n - r_0 = L_n \times \cos(\alpha) \tag{7.3}$$

where

$$L_n = L_{\text{CoSIW}} - L_d \tag{7.4}$$
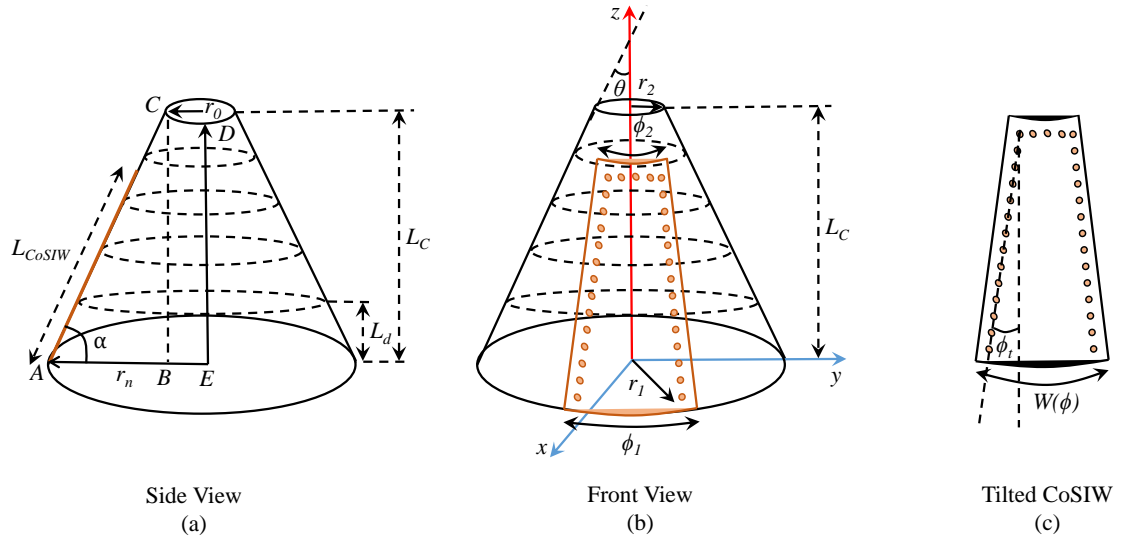
FIGURE 7.2: Cross-sectional view of nose-cone conformal SIW.

As long as L_d sweeps from 0 to L_C, L_n traverse along the generatrix of nose-cone. In Eq. (7.4), L_{CoSIW} corresponds to the length of conformal SIW, which can be calculated through triangle ΔABC as shown in Fig. 7.2(a). In the figure, the lines $\overline{AC} = L_{\text{CoSIW}}$, $\overline{BC} = L_C$, and $\overline{AB} = r_n - r_0$. By using Pythagoras theorem, L_{CoSIW} can be represented as:

$$L_{\text{CoSIW}} = \sqrt{(r_n - r_0)^2 + L_C^2} \qquad (7.5)$$

In Eq. (7.3), the variable α represents cone angle. A number of HFSS simulations of conformal SIW have been carried out for β_n curves against the tilted cylindrical conformed SIW and the results are shown in Fig. 7.3(a). One can observe from Fig. 7.3(a) that the slope of β curves by increasing the value of L_C, as evident from Fig. 7.2(b), is reducing. Examination of Fig. 7.3(a) also shows that all the β_n curves are passing through a region labeled as area of interest. It is worth mentioning that all the β_n curves converge for a range of $\phi_t \sim 0.3°-0.5°$. This range of ϕ_t provides unchanged β along the conformal SIW thus, for an appropriate design, a value of $\phi_t \approx 0.43°$ has been selected, which gave $\beta = 230.5$ rad/m as marked area of interest in Fig. 7.3(a).

In the second case, the geometrical structure has been modified, and now it is truly represented by a cone having bottom radius, r_1 and top radius, r_2 as shown
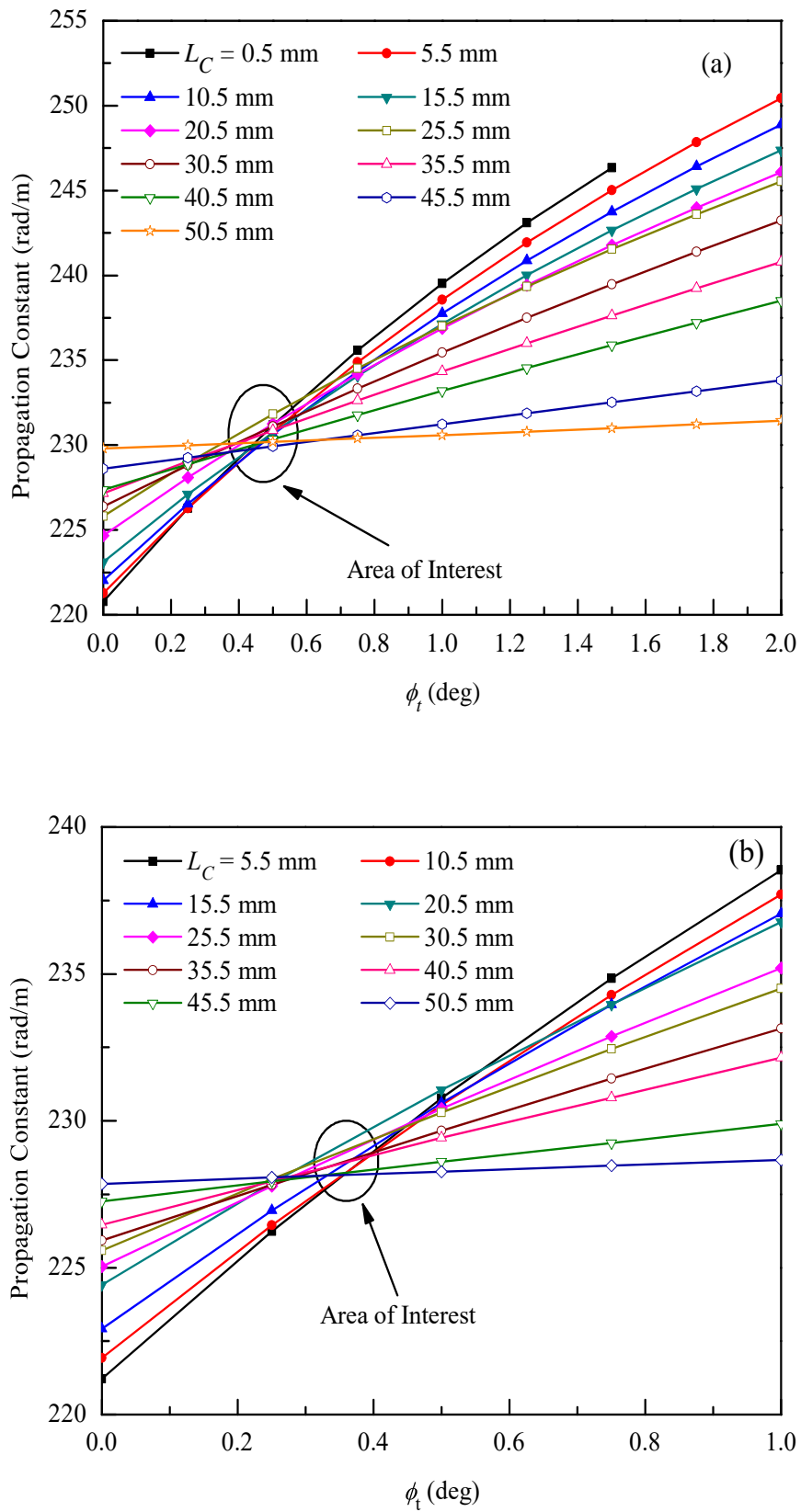
FIGURE 7.3: Wave propagation characteristics of conformal SIW along distance, L_C and tilted width, $W(\phi)$ [Fig. 7.2(c)]: (a) cylindrical (b) nose-cone.

in Fig. 7.2(b). Series of simulations were performed by moving the probe from higher to the lower radius (r_1 to r_2), and the variation in β has been observed. It has been noted that for $\phi_t \approx 0.43°$ where the $\beta \approx 228$ rad/m, is the value which is independent of L_C. Thus, this value is taken to calculate the length L_{CoSIW} of conformed SIW, which is equal to two guided-wavelength, $2\lambda_g$. Whereas, the tapering of via-holes along the longitudinal direction increases the width of SIW at the base (near to r_1) as shown in Fig. 7.2(b). A new variable $W(\phi)$ is introduced, shown in Fig. 7.2(c), while keeping the width of SIW fixed at the vertex of the cone and the arrays of conducting via holes are being tilted as shown in Fig. 7.2(c). The simulated data of geometrical variables such as ϕ_t, L_C and β have been analyzed in Fig. 7.3(b), and it is noted that the region of convergence of β_n curves is little bit expanded compared to the cylindrical case (Fig. 7.3a). The vias of conformal SIW are tilted outward as shown in Fig. 7.2(c) therefore, the width $W(\phi) > \lambda_0/2$. In conformal SIW, there is a possibility that multiple propagation modes will exist due to the structural modifications in SIW. In the presented design, the SIW is modified in such a way that it should adopt the first propagation mode, which is TE_{10}. On the other hand, higher-order propagation modes also exist outside the band of interest.

7.4   Design of Conformal SIW Slotted Array

This section describes the steps involved in the designing of nose-cone conformal SIW slot array including feeding structure.

7.4.1   Array Feeding

To excite the array, two feeding techniques are considered: the first one is microstrip to SIW feeding and the second one is RWG to SIW feeding. The first technique is relatively easy to fabricate as the flexible substrate can be conformed comfortably to a predefined surface [11]. However, this could cause spurious radiations, which can possibly affect the overall performance of the system [19].

RWG to SIW feeding is a better option if adopted for conformal array design. One major advantage of RWG to SIW feed is that it suppresses spurious radiations. The half cosine incident wave will intersect with the lower coupling slot of SIW and can be tuned by off-setting from the center. The coupling slot is similar to the radiating slot [75], and it is located on SIW where the magnetic field is maximum. This kind of technique was utilized in Ref. [108] where the authors designed SIW slot array antenna on a cylindrical platform. They utilized RWG to SIW feed structure to excite 1×6 elements slot array. Their simulation results showed that the presented array had SLL of -21.72 dB with a gain of 9.8 dBi.

Figure 7.4 illustrates RWG to SIW feeding structure. From the figure, it can be observed that two coupling slots are placed on SIW structure. The distance from the center of the slot to conducting vias is $3\lambda_g/4$ as shown in Fig. 7.4. Two rectangular waveguides represented as input and output ports are used to calculate the power transfer characteristics from one port to another.

The S-parameters of RWG to SIW feeding structure are shown in Fig. 7.5. It can be observed from Fig. 7.5(a) that the proposed feeding technique is operating well for the frequency of interest, which is 10 GHz. Therefore, from Fig. 7.5(a), it can be noted that the proposed feeding structure provides 100 MHz bandwidth from 9.93 to 10.03 GHz. The reason behind such a narrow bandwidth is that the conducting vias are tightly spaced, which tend to cause electric field leakage. The dielectric losses could be another reason for the observed narrow bandwidth for the proposed feeding structure [109]. On the other hand, the broadband transition,
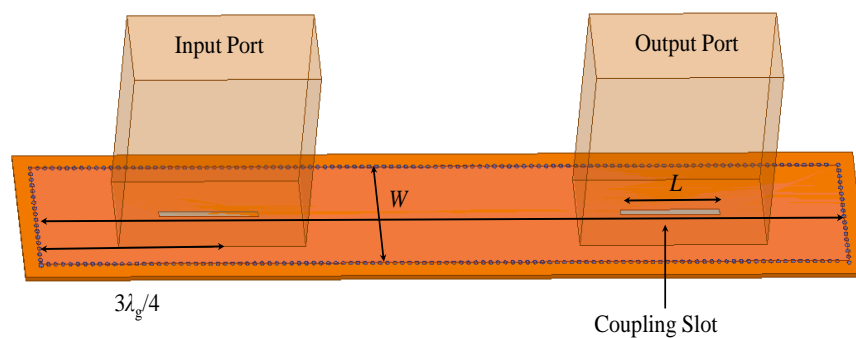
FIGURE 7.4: Represents a scheme in which RWGs are used to excite and observe field pattern of SIW.
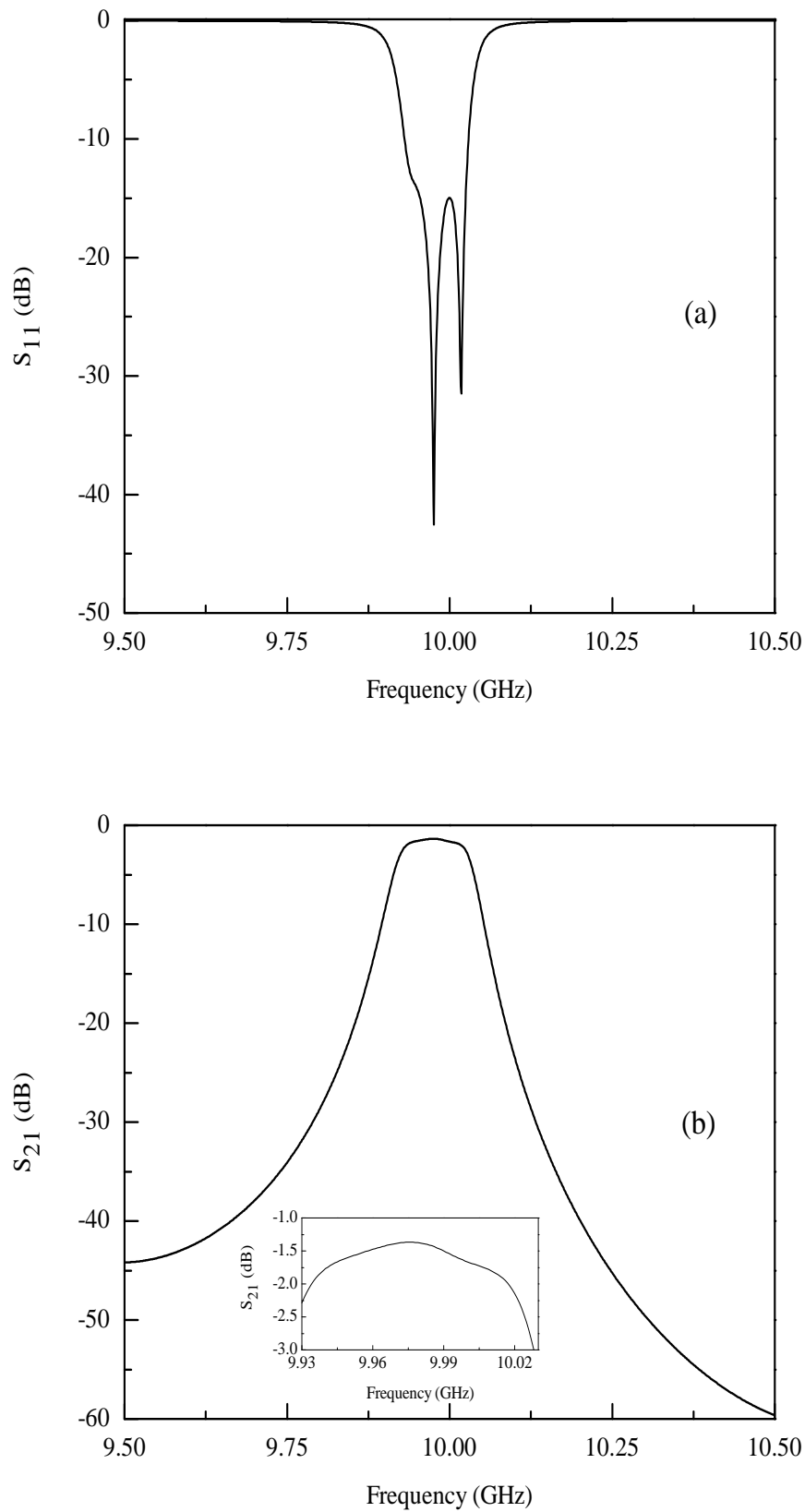
FIGURE 7.5: S-parameters of RWG to SIW feeding structure (a) reflection parameter and (b) insertion loss; the inset of Figure 7.5(b) represents a zoomed view of region of interest.

such as reported in [110], cannot be implemented directly in the proposed design, because it is difficult to conform E-plane iris of RWG on the nose-cone surface.

Figure 7.5(b) shows insertion loss of the proposed feeding structure. From the figure, it is observed that the variation in insertion transition is 1.25 dB, which could primarily be associated with dielectric losses of the medium [109] and coupling losses of both the ports of the proposed design.

7.4.2 Array Design and Simulation

The graphical view of longitudinal slot array on the nose-cone surface is represented in Fig. 7.6. It is pertinent to mention here that a hollow conical surface has been selected for the proposed design. Moreover, substrate chosen for the design of slotted array is Rogers RT/Duroid 5880 having $h = 0.508$ mm, $\varepsilon_r = 2.2$ and $\tan \delta = 0.0009$. The center frequency of the designed array is 10 GHz. The array is projected on the conical surface of lower radius, r_1 and upper radius, r_2 as shown in Fig. 7.2(b), while the width W of the nose-cone conformal SIW is selected according to the process defined in Section 3. The diameter of the metal vias is 0.5 mm and the separation between them is 0.9 mm. The rest of the design parameters are listed in Table 7.1. This table provides variables for two different design: one deals with the proposed nose-cone design listed in column 1, whereas for comparison purposes, a cylindrical design parameters are also provided in the table.

TABLE 7.1: Design parameters of nose-cone and cylindrical conformal SIW slot array antennas.

Nose-cone Parameters	Values	Cylinder Parameters	Values
r_1 (mm)	$5\lambda_0$	r (mm)	$1.66\lambda_0$
r_2 (mm)	$4\lambda_0$	L_C (mm)	$5\lambda_0$
L_C (mm)	$5\lambda_0$	L_{CSIW} (mm)	$5\lambda_g$
L_{CoSIW} (mm)	$5\lambda_g$	W (mm)	$\lambda_0/2$
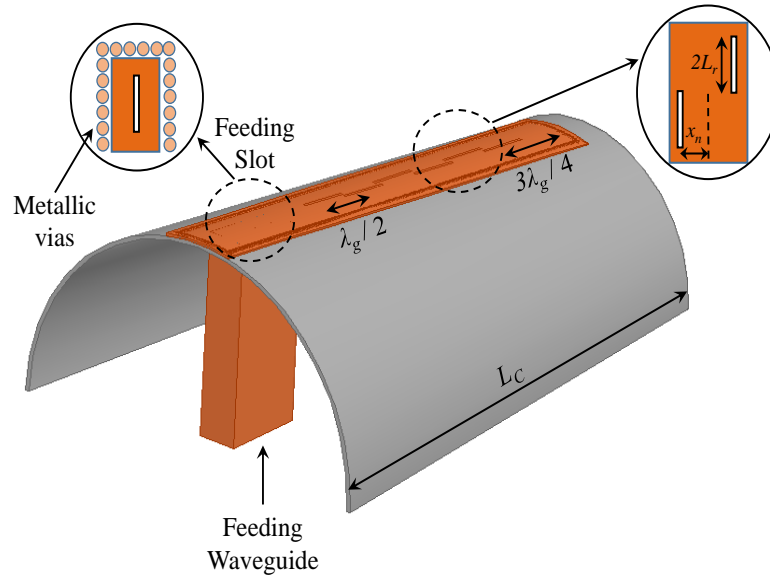
FIGURE 7.6: Configuration of hollow nose-cone conformal SIW slot array antenna.

The road map for the designed array is the same as that of Elliot's design technique [67, 74]. To get optimum radiation characteristics with low SLL, the slot off-sets and their corresponding lengths, listed in Table 7.2, are obtained by using Method of least square (MLS) [17, 93]. The error function, which is used for pattern synthesis is given in Eq. (7.6) [17]:

$$\varepsilon_{\text{syn}} = W^{\text{upper}} \sum_{m=1}^{M} |S(\theta_m) - h_m^{\text{upper}}| + W^{\text{lower}} \sum_{m=1}^{M} |S(\theta_m) - h_m^{\text{lower}}| \qquad (7.6)$$

where, W^{upper} and W^{lower} are the weights, while h_m^{upper} and h_m^{lower} represent upper and lower limits of SLL, respectively; $S(\theta_m)$ denotes array factor, and M represents maximum number of iterations.

Once the conformal SIW slot array is designed, then its equivalent circuit model can be implemented by the classical slot array theory [68] as shown in Fig. 7.7. Wherein, the inter element spacing is $\lambda_g/2$, Y represents admittance of the elements, G_0 is the normalized conductance of slots, Z_{in} is the input impedance of the array, and the array is short circuited at $3\lambda_g/4$.

The proposed nose-cone conformal SIW slot array antenna is validated by comparing its radiation characteristics, shown in Fig. 7.8, with planar and cylindrical

TABLE 7.2: Slot parameters for nose-cone conformal antenna with inter-element spacing of $\lambda_g/2$.

S. No.	x_n (mm)	$2L_r$ (mm)
1	0.630	11.333
2	0.858	11.515
3	0.974	11.583
4	0.980	11.591
5	0.875	11.508
6	0.672	11.290
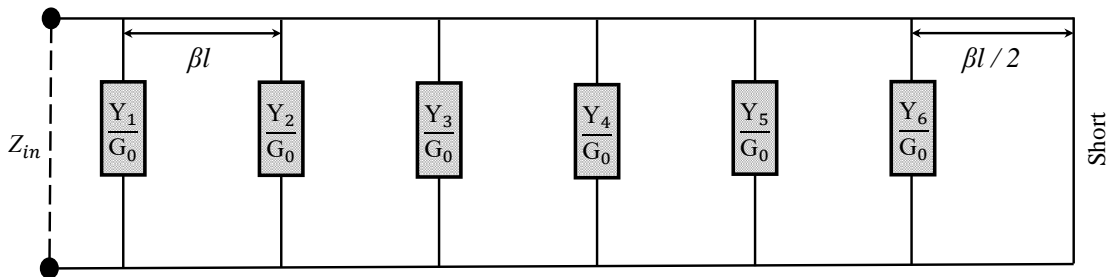
FIGURE 7.7: Equivalent circuit model of slotted array.

conformal [108] SIW slot arrays. From the figure, it can be observed that the radiation characteristics are almost the same for all the three cases but, nose-cone conformal array provides low SLLs, which could be considered as a major achievement of nose-cone conformal design. From Fig. 7.8, it can also be observed that the arrays have the main beam position in the broadside direction ($\theta = 0°$). Different electrical parameters of all the three distinct surfaces are listed in Table 7.3, where the comparative analysis for the presented cases is given.

In nose-cone conformal case, the 1st SLL, given in Table 7.3, is equal to -20.82 dB, while the 2nd SLL is equal to -27.63 dB. Such low values of SLL could possibly be associated with the conformity of the radiating array with the supporting surface. The maximum gain of the nose-cone conformal slot array antenna at 10 GHz is 11.91 dBi, while HPBW is 19.80°. The maximum gain values for planar and cylindrical conformal arrays are 9.36 dBi and 9.8 dBi, respectively; as listed in Table 7.3. In nutshell, it can be claimed that nose-cone conformal SIW array antenna provides better gain, and low SLLs.
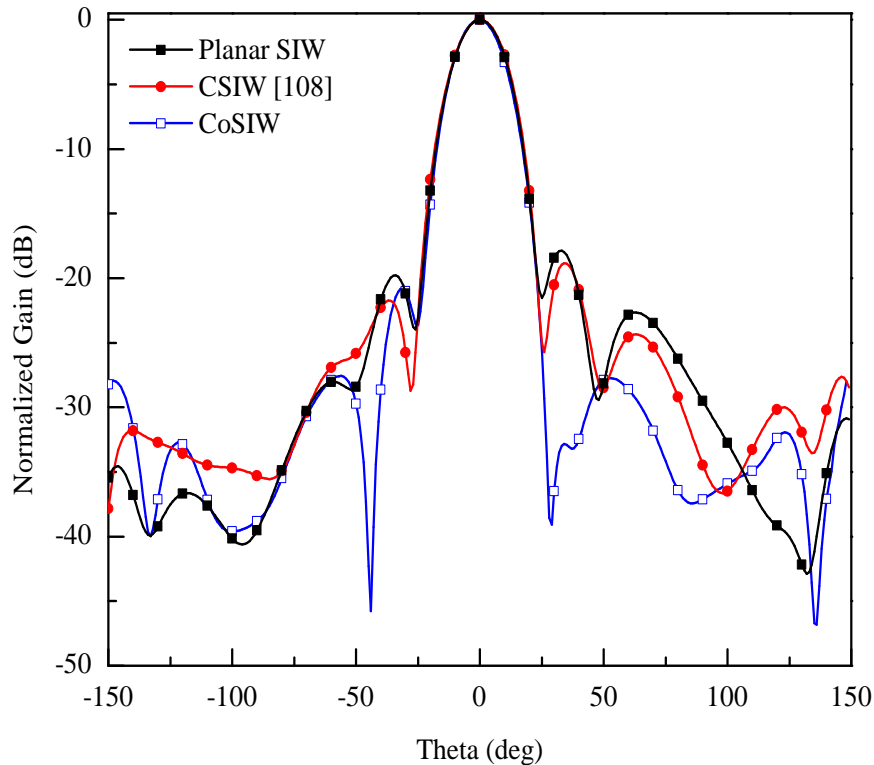
FIGURE 7.8: H-plane radiation characteristics of planar, cylindrical and nose-cone conformal slot arrays.

TABLE 7.3: Comparative analysis for planar, cylindrical and nose-cone conformal SIW slot arrays ($N = 6$ and $d = \lambda_g/2$).

Parameters	Planar SIW	Cylindrical SIW [108]	Nose-cone SIW
1st SLL (dB)	-19.78	-21.72	-20.82
2nd SLL (dB)	-17.85	-18.83	-27.63
SIW tilt (deg)	0°	0°	0.43°
Beam position (deg)	0°	0°	0°
HPBW (deg)	20.29°	21.24°	19.80°
Max. Gain (dBi)	9.36	9.8	11.91

Figure 7.9 shows the effect of large curvature and carrier surface on antenna's performance. It has been observed from Fig. 7.9 that if the curvature of the nose-cone is increased as large as $10\lambda_0$, then the effect of conformity tends to be minimum and the surface will behave as a planar surface [44]. Accordingly, the radiation pattern due to the large curvature of the nose-cone conformal antenna is approximately equal to planar antenna as shown in Fig. 7.9. On the other hand, when nose-cone conformal antenna is embedded with carrier surface, shown
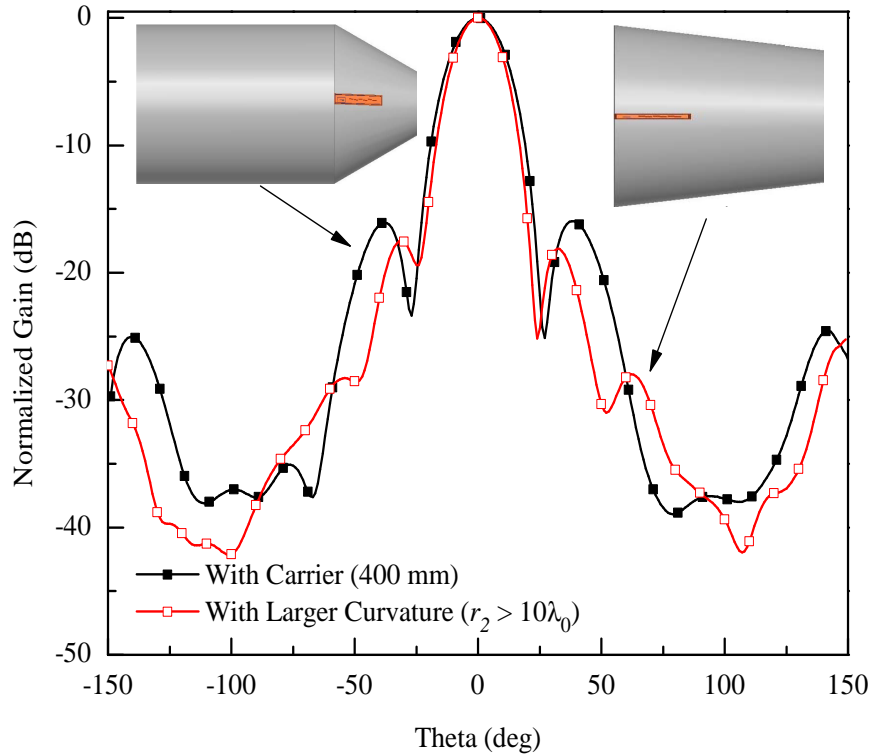
FIGURE 7.9: Effect of large curvature and carrier surface on antenna's radiation characteristics.

in inset of Fig. 7.9, an increase in SLLs and beamwidth has been observed. This is due to the fact that the carrier surface provides extra reflections at the edges of nose-cone conformal antenna.

Figure 7.10(a) shows the simulated radiation patterns for different values of L_C. It has been noted from the figure that for $L_C = 150$-250 mm, the SLLs are reducing. For values > 250 mm, the SLLs increases with the spread in the main beam up to some extent as shown in Fig. 7.10(a). The effect of r_1 and r_2 on antenna's performance is illutrated in Fig. 7.10(b). From the figure, it has been observed that SLLs tends to reduce with the increase in r_1 and r_2 value, while the gain variation is about 0.5 dB.

7.4.3   Fabrication and Measurements

The prototype of the proposed nose-cone conformal SIW slot array antenna is shown in Fig. 7.11.
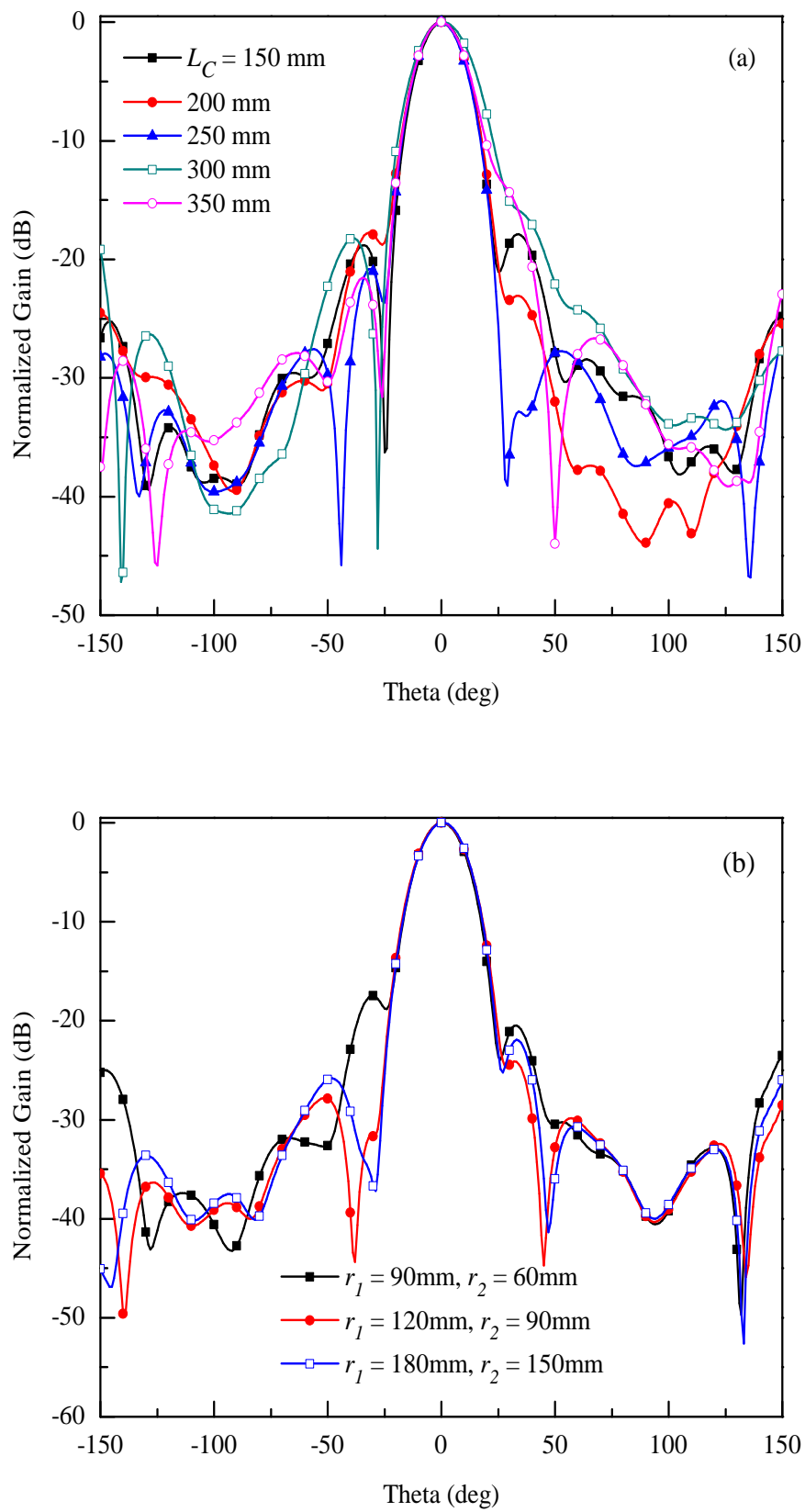
FIGURE 7.10: Effect of nose-cone parameters (a) L_C and (b) r_1, r_2 on antenna's performance.

(a) Slotted array conformed on conical platform   (b) Rectangular waveguide with SMA connector

FIGURE 7.11: Prototype of the fabricated nose-cone conformal slot array antenna.

Four major steps are involved in the fabrication of the proposed antenna array. First, fabrication of SIW, which involves the etching of slot elements, drilling, and metallization of via holes. Second, a cone is fabricated in accordance with the design parameters listed in Table 7.1 by using a metallic sheet of thickness 14 AWG as shown in Fig. 7.11(a). Third, RWG (WR-90) having one end compatible to the conical surface is attached to the inner surface of the cone through a machined window as shown in Fig. 7.11(b), while an SMA connector is inserted at a distance of $\lambda_g/4$ from shorted end of a waveguide. The last step is to wrap SIW slot array on the conical surface to excite the array by feeding slot.

The return loss characteristics of the fabricated antenna are measured using Agilent Technologies N5232A Vector Network Analyzer (VNA) and compared to the simulated results. From Fig. 7.12, a reasonable match is observed between simulated and measured return loss. An acceptable match between simulated and measured results validate the proposed nose-cone SIW design. Some discrepancies are observed between the simulated and measured return losses, which could
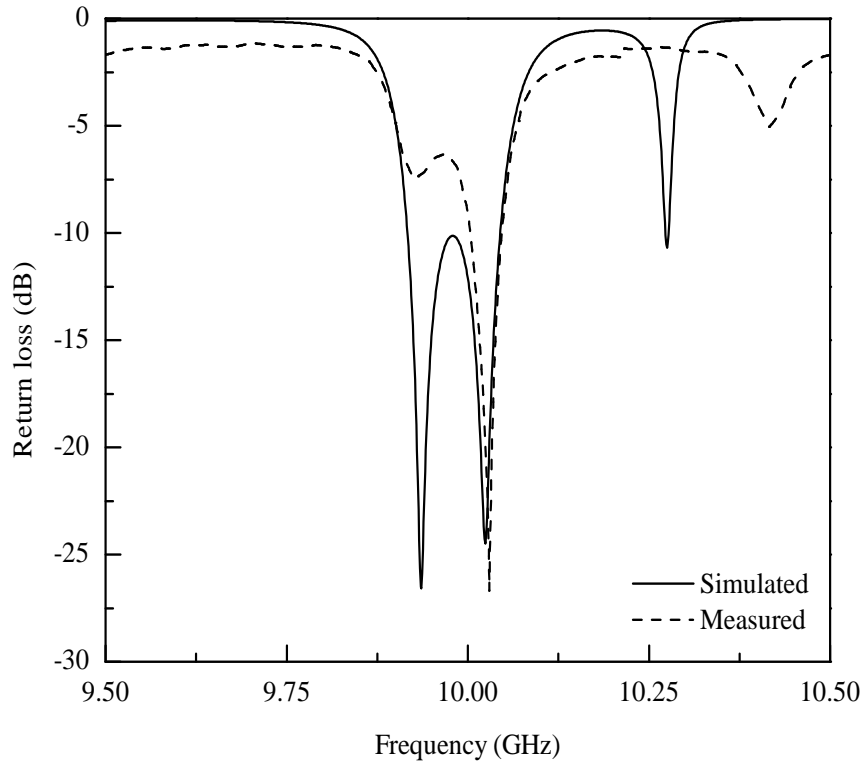
FIGURE 7.12: Return loss characteristics of the proposed nose-cone conformal slot array.

be associated with the fabrication tolerances especially the mounting of RWG on conical platform.

The far-field characteristics of the proposed antenna were measured inside the anechoic chamber. Figure 7.13 illustrates the graphical representation of measurement setup. In Figs. 7.14 and 7.15, a comparison between simulated and measured H-plane and E-plane radiation patterns is shown for the proposed nose-cone conformal SIW slot array. For H-plane, shown in Fig. 7.14, the simulated results offer SLLs of -20.82 dB and -27.63 dB, respectively; while the measured SLLs are -20.82 dB and -16 dB, respectively. An obvious reason of the observed discrepancy could be that the feeding part of the conformed array is located at the base of hollow nose-cone as shown in Fig. 7.11(b), and a mismatch between RWG and SIW, because of its tapered nature, caused an extra reflections and hence, increased SLL, which ultimately degrades radiation characteristics of the proposed antenna. On the other hand, the designed antenna consists of only one row of radiating slots therefore, its radiation characteristics are deteriorated in the E-plane by the fixed
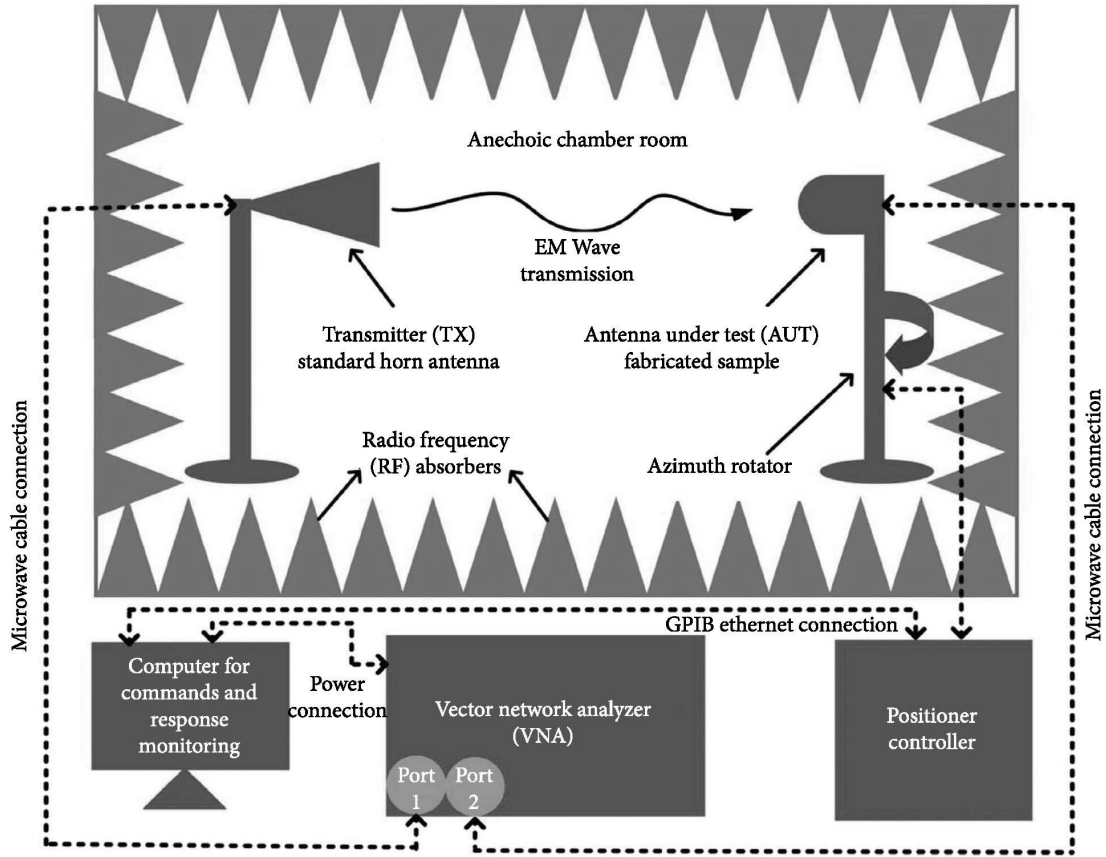
FIGURE 7.13: Return loss characteristics of the proposed nose-cone conformal slot array.

screw blockage and the lateral size of an SIW slot array antenna as shown in Fig. 7.15.

The radiation efficiency of the proposed antenna is shown in Fig. 7.16. From the plot of Fig. 7.16, it is observed that the average radiation efficiency of the antenna is ≈70%. The maximum radiation efficiency is equal to 76% at 9.5 GHz, while the minimum radiation efficiency is noted to be 68% at 10.5 GHz. Furthermore, by using the proposed nose-cone conformal SIW array antenna, the main beam can be steered by changing the frequency to increase the coverage. The patterns thus, achieved indicating the position of main beam as a function of frequency are shown in Fig. 7.17.

A comparative analysis between proposed and previously presented conformal arrays is given in Table 7.4. By examining the values of return loss and the gain as shown in the table, it can be noted that the proposed array has better performance
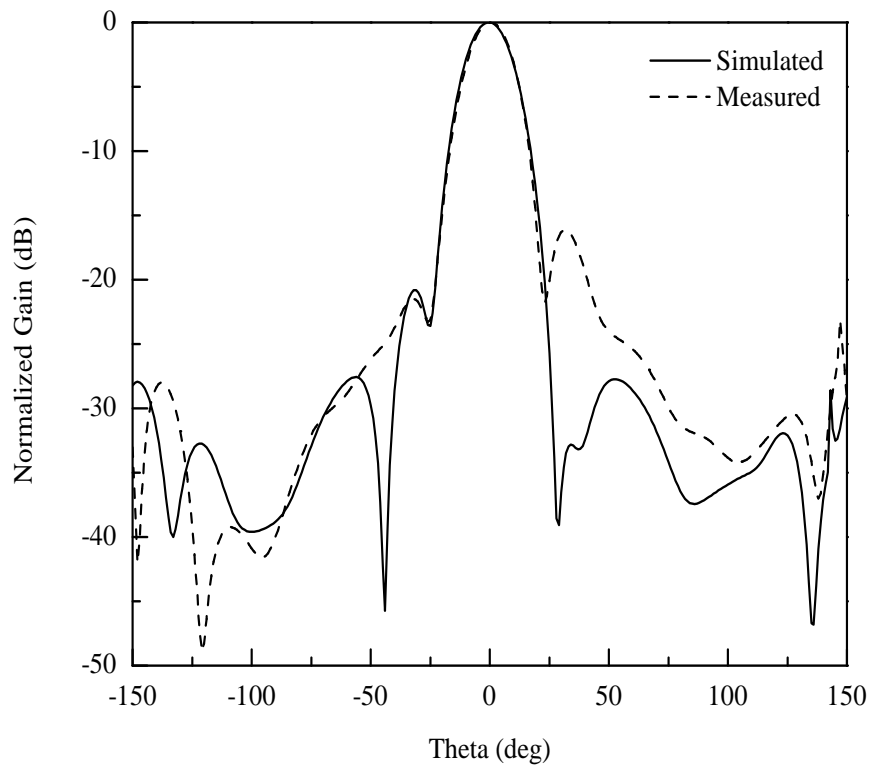
FIGURE 7.14: H-plane radiation characteristics of the proposed nose-cone conformal slot array.
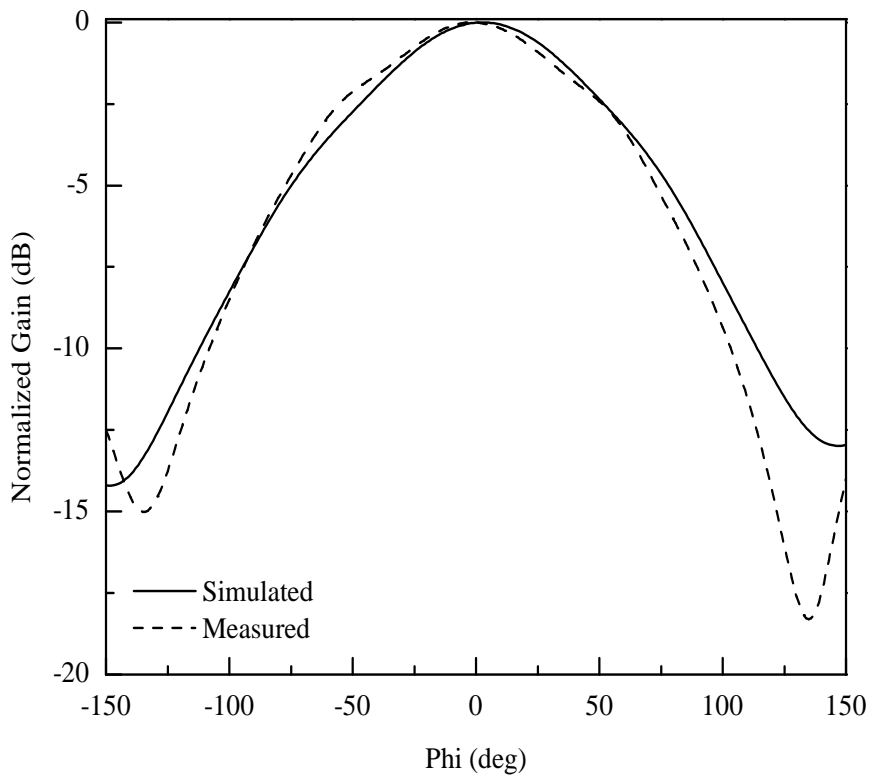
FIGURE 7.15: E-plane radiation characteristics of the proposed nose-cone conformal slot array.
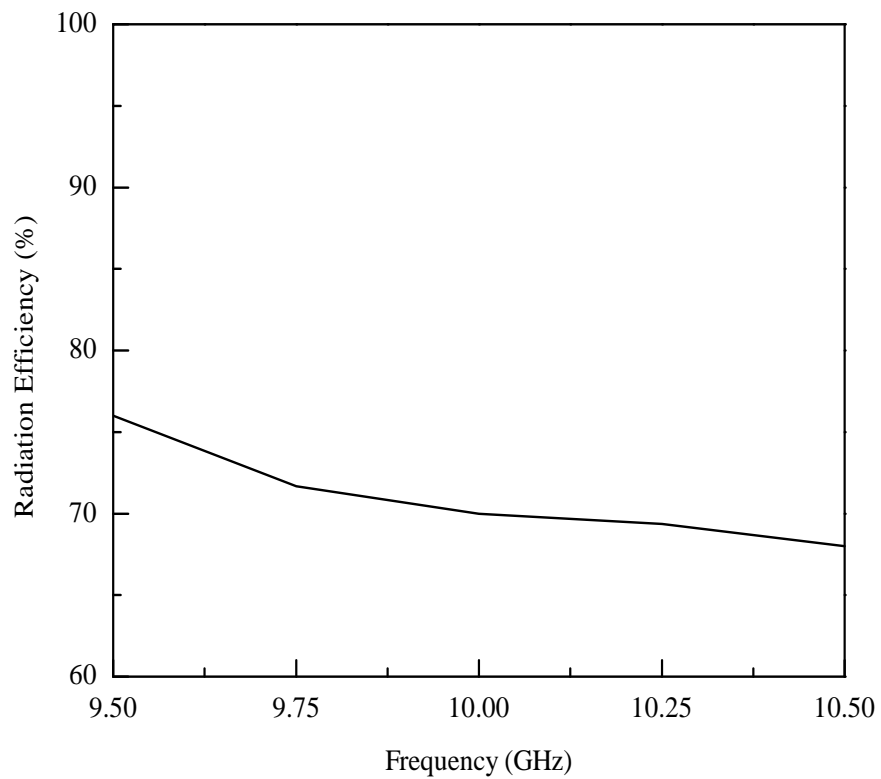
FIGURE 7.16: Radiation Efficiency of the proposed nose-cone conformal slot array.
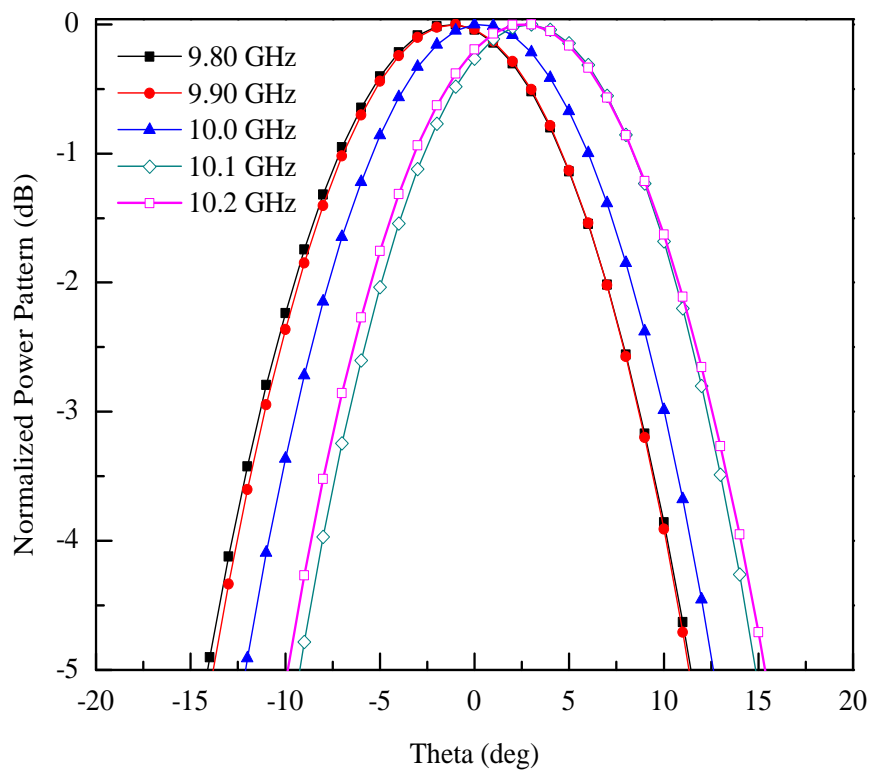
FIGURE 7.17: Main beam positioning vs. frequency.

TABLE 7.4: Comparative study of proposed and previously presented antenna arrays.

Parameters	[63]	Proposed
Array size	1×8	1×6
Cone type	Solid cone	Hollow nose-cone
Waveguide type	Wire-cut waveguide	Suspended waveguide
Design procedure	β and Z_{in} optimization on cylindrical surface	β optimization on conical surface
Return loss	> -10 dB	< -10 dB
Gain	9.9 dBi	11.91 dBi

than the design presented in [63]. It is worth mentioning here that the proposed nose-cone conformal array offers high gain even with less number of elements.

In the presented design of the nose-cone conformal antenna array, the main beam is positioned on the broadside of the nose-cone. However, the proposed antenna has the limitations to receive the scattering from the broadside, but the beam scanning of such an array can increase the angular coverage.

7.5 Summary

This chapter presents a design of an X-band nose-cone conformal substrate integrated waveguide longitudinal slot array antenna. The wave propagation on the nose-cone has been investigated, and a rectification process has been proposed through EM simulations. The simulated radiation characteristics of the proposed array are compared with planar and cylindrical conformal arrays, and it is observed that the proposed nose-cone conformal array offers relatively high gain with low SLLs. Furthermore, the nose-cone conformal array is validated through fabrication and a good agreement is observed between the measured and the simulated data. The presented study demonstrates that the proposed antenna array can be utilized with beam sweeping in modern radars, and on the conical surface of aircraft and missiles.

Chapter 8

Dual-beam Nose-cone Conformal Slot Array Antenna

8.1   Introduction

In modern aircraft and UAVs, generally, planar array antennas are utilized, but their use can increase the payload of the system and also cause more fuel consumption [101]. To overcome these problems, now-a-days, conformal array antennas are being used on the surface of an aircraft and missile [1, 102]. Furthermore, SIW based conformal arrays are considered a good candidate for airborne applications. SIW has the inherent property of microstrip line with an added advantage of a waveguide. Moreover, it is compact in size, cost-effective, has low insertion loss and integration capability for microwave circuits [96, 104]. The closed configuration of SIW suppresses the spurious radiations from the feeding structure, which leads to achieving narrow beamwidth [93]. Therefore, many conformal arrays, with and without SIW, have been presented in the literature for multiple applications.

In [111], a conical conformal phased array antenna was presented for radar applications. The presented array can steer the beam electronically both in elevation and azimuth plane. GA was applied to the design equations to achieve narrow beamwidth and low SLLs. It was observed from the results that SLLs of less than

-20 dB was achieved by optimizing the array factor of the conical conformal antenna. But the authors did not present the practical validation of the design. In [112], a microstrip patch antenna array was conformed on the surface of a missile for tracking applications. From the presented design, authors achieved an AR of 3 dB and an omni-axis ratio less than 6 dB. The problem of microstrip fed radiating structures is, that the feed line can generate unwanted radiations when conformed on the curved surface.

A low-profile 16×8 cavity-backed slot antenna array was presented in Ref. [63] for tracking applications. The designed array can operate in the frequency range of $0.9f_0$-$1.04f_0$ with a VSWR <2.5. Furthermore, the presented array had a beam scanning capability from 0° to 60° in the azimuth plane. In [59], the design of a conformal dipole array was presented for aircraft applications. Six element array of planar dipoles was conformed on the wing of an aircraft. The presented array had an operational bandwidth from $0.88f_0$ to $1.1f_0$ and had a scanning angle of 30° in the azimuth plane. The designs presented in Ref. [59, 63] can lead to a power loss because of high impedance at the input. Wu et al. [113] presented a conical conformal SIW array antenna for millimeter-wave applications. For the efficient transition between a conical surface and a cylindrical surface, and for good impedance matching, a flexible SIW transition was designed. From the presented design, SLLs of -28 dB was observed in H-plane with a gain of 9.9 dBi.

Chen et al. [114] designed a dual-band conformal antenna on the surface of a missile. To achieve dual-band characteristics, the patch was loaded with an open stub and for miniaturization, the upper end of the patch element was shorted to the missile's body. Furthermore, for omnidirectional radiation characteristics, two antenna elements were designed and fed with a coaxial line of equal amplitude and phase. In [50], different conformal arrays were designed for full solid-angle scanning applications. Firstly, a microstrip Yagi antenna was designed and then an array of Yagi antenna was developed on a cylindrical platform. Secondly, a conformal microstrip patch antenna array was realized on cylindrical and conical surfaces for broadside beam scanning. In the last, a feeding network was designed

to obtain a full solid angle scanning. In the presented design, authors, however, did not take into account the coupling effect between radiating elements.

In [40], 16-element based conformal antenna array was presented for missile-borne applications. The radiation element consists of a rectangular patch and a parasitic patch with an open-circuit stub. All the array elements were connected to the power divider and conformed on a cylindrical surface. A multi-beam cylindrical conformal SIW slot antenna array of 10×10 elements was designed and implemented at 10 GHz by Liu et al. [115]. The presented array was based on a modified Rotman lens concept. The designed array had -20 dB SLLs in H-plane with a scanning angle of 35°, which could be considered for aircraft and high-speed vehicles applications.

In this chapter, a design of a conical conformal SIW slotted array at X-band is presented for multiple target tracking applications. The proposed antenna system consists of two sub-arrays conformed on either side of the conical surface having lower and upper radius r_1 and r_2 respectively. An RWG to SIW 1×2 balanced T-junction power divider is used to feed the sub-arrays. Simulation results show that the proposed antenna system has offered two main beams located at $\theta = \pm 90°$, and the SLLs are noted to be -22.80 dB and -20.12 dB, respectively. The proposed conformal array overcomes the dielectric loss of radome and dead radar coverage zone. Furthermore, the proposed design is compact in size than the previously presented conformal arrays and hence; more feasible for airborne applications.

8.2 Array Factor

In Fig. 8.1, a single element is extended to an array of N elements to form a beam with required radiation characteristics. For this purpose, M number of longitudinal linear nose-cone conformal sub-arrays are incorporated. As the object is considered in spherical coordinates system, and elements are distributed in spatial distribution therefore, Array Factor (AF) can be written as:
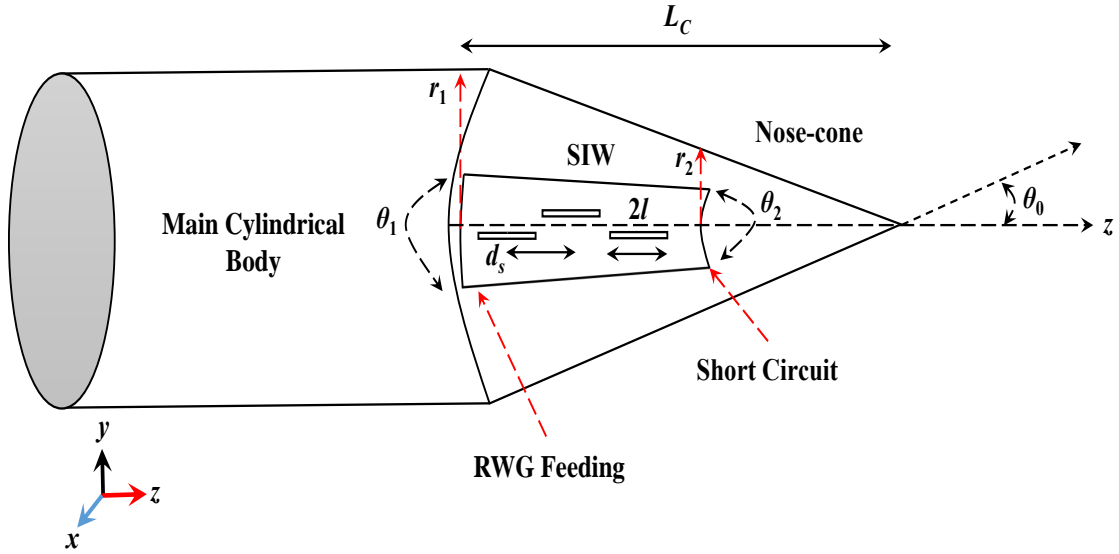
FIGURE 8.1: General diagram of a nose-cone conformal sub-array.

$$\text{AF}(\theta, \phi) = \sum_{n=1}^{N} \left| \frac{V_n^s}{V_n} \right|^2 W_n e^{j(nkd_s \cos(\alpha_n) + \beta_n)} \tag{8.1}$$

where V_n^s/V_n is the normalized slot voltages, W_n represents element's weights, α_n denotes solid angle between n^{th} element and β_n represents phase shift. The maximum array factor $\text{AF}(\theta, \phi)$ can be written as [111]:

$$nkd_s \cos(\alpha_n) + \beta_n = 0 \tag{8.2}$$

Observing the electromagnetic field at the tip of nose-cone from arbitrary position of target in spherical coordinates system, shown in Fig. 8.2, the unit vectors of the target and the nth element are $\hat{a_r}$ and $\hat{a_n}$, respectively. The unit vectors $\hat{a_{r1}}$ and $\hat{a_{r2}}$ belong to target-1 and 2, respectively; located in θ direction, while the unit vectors of slot elements are represented as $\hat{a_{n1}}$ and $\hat{a_{n2}}$, respectively. The dot product of both the unit vectors can be expressed as:

$$\hat{a_r} \cdot \hat{a_n} = \left[\left(\sin(\theta) \cos(\phi) \hat{a_x} + \sin(\theta) \sin(\phi) \hat{a_y} + \cos(\theta) \hat{a_z} \right) \right.$$
$$\left. \cdot \left(\sin(\theta_0) \hat{a_x} + \cos(\phi_n) \hat{a_y} - \cos(\theta_0) \hat{a_z} \right) \right] \tag{8.3}$$

$$\hat{a_r} \cdot \hat{a_n} = \cos(\alpha_n) \tag{8.4}$$

According to [60], Eq. (8.3) can be deduced to:
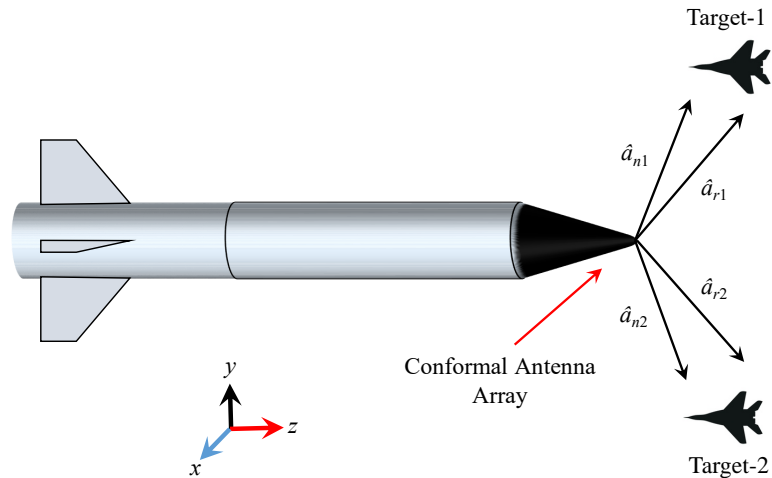
FIGURE 8.2: Nose-cone conformal sub-array for multiple target tracking.

$$\hat{a}_r \cdot \hat{a}_n = \sin(\theta_i)\sin(\theta_0)\cos(\phi_i - \phi_n) - \cos(\theta_i)\cos(\phi_n) \tag{8.5}$$

where θ_i and ϕ_i represent the position of the main lobe in elevation and azimuth plane, respectively. By comparing Eqs. (8.4) and (8.5), one can have the expression to calculate the array factor of two sub-arrays based antenna system.

$$\left[\begin{array}{c} \hat{a}_r \cdot \hat{a}_n \end{array}\right] = \left[\begin{array}{c} \hat{a_{r1}} \cdot \hat{a_{n1}}, \hat{a_{r2}} \cdot \hat{a_{n2}} \end{array}\right] \tag{8.6}$$

Once the array factor is obtained, then one can synthesize two sub-arrays in order to achieve the requirement of minimum SLL.

8.3 RWG to SIW T-juncton Power Divider

8.3.1 Power Divider Design

A balanced power divider design is the basic requirement to feed two conformal sub-arrays. In the literature, most of the conformal arrays had been fed using microstrip structures, which radiate the EM waves as the substrate is being conformed [56] therefore, an RWG based T-junction power divider can be the right choice to feed two sub-arrays located at $\phi = 0°$ and $180°$, respectively. Figure 8.3
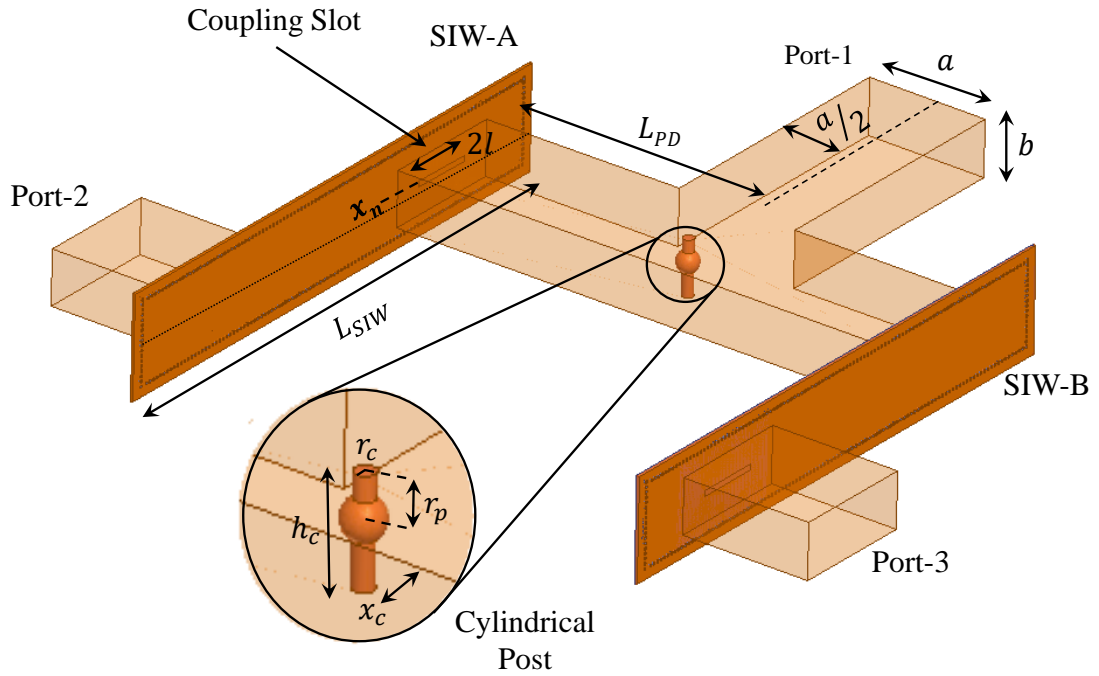
FIGURE 8.3: Design of the proposed RWG to SIW 1×2 T-junction power divider.
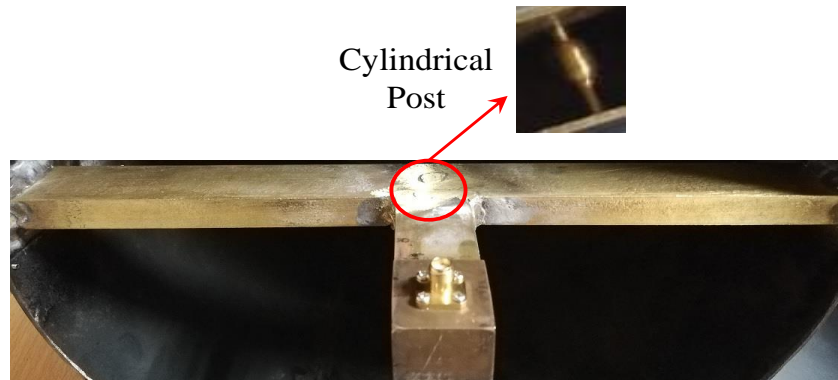
FIGURE 8.4: Fabricated prototype of the proposed RWG to SIW 1×2 T-junction power divider.

shows the structure of the proposed power divider, while the fabricated prototype is shown in Fig. 8.4. A T-junction is formed with WG-90, which is a three port network that couples the EM waves to SIW through coupling slot. Port-1 is used as an input port, while port-2 and 3 are attached to SIW based slotted arrays, and dummy waveguides are attached at port-2 and 3, shown in Fig. 8.3, to analyze the power division ratio.

The coupling slot is similar to slot antenna, which is matched to the required frequency by the length $2l$ and off-set x_n. Theoretically, the coupling slot should

TABLE 8.1: Design parameters of the proposed T-junction power divider.

Parameters	Values (mm)
a	22.86
b	10.16
L_{PD}	49.32
L_{SIW}	98.64
$2l$	11.8
x_n	0.35
h_c	6.08
r_c	1
x_c	2
r_p	4.08

perfectly match to waves propagating in RWG, but it causes transmission losses that are considered as a function of nose-cone parameters especially, the radius of nose-cone. A semi-sphere embedded cylindrical post is also designed between the output ports of power divider to balance power division ratio on both the output ports. The overall design parameters of Fig. 8.3 are listed in Table 8.1 with their respective values.

8.3.2 Results and Discussion

The power divider, shown in Fig. 8.3, is analyzed using the design procedure given in [116] and its characteristics are shown in Fig. 8.5. From the figure, it is observed that the proposed power divider is offering return loss characteristics < -15 dB in the desired frequency band. It can also be observed from Fig. 8.5 that the power is equally distributed on both the output ports.

For the verification of theoretical results, shown in Fig. 8.5, the proposed power divider design is simulated in Ansys HFSS [117] and the results are illustrated in Fig. 8.6(a, b). From Fig. 8.6(a), it is observed that the power divider is operating well in the band of interest, but the power division is unbalanced at the
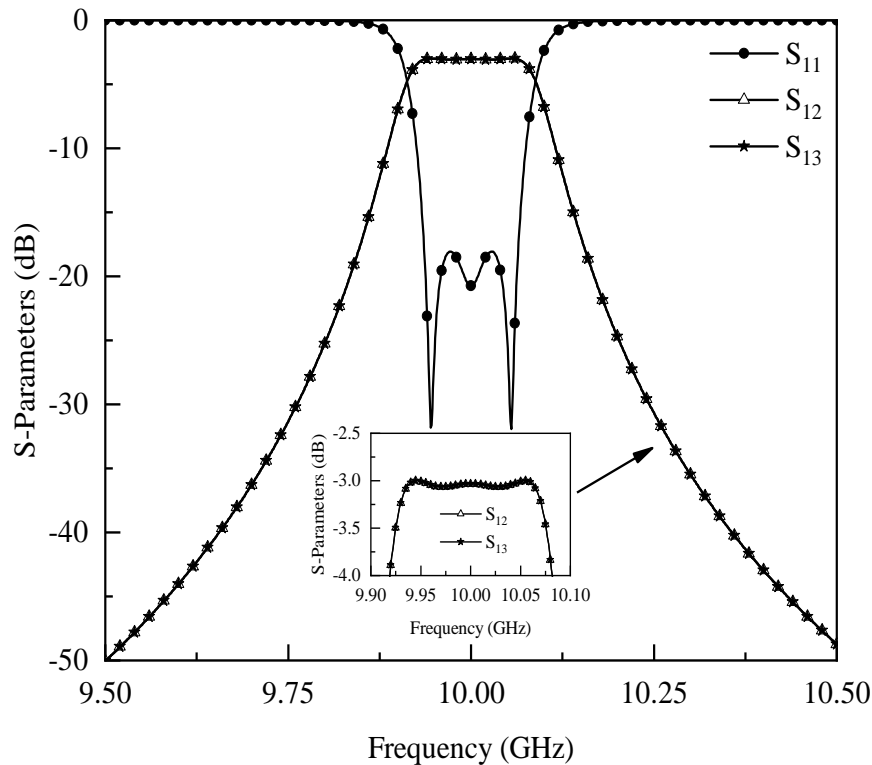
FIGURE 8.5: Theoretical results of the proposed 1×2 T-junction power divider (the inset of figure represents a zoomed view of region of interest).

output ports. To overcome the unbalanced output characteristics, a metallic post, discussed in the previous sub-section, is designed as shown in Fig. 8.3. As a result of this modification, the power is equally distributed at the output ports of power divider with 1 dB dielectric loss, while the return loss characteristics remained unaffected as shown in Fig. 7.3(b).

The prototype of the fabricated T-junction power divider, shown in Fig. 8.4, is measured for the verification of simulation results. Figure 8.7 shows the measured S-parameters of the proposed power divider. It can be observed from the figure that the measured parameters are well in agreement with the simulated one. Some discrepancies are observed between the simulated and the measured results because the cylindrical post is inserted in the T-junction through a soldering process.

Figures 8.8(a) and 8.8(b) show the simulated E-field distribution results of the proposed power divider. From the figures, it can be noted that the use of metallic post between the output ports of the power divider, equally distributes the electric field on RWG power divider as well as on SIW arrays.
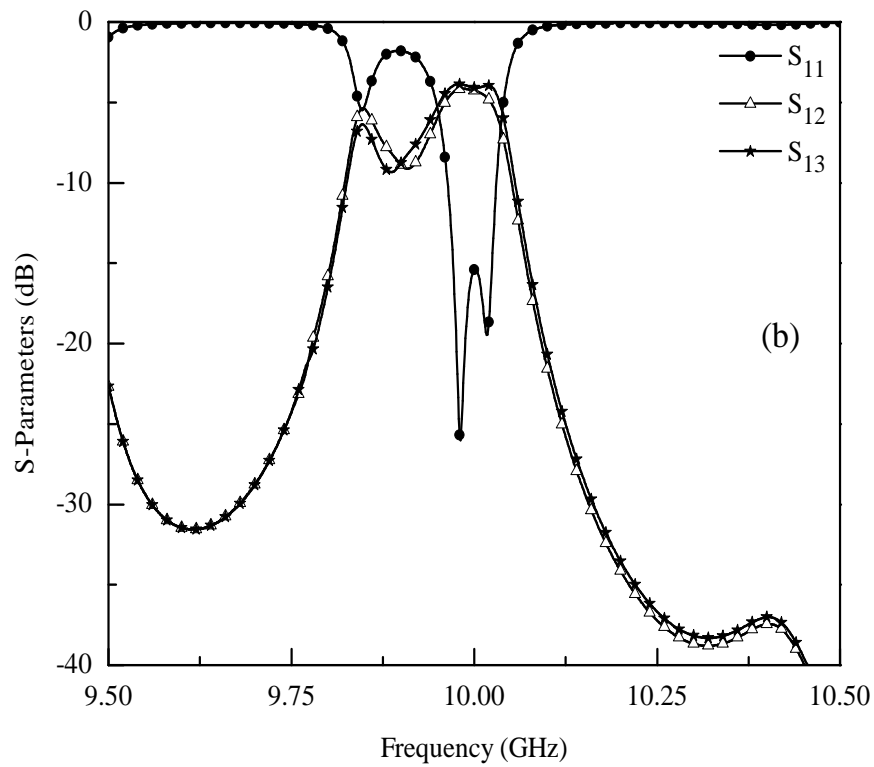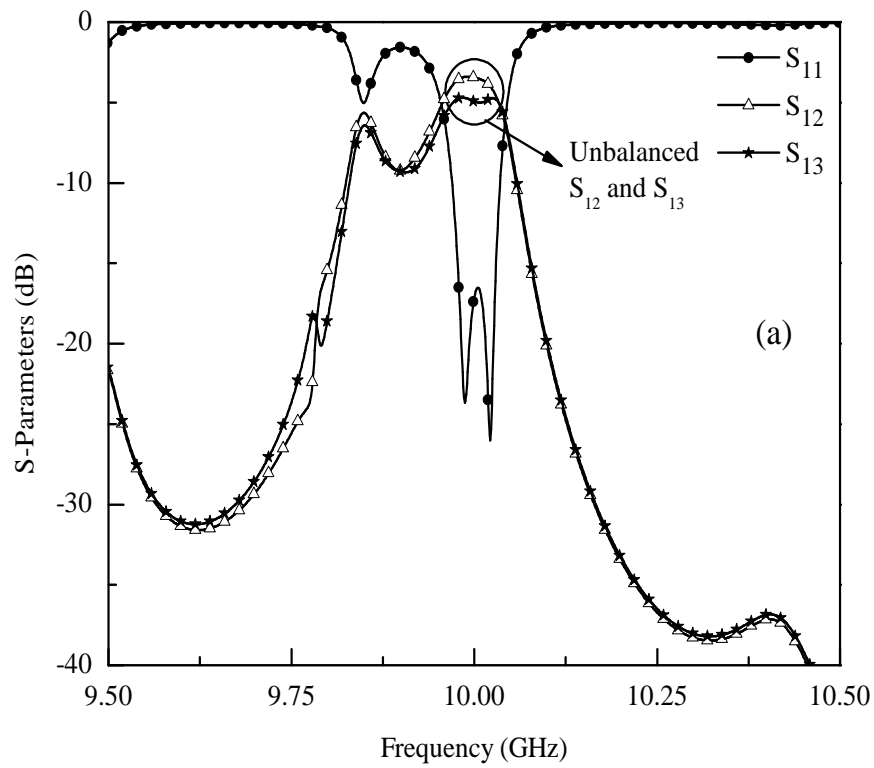
FIGURE 8.6: Full wave EM simulation results of the proposed 1×2 T-junction power divider (a) without cylindrical post (b) with cylindrical post.
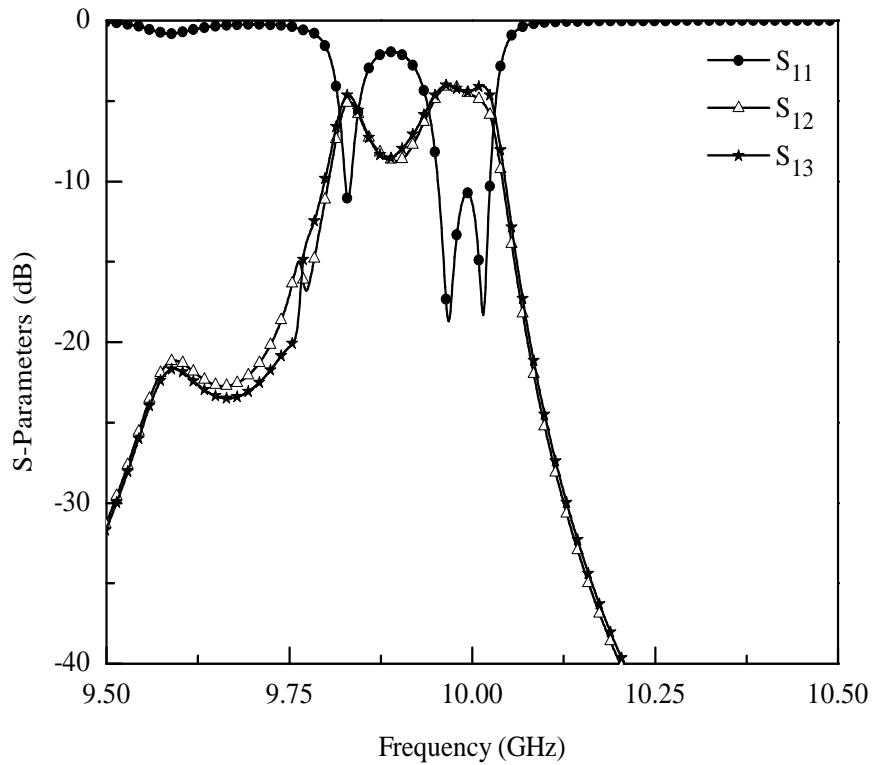
FIGURE 8.7: Measured S-parameters of the proposed 1×2 T-junction power divider.

(a)

(b)
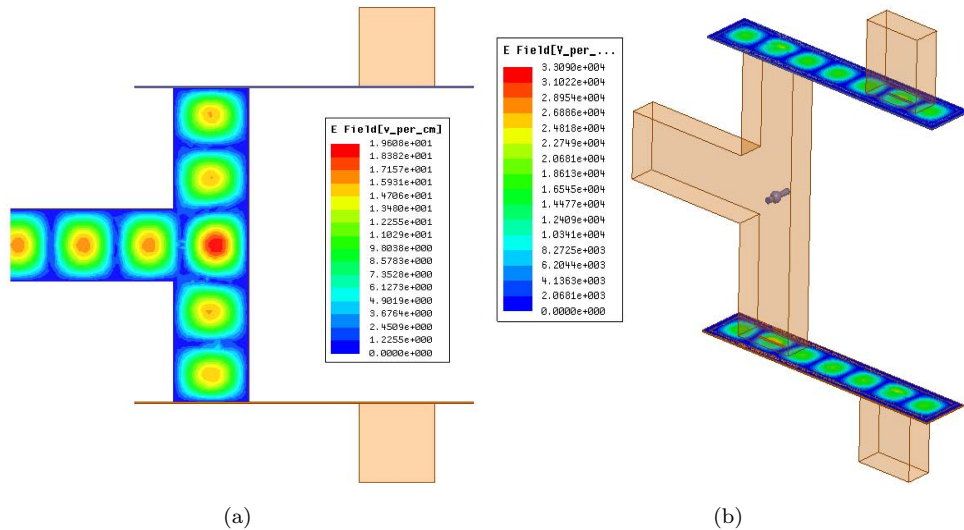
FIGURE 8.8: Electric-field distribution in (a) RWG T-junction power divider (b) SIW.

8.4   Conformal Array Design

SIW based longitudinal slot antenna array is considered a good candidate for RADAR applications due to its shaped radiation pattern (sum or difference) and

high gain. The precise control of the aperture distribution of slot antenna array increased its use in communication systems, as well as in radars.

In this work, SIW based slot antenna array is designed, which contains six elements, shown in Fig. 8.9(a), designed on the top side of Rogers/RT Duroid 5880 substrate having a thickness, $h = 0.508$ mm and relative permittivity, $\varepsilon_r = 2.2$. The conducting via has a diameter of 0.5 mm and the separation between two consecutive vias is 0.9 mm. The conducting vias are arranged in a tapered manner ($\phi = 0.43°$) so that the surface waves can propagate along the conformed array. The tapered width $W(\theta)$ at R_1 is wider than the width at R_2 as shown in Fig. 8.9(a). The distance between slot radiators is taken one half of the guided wavelength at the center frequency of 10 GHz. The width of the SIW array is taken one half of the free space wavelength, shown in Fig. 8.9(a), to avoid the grading lobes generated in H-plane. A coupling slot is designed on the bottom side of the substrate to allow the energy to couple for radiating slots.

Figure 8.9(b) shows a side view of the proposed antenna system. From the figure, it can be seen that two slotted arrays are placed on a nose-conical surface having lower radius, $R_1 = 4\lambda_0$ and upper radius, $R_2 = 5\lambda_0$ at $\phi = 0°$ and 180°, respectively. The length of the conducting conical platform is chosen to be $5\lambda_g$. To feed both the arrays, 1×2 T-junction power divider is used whose detail is given in the previous section.

The feeding slots, in a T-junction power divider, are $3\lambda_g/4$ away from the first element both for $\phi = 0°$ and 180° positions and is fed with the antipodal EM waves. This effect was taken into account by alternating slot off-sets in the sub-arrays as shown in Fig. 8.9(a).

The prototype of the proposed nose-cone conformal SIW antenna array is shown in Fig. 8.10. Four major steps are involved in the fabrication of the proposed antenna array. First, fabrication of SIW slot antenna array involves the etching of slot elements, drilling, and metallization of via holes. Second, a cone is fabricated by wrapping a metal sheet of thickness 14 AWG according to design parameters shown in Fig. 8.9. Third, the proposed T-junction power divider, shown in Fig.

, is placed on the lower side of conformed SIW slotted arrays through a machined window in the cone, while an SMA connector is inserted at a distance of $\lambda_g/4$ from shorted end of a waveguide. The last step is to wrap SIW based slot antenna array on the conical surface to excite the feeding slots.
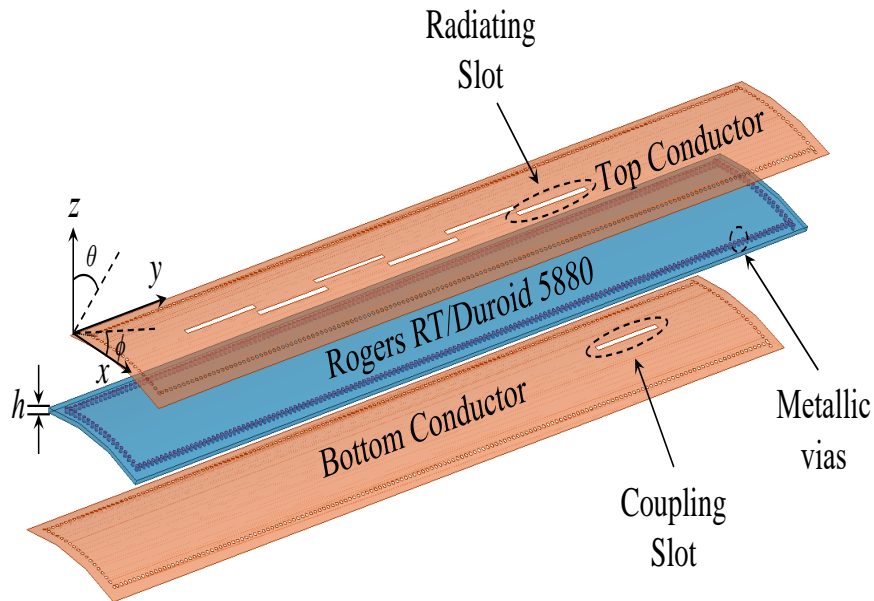
(a)
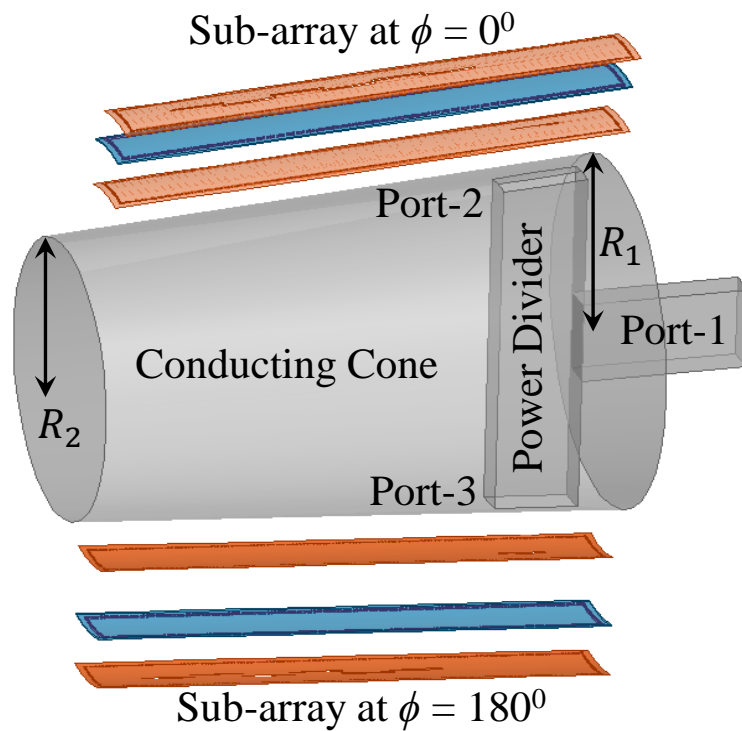
(b)

FIGURE 8.9: (a) Design of the proposed slot antenna array. (b) Side view of the proposed antenna system.

(a)
(b)
(c)

FIGURE 8.10: Fabricated prototype of the proposed conformal slot antenna array (a) sub-array 1 (b) sub-array 2 (c) side view including T-junction power divider.

8.4.1 Results and Discussion

Initially, the array is synthesized using MLS algorithm [17] by complying to -20 dB SLL criterion. After that, the proposed antenna system is simulated in Ansys HFSS, a commercially available electromagnetic software. Figure 8.11 shows return loss results of the proposed conformal array. It is observed from the results that the designed array is resonating well in the band of interest, and has an impedance bandwidth of 127 MHz in the frequency range of 9.917-10.044 GHz. To verify the results obtained from HFSS simulation, the proposed design is measured
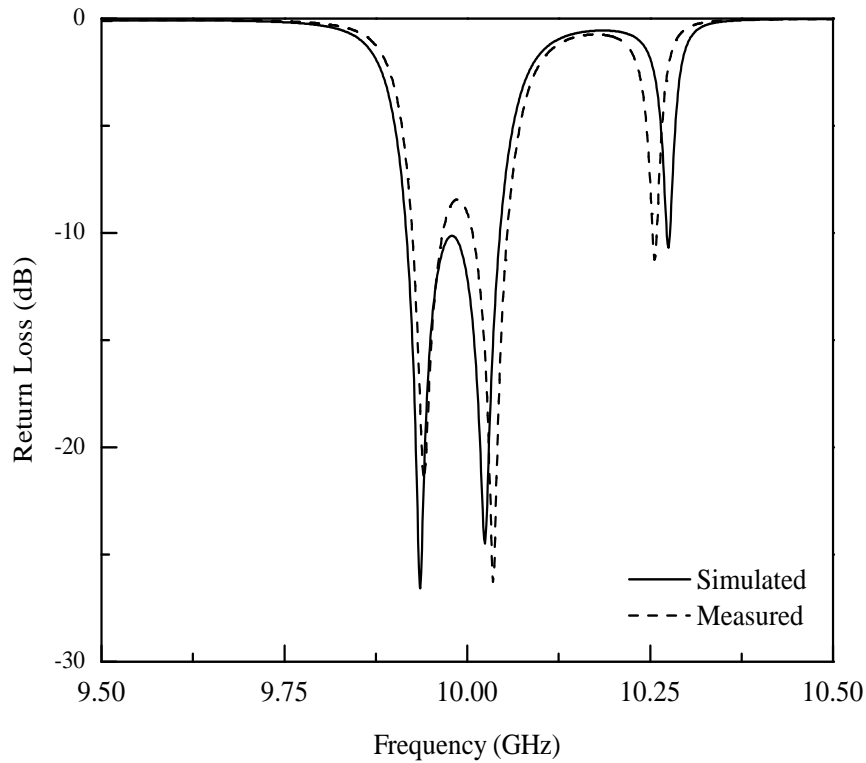
FIGURE 8.11: Return loss characteristics of the proposed slot antenna array.

using Agilent Technologies N5232A VNA, and the result is also shown in Fig. 8.11. From the figure, it is observed that the return loss characteristics obtained from measurements are in good agreement with the simulated data. Furthermore, measurements show that the proposed antenna offers two frequency ranges from 9.925 GHz to 9.966 GHz having impedance bandwidth of 41 MHz, and from 10.009 GHz to 10.054 GHz having impedance bandwidth of 45 MHz, respectively, as shown in Fig. 8.11. A minor discrepancy in measured and simulated results is noted, which could be associated with fabrication tolerance because the power divider is installed in the conical platform using gas welding process. Furthermore, such deficiencies could also arise due to imperfect soldering of the SMA connector.

The simulated and measured results of the H-plane radiation pattern at 10 GHz are shown in Fig. 8.12. It is observed that the antenna offers two main beams located at $\theta = \pm 90°$. The right and left SLLs of main beam located at $\theta = 90°$ are -24.47 dB and -20.12 dB, respectively; while the other beam located at $\theta = -90°$ has SLLs at -22.80 dB and -23 dB, respectively. From Fig. 8.12, one can again observe that the radiation characteristics obtained from simulations and measurements are
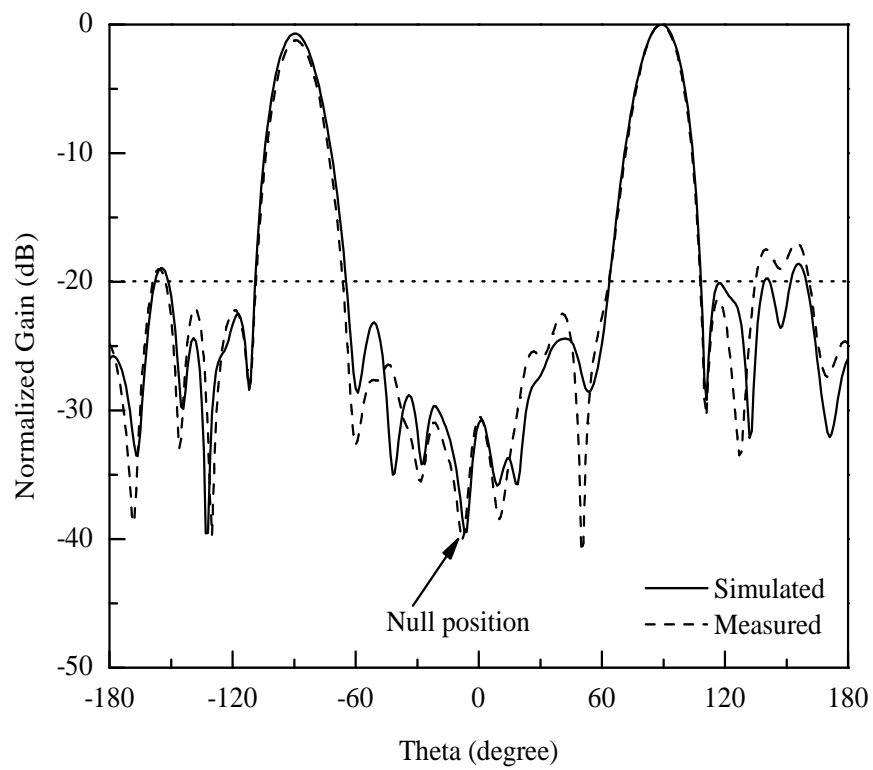
FIGURE 8.12: H-plane radiation pattern of the proposed slot antenna array.
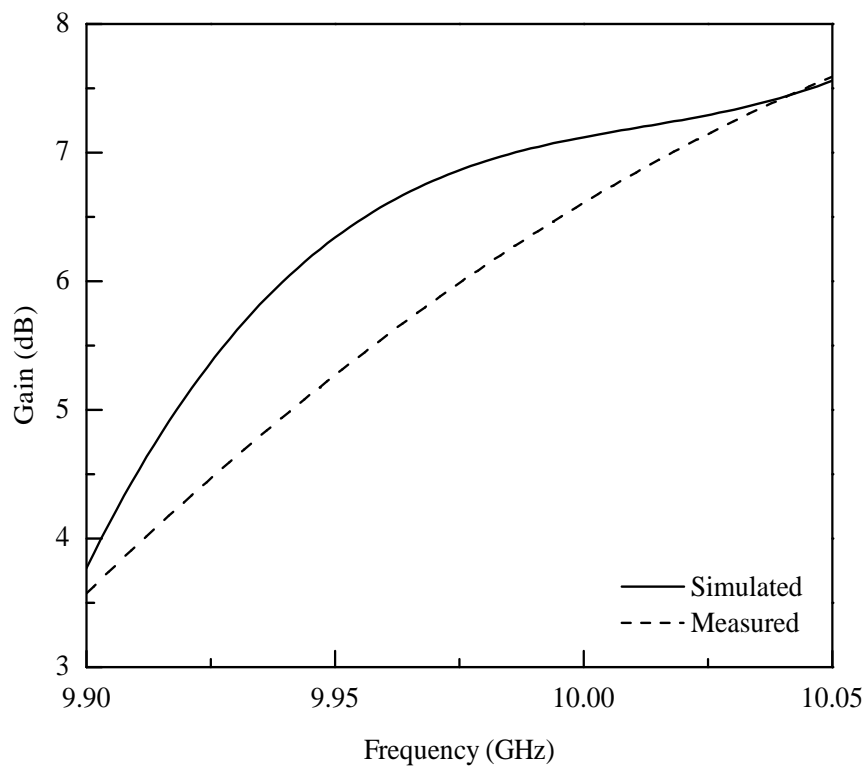
FIGURE 8.13: Simulated gain of a single slotted sub-array.

in good agreement. Figure 8.13 presents the simulated and measured gain of a single slotted sub-array from 9.9 to 10.05 GHz. From Fig. 8.13, it is noted that the gain is increasing with the increase in frequency. At 10 GHz, the simulated gain value is $\approx$ 7dBi, while the measured gain value is 6.72 dBi.

Table 8.2 demonstrates a comparative study between the existing and the proposed conformal arrays. From the data of the table, it can be seen that the designed array utilizes less number of elements than the designs presented in [63, 113, 115], and its performance in terms of SLL is relatively better than the designs presented in [112, 115]. The observed gain is relatively low than Ref. [113], which is close to the proposed array structure in terms of array elements. The same can be improved further by increasing number of elements. Moreover, by utilizing the proposed array design, the beam scanning capabilities can be increased.

TABLE 8.2: Comparison between proposed and previously presented conformal arrays.

Ref.	Array Elements	Frequency (GHz)	SLL (dB)	Gain (dBi)	HPBW (deg)
[63]	16×8	$0.96f_0 - 1.04f_0$	-15.8	25.8	–
[112]	–	1.18−1.36	-20	–	–
[113]	1×8	35	-28	9.9	–
[115]	10×10	10.05	-20	19.3	12
Proposed	1×6	10	-22.80	6.72	16

8.5   Summary

This chapter presents a design of a nose-cone conformal SIW slot antenna array for tracking applications. A balanced 1×2 T-junction power divider is also designed to feed the sub-arrays located on both sides of the conical platform. Results showed that the designed conformal antenna system has two broadside main beams located at $\theta = \pm 90°$ with SLLs of -22.80 dB and -20.12 dB, respectively; which is useful to track multiple targets on broadside. Furthermore, the proposed antenna system

is fabricated and measured, and it is observed that the simulated and measured characteristics are in good conformity.

Chapter 9

Conclusion and Future Work

Conformal array antennas have been the topic of great interest for aerodynamic applications, because they can easily be integrated on the surface of aircraft and UAVs. Furthermore, SIW based conformal array antennas are considered to be good candidates for airborne applications. For this purpose, different conformal array designs have been presented in this thesis, which can easily be used for airborne and radar applications.

It has been described that the demand of domestic purpose UAVs is increasing day-by-day, and the issue for accuracy of instrumentation landing systems needs to be improved to ensure the human safety during landing. So, there is a need to design an antenna array, which can provide both $\sum$ and Δ radiation characteristics. Therefore, for this purpose, in the 1$^{\text{st}}$ part of this research, a planar slotted array is designed and simulated to generate $\sum$ and Δ radiation patterns. The presented array is synthesized by using the design principle presented by Elliot to generate $\sum$ pattern. On the other hand, Bayliss's current distribution is used to generate an H-plane Δ pattern. The results obtained from the designed array are in good agreement with theoretical data. It is also observed from the presented results that the gain of the proposed array for Δ pattern array is 8 dBi and has a SLL of -23 dB. In Δ pattern, the principle null of the main beam is located at 0°. On the other hand, the simulated gain of $\sum$ pattern array is 11.75 dBi and observed SLL is -8 dB directed to 50°.

From the above presented results, it is observed that the SLL of $\sum$ pattern array is high. Therefore, in the 2nd part of this work, a slotted array is designed with the aim to improve the SLL of $\sum$ pattern slotted array. This part is further divided into two sub-sections such as the optimization of array parameter through PSO, while the second sub-section consists of the design and simulation of the optimized array. A number of linear arrays have been synthesized and optimized to achieve minimum SLL with high gain. After that, two design examples have been simulated with optimized parameters for -20 dB and -30 dB SLLs. Finally, the $\sum$ radiation pattern arrays, which were synthesized through the earlier mentioned optimization have been designed and simulated, and it is observed that the designed arrays offer significantly low SLLs of -18.59 dB and -26.99 dB, respectively.

In the modern era of communication systems, CubeSats have widely been used for space missions. The use of CubeSats is a more affordable solution for deep space and remote sensing applications compared to conventionally used satellites. Normally, CubeSats are deployed at lower earth orbit for applications like earth imaging, and weather forecast applications, etc. The major problem in utilizing CubeSats is that the information signals can suffer from path loss. To overcome this issue, the antenna system of CubeSats needs to be efficient. In order to meet these requirements, in the 3rd part of this thesis, an SIW based slotted array is designed with a broadband feeding network for CubeSats applications. A dumbbell-shaped coupling slot is introduced, which is designed on another SIW placed at the lower side of the radiating part. The proposed array is designed and simulated in Ansys HFSS, and it is observed that the SLL, H-plane gain, and VSWR are -19.62 dB, 11.15 dBi, and $\leq$2, respectively; at a center frequency of 10 GHz. Furthermore, from the presented results, it is observed that the designed slotted array offers wide operational bandwidth compared to conventional slot arrays.

In modern aircraft, the antenna system must integrate on the curved surface to decrease the drag and fuel consumption. Therefore, the perfect attachment of antenna arrays on the surface of an aircraft can be achieved by using flexible and low profile antennas. In the 4th part of this research work, a cylindrical

conformal SIW slot array antenna for X-band applications is presented. RWG to SIW feeding structure is used to excite SIW based slot array of 1×6 elements. In fact, the response of conformal SIW keeps on changing along the cross-section of the cylinder, which contributes to the total design error. Therefore, an error function has been designed and optimized. Furthermore, the designed array has been optimized using MLS algorithm. From the presented results, it is observed that the proposed SIW based slot array antenna on cylindrical surface offers a gain and SLL of 9.8 dBi and -21.72 dB, respectively; at a center frequency of 10 GHz.

In the current state of conformal arrays, there is a need to investigate the integration of antenna arrays on the surface of high-speed jets. Owing to this, in the 5$^{\text{th}}$ part, a nose-cone conformal SIW slotted array is designed, fabricated and characterized at X-band. Since, the conical surface is an essential part of aerodynamic applications such as space rockets, supersonic aircraft, and missiles therefore, design consideration of nose-cone conformal SIW is emphasized in this work. It has been investigated through EM simulation that the propagation constant will change with the increase in length of SIW along the direction of nose-cone. Therefore, a modification in SIW design has been proposed in order to get constant wave propagation along the conformed surface. A design process is also proposed for a doubly curved surface. Furthermore, RWG is integrated for the feeding of a conformal array. The nose-cone conformal SIW slot array antenna is validated through fabrication, and a good agreement is observed between measured and simulated data.

Moreover, the simulated radiation characteristics of the proposed array are compared with planar and cylindrical conformal arrays, and it is observed that the proposed nose-cone conformal array offers relatively high gain (11.91 dBi) with low SLLs (-20.82 dB). The presented study demonstrates that the proposed antenna array can be utilized in modern radars, and on the conical surface of aircraft and missiles.

In the last part of this thesis, a conical conformal slot array antenna is presented for multi-target tracking applications. Two conformal slotted arrays of 1×6 elements

are used to achieve dual-beam response. A balanced 1×2 T-junction power divider is designed to feed the sub-arrays located on both sides of the conical platform. The simulated results show that the designed conformal antenna system has two main beams located at $\theta = \pm90°$ with SLLs of -22.80 dB and -20.12 dB, respectively; which is useful to track multiple targets at a time. Furthermore, the proposed antenna system is fabricated and measured, and it is observed that the simulated and measured characteristics are in good agreement.

9.1   Future Recommendations

The current research can be extended further into following possible areas:

i. The cylindrical and nose-cone conformal slot array antenna designs can be modified to achieve electronic beam scanning capability. In order to achieve above mentioned requirement, an SIW based slotted array needs to be designed with phase shifting capabilities. This kind of conformal antenna can also be utilized in early warning systems for airborne applications. Furthermore, for high gain, the large number of antenna elements can conform on the surface of an aircraft.

ii. The design of a multi-band circularly polarized conformal antenna array for satellite applications can be considered for future work. For this particular application, the array must be efficient in terms of axial ratio and gain.

iii. The use of ink-jet printed conformal antennas is increasing day-by-day due to their low fabrication cost and easy installation on any surface. This kind of array can be useful for health monitoring applications, e.g. breast and brain cancer detection.

Bibliography

[1] R. J. Mailloux, *Conformal Array Antenna Theory and Design: Reviews and Abstracts*, vol. 49. Wiley-Interscience Publication, Oct 2007.

[2] H. Chireix, "Antennes à rayonnement zénithal réduit,," *L'Onde Electrique*, vol. 15, pp. 440–456, 1936.

[3] H. L. Knudsen, "The field radiated by a ring quasi-array of an infinite number of tangential or radial dipoles," *Proceedings of the IRE*, vol. 41, no. 6, pp. 781–789, 1953.

[4] P. J. D. Gething, "High-frequency direction finding," *Proceedings of the Institution of Electrical Engineers*, vol. 113, no. 1, pp. 49–61, 1966.

[5] A. Hessel, "Mutual coupling effects in circular arrays on cylindrical surfaces-aperture design implications and analysis," in *Proceedings of Phased Array Symposium*, Polytechnic Institute of Brooklyn., 1970.

[6] E. Christopher, "Electronically scanned TACAN antenna," *IEEE Transactions on Antennas and Propagation*, vol. 22, no. 1, pp. 12–16, 1974.

[7] J. Colin, "Phased array radars in france: Present and future," in *Proceedings of International Symposium on Phased Array Systems and Technology*, pp. 458–462, 1996.

[8] S. V. Bearse, "Planar array looks through lens to provide hemispherical coverage," *Microwaves*, vol. July, pp. 9–10, 1975.

[9] P. Knott, C. Loker, and S. Algermissen, "Antenna element design for a conformal antenna array demonstrator," in *2011 Aerospace Conference*, pp. 1–5, March 2011.

[10] J. F. Xu, W. Hong, P. Chen, and K. Wu, "Design and implementation of low sidelobe substrate integrated waveguide longitudinal slot array antennas," *IET Microwaves, Antennas Propagation*, vol. 3, no. 5, pp. 790–797, 2009.

[11] L. Li, X. Chen, R. Khazaka, and K. Wu, "A transition from substrate integrated waveguide (SIW) to rectangular waveguide," in *2009 Asia Pacific Microwave Conference*, pp. 2605–2608, Dec 2009.

[12] M. Ohira, A. Miura, and M. Ueba, "60-GHz wideband substrate-integrated-waveguide slot array using closely spaced elements for planar multisector antenna," *IEEE Transactions on Antennas and Propagation*, vol. 58, no. 3, pp. 993–998, 2010.

[13] D. Kim, W. Chung, C. Park, S. Lee, and S. Nam, "A series slot array antenna for 45 °-inclined linear polarization with SIW technology," *IEEE Transactions on Antennas and Propagation*, vol. 60, no. 4, pp. 1785–1795, 2012.

[14] E. Gandini, M. Ettorre, M. Casaletti, K. Tekkouk, L. L. Coq, and R. Sauleau, "SIW slotted waveguide array with pillbox transition for mechanical beam scanning," *IEEE Antennas and Wireless Propagation Letters*, vol. 11, pp. 1572–1575, 2012.

[15] J. Wei, Z. N. Chen, X. Qing, J. Shi, and J. Xu, "Compact substrate integrated waveguide slot antenna array with low back lobe," *IEEE Antennas and Wireless Propagation Letters*, vol. 12, pp. 999–1002, 2013.

[16] M. Karami, R. A. Sadeghzadeh, M. Noferesti, and M. Chegeni, "Suppressed back-lobe substrate-integrated waveguide slot array antenna for X-band," *Electronics Letters*, vol. 51, no. 11, pp. 811–813, 2015.

[17] S. E. Hosseininejad and N. Komjani, "Optimum design of traveling-wave SIW slot array antennas," *IEEE Transactions on Antennas and Propagation*, vol. 61, pp. 1971–1975, April 2013.

[18] J. Xu, Z. N. Chen, and X. Qing, "Cpw center-fed single-layer siw slot antenna array for automotive radars," *IEEE Transactions on Antennas and Propagation*, vol. 62, pp. 4528–4536, Sep. 2014.

[19] M. I. Nawaz, Z. Huiling, and M. Kashif, "Substrate integrated waveguide (SIW) to microstrip transition at X-band," in *Proceedings of the 2014 International Conference on Circuits, Systems and Control*, pp. 61–63, 2014.

[20] A. Mallahzadeh and S. Mohammad-Ali-Nezhad, "A low cross-polarization slotted ridged SIW array antenna design with mutual coupling considerations," *IEEE Transactions on Antennas and Propagation*, vol. 63, no. 10, pp. 4324–4333, 2015.

[21] L. Qiu, K. Xiao, S. L. Chai, H. Y. Qi, and J. J. Mao, "A double-layer shaped-beam traveling-wave slot array based on SIW," *IEEE Transactions on Antennas and Propagation*, vol. 64, no. 11, pp. 4639–4647, 2016.

[22] P. Wu, S. Liao, and Q. Xue, "A substrate integrated slot antenna array using simplified feeding network based on higher order cavity modes," *IEEE Transactions on Antennas and Propagation*, vol. 64, no. 1, pp. 126–135, 2016.

[23] I. Mohamed and A. Sebak, "Linearly tapered slot antenna array with SIW feed network for 60 GHz applications," in *2016 17th International Symposium on Antenna Technology and Applied Electromagnetics (ANTEM)*, pp. 1–2, 2016.

[24] Y. Wen, B. Wang, and X. Ding, "Wide-beam SIW-slot antenna for wide-angle scanning phased array," *IEEE Antennas and Wireless Propagation Letters*, vol. 15, pp. 1638–1641, 2016.

[25] F. Cao, D. Yang, J. Pan, D. Geng, and H. Xiao, "A compact single-layer substrate-integrated waveguide (SIW) monopulse slot antenna array," *IEEE Antennas and Wireless Propagation Letters*, vol. 16, pp. 2755–2758, 2017.

[26] Nasimuddin, X. Qing, and Z. N. Chen, "A tapered leaky-wave slot antenna with wideband boresight radiation," in *2017 Progress in Electromagnetics Research Symposium - Fall (PIERS - FALL)*, pp. 2936–2939, Nov 2017.

[27] D. Yang, F. Cao, and J. Pan, "A single-layer dual-frequency shared-aperture SIW slot antenna array with a small frequency ratio," *IEEE Antennas and Wireless Propagation Letters*, vol. 17, no. 6, pp. 1048–1051, 2018.

[28] P. Vasina, T. Mikulasek, J. Lacik, and H. Arthaber, "Beam- and polarisation-reconfigurable SIW ring-slot antenna array," *IET Microwaves, Antennas Propagation*, vol. 12, no. 15, pp. 2313–2319, 2018.

[29] Y. Li and Y. Li, "Investigation on SIW slot antenna array with beam scanning ability," *International Journal of Antennas and Propagation*, vol. Vol. 2019, pp. 1–8, 2019.

[30] Z. Wang, X. Dai, and W. Sun, "Tri-beam slot antenna array based on substrate integrated waveguide (SIW) technology," *International Journal of Microwave and Wireless Technologies*, vol. 12, no. 3, p. 246–251, 2020.

[31] A. Herschlein, G. Gottwald, and W. Wiesbeck, "Patch antennas on finite and infinite cylindrical surface structures," in *Proceedings of International Symposium on Phased Array Systems and Technology*, pp. 168–170, 1996.

[32] Niu Jun-wei and Zhong Shun-shi, "Cylindrical conformal microstrip bow-tie antennas," in *6th International SYmposium on Antennas, Propagation and EM Theory*, pp. 74–76, 2003.

[33] Q. Wu, F. Sun, J. Fu, Z. Feng, and G. Yang, "A cylindrical conformal 2×2 microstrip antenna array," in *2007 Asia-Pacific Microwave Conference*, pp. 1–4, 2007.

[34] A. Traille, J. Ratner, G. D. Hopkins, and V. Tripp, "Development of a novel faceted, conformal, slotted-waveguide subarray for sensor applications with full 360^0 azimuth tracking capabilities," in *2007 IEEE Antennas and Propagation Society International Symposium*, pp. 3828–3831, June 2007.

[35] L. Song, S. Fu, Q. Fang, and Q. Wu, "Performance simulation and analysis of two kinds of cylindrical conformal microstrip Yagi antennas," in *2009 3rd IEEE International Symposium on Microwave, Antenna, Propagation and EMC Technologies for Wireless Communications*, pp. 576–579, 2009.

[36] C.-H. Ahn, Y.-J. Ren, and K. Chang, "A dual-polarized cylindrical conformal array antenna suitable for unmanned aerial vehicles," *International Journal of RF & Microwave Computer-Aided Engineering*, vol. 21, pp. 91–98, 2010.

[37] Z. Zhang, X. Gao, W. Chen, Z. Feng, and M. F. Iskander, "Study of conformal switchable antenna system on cylindrical surface for isotropic coverage," *IEEE Transactions on Antennas and Propagation*, vol. 59, no. 3, pp. 776–783, 2011.

[38] Y. Y. Liu, M. Guo, and S. S. Zhong, "Conformal slotted waveguide array antenna," in *2012 IEEE International Workshop on Antenna Technology (iWAT)*, pp. 56–59, March 2012.

[39] K. Labowski, C. Penney, and J. F. Stack Jr, "Conformal antenna array design on a missile platform," *Microwave Journal*, vol. 56, no. 1, pp. 112–113, 2013.

[40] O. Bayraktar and O. A. Civi, "Circumferential traveling wave slot array on cylindrical substrate integrated waveguide (CSIW)," *IEEE Transactions on Antennas and Propagation*, vol. 62, pp. 3557–3566, July 2014.

[41] A. J. Martinez-Ros, J. L. Gómez-Tornero, and G. Goussetis, "Conformal tapered substrate integrated waveguide leaky-wave antenna," *IEEE Transactions on Antennas and Propagation*, vol. 62, pp. 5983–5991, Dec 2014.

[42] J. Wang, W. Cao, S. Li, X. Yu, X. Gao, and Y. Jiang, "Design and simulation of cylindrical conformal traveling wave slot array antenna at 35 GHz," in *2015 IEEE International Conference on Communication Problem-Solving (ICCP)*, pp. 294–296, Oct 2015.

[43] K. K. Fan and Z.-C. Hao, "Cylindrical conformal array antenna with tilted h-plane fan-shaped beam for millimeter-wave application," *Microwave and Optical Technology Letters*, vol. 58, no. 7, pp. 1666–1671, 2016.

[44] H. Yang, Z. Jin, G. Montisci, Y. Liu, X. He, G. A. Casula, and G. Mazzarella, "Design equations for cylindrically conformal arrays of longitudinal slots," *IEEE Transactions on Antennas and Propagation*, vol. 64, pp. 80–88, Jan 2016.

[45] L. Tao, S. Lizhong, L. Shangji, W. Yongjian, and L. Zexiu, "Novel conformal vivaldi antenna fed by CPW," in *2016 IEEE International Conference on Microwave and Millimeter Wave Technology (ICMMT)*, vol. 2, pp. 725–727, June 2016.

[46] X. Chen, J. Su, L. Han, X. Chen, and W. Zhang, "A conformal antenna array with coplanar waveguide series feed configuration," in *2016 IEEE International Conference on Computational Electromagnetics (ICCEM)*, pp. 275–277, Feb 2016.

[47] N. Agnihotri, K. G. S, K. Veeramalai, A. Prasanna, and S. S. Siddiq, "Super wideband conformal antenna array on cylindrical surface," in *21st International Conference on Microwave, Radar and Wireless Communications (MIKON)*, pp. 1–4, May 2016.

[48] T. Pelham, G. Hilton, E. Mellios, and R. Lewis, "Predicting conformal aperture gain from 3D aperture and platform models," *IEEE Antennas and Wireless Propagation Letters*, vol. PP, no. 99, pp. 1–1, 2016.

[49] M. Angelilli, L. Infante, and P. Pacifici, "A family of secondary surveillance radars based on conformal antenna array geometries," in *2017 IEEE Radar Conference (RadarConf)*, pp. 1681–1684, May 2017.

[50] Y. Liu, H. Yang, Z. Jin, F. Zhao, and J. Zhu, "A multibeam cylindrically conformal slot array antenna based on a modified rotman lens," *IEEE Transactions on Antennas and Propagation*, vol. 66, pp. 3441–3452, July 2018.

[51] I. Serhsouh, H. Lebbar, and M. Himdi, "A new design of reconfigurable SIW antenna conformal to cylindrical surface," in *2018 International Symposium on Advanced Electrical and Communication Technologies (ISAECT)*, pp. 1–4, 2018.

[52] A. Munger, G. Vaughn, J. Provencher, and B. Gladman, "Conical array studies," *IEEE Transactions on Antennas and Propagation*, vol. 22, no. 1, pp. 35–43, 1974.

[53] D. Augustin, R. Staraj, and E. Cambiaggio, "Performance of an original microstrip ring array antenna laid on a conical structure," in *1995 Ninth International Conference on Antennas and Propagation*, vol. 1, pp. 423–427 vol.1, 1995.

[54] Y. Yu and W. Wu, "Analysis of millimeter wave conformal antenna array on conical surface," in *2006 Joint 31st International Conference on Infrared Millimeter Waves and 14th International Conference on Teraherz Electronics*, pp. 280–280, 2006.

[55] T. E. Morton and K. M. Pasala, "Performance analysis of conformal conical arrays for airborne vehicles," *IEEE Transactions on Aerospace and Electronic Systems*, vol. 42, no. 3, pp. 876–890, 2006.

[56] T. Kaifas, K. Siakavara, E. Vafiadis, T. Samaras, and J. Sahalos, "On the design of conformal slot arrays on a perfectly conducting elliptic cone," *Electrical Engineering*, vol. 89, no. 2, pp. 95–105, 2006.

[57] M. Liu, Z. Feng, and Q. Wu, "Design of a millimeter-wave conformal low sidelobe microstrip antenna array on a cone surface," in *2008 China-Japan Joint Microwave Conference*, pp. 121–124, 2008.

[58] X. Zhang, X. Ma, and Q. Lai, "Two kind of conical conformal GPS antenna arrays on projectile," in *2009 3rd IEEE International Symposium on Microwave, Antenna, Propagation and EMC Technologies for Wireless Communications*, pp. 659–662, 2009.

[59] M. Li, L. Xu, W. B. Zeng, and G. Liu, "Design and implementation of a new missile-borne conical conformal antenna.," in *PIERS Proceedings*, 2014.

[60] A. K. Aboul-Seoud, A. D. S. Hafez, A. M. Hamed, and M. Abd-El-Latif, "A conformal conical phased array antenna for modern radars," in *2014 IEEE Aerospace Conference*, pp. 1–7, March 2014.

[61] V. Jaeck, L. Bernard, K. Mahdjoubi, R. Sauleau, S. Collardey, P. Pouliguen, and P. Potier, "A conical patch antenna array for agile point-to-point communications in the 5.2-GHz band," *IEEE Antennas and Wireless Propagation Letters*, vol. 15, pp. 1230–1233, 2016.

[62] Z. Chen and Z. Shen, "Conformal cavity-backed slot antenna embedded in a conical platform for end-fire radiation," in *2017 IEEE International Symposium on Antennas and Propagation USNC/URSI National Radio Science Meeting*, pp. 2239–2240, 2017.

[63] Y. F. Wu and Y. J. Cheng, "Conical conformal shaped-beam substrate integrated waveguide slot array antenna with conical-to-cylindrical transition," *IEEE Transactions on Antennas and Propagation*, vol. PP, no. 99, pp. 1–1, 2017.

[64] H. Xu, B. Zhang, J. Duan, J. Cui, Y. Xu, Y. Tian, L. Yan, M. Xiong, and Q. Jia, "Wide solid angle beam-switching conical conformal array antenna with high gain for 5G applications," *IEEE Antennas and Wireless Propagation Letters*, vol. 17, no. 12, pp. 2304–2308, 2018.

[65] Y. Gao, W. Jiang, T. Hong, and S. Gong, "A high-gain conical conformal antenna with circularly polarization and axial radiation in X-band," in *2019 13th European Conference on Antennas and Propagation (EuCAP)*, pp. 1–4, 2019.

[66] Y. Xiaole, N. Daning, L. Shaodong, L. Zhengjun, and W. Wutu, "Design of a wideband waveguide slot array antenna and its decoupling method for synthetic aperture radar," in *38th European Microwave Conference*, pp. 135–138, Oct 2008.

[67] R. Elliott and L. Kurtz, "The design of small slot arrays," *IEEE Transactions on Antennas and Propagation*, vol. 26, pp. 214–219, Mar 1978.

[68] R. S. Elliot, *Antenna theory and design.* John Wiley & Sons, 2006.

[69] P. Rocca, L. Manica, L. Poli, and A. Massa, "Synthesis of compromise sum-difference arrays through time-modulation," *IET Radar, Sonar Navigation*, vol. 3, no. 6, pp. 630–637, 2009.

[70] J. Liu, Z. Zhao, K. Yang, and Q. H. Liu, "Sum and difference pattern synthesis with antenna correction," in *2014 IEEE Antennas and Propagation Society International Symposium (APSURSI)*, pp. 113–114, 2014.

[71] J. R. Mohammed, ""an alternative method for difference pattern formation in monopulse antenna,," *Progress In Electromagnetics Research Letters*, vol. 42, pp. 45–54, 2013.

[72] S. Sekretarov and D. M. Vavriv, "A wideband slotted waveguide antenna array for sar systems," *Progress In Electromagnetics Research M*, vol. 11, pp. 165–176, 2010.

[73] R. Elliott and W. O'Loughlin, "The design of slot arrays including internal mutual coupling," *IEEE Transactions on Antennas and Propagation*, vol. 34, pp. 1149–1154, Sep 1986.

[74] R. Elliott, "An improved design procedure for small arrays of shunt slots," *IEEE Transactions on Antennas and Propagation*, vol. 31, pp. 48–53, Jan 1983.

[75] M. Orefice and R. S. Elliott, "Design of waveguide-fed series slot arrays," *Microwaves, Optics and Antennas, IEE Proceedings H*, vol. 129, pp. 165–169, August 1982.

[76] T. Girard, R. Staraj, E. Cambiaggio, and F. Muller, "A simulated annealing algorithm for planar or conformal antenna array synthesis with optimized polarization," *Microwave and Optical Technology Letters*, vol. 28, no. 2, pp. 86–89, 2001.

[77] D. Marcano and F. Duran, "Synthesis of antenna arrays using genetic algorithms," *IEEE Antennas and Propagation Magazine*, vol. 42, pp. 12–20, June 2000.

[78] D. I. Abu-Al-Nadi, T. H. Ismail, and M. J. Mismar, "Synthesis of linear array and null steering with minimized side-lobe level using particle swarm optimization," in *Proceedings of the Fourth European Conference on Antennas and Propagation*, pp. 1–4, April 2010.

[79] M. M. Khodier and C. G. Christodoulou, "Linear array geometry synthesis with minimum sidelobe level and null control using particle swarm optimization," *IEEE Transactions on Antennas and Propagation*, vol. 53, pp. 2674–2679, Aug 2005.

[80] J. Song, H. Zheng, and L. Zhang, "Application of particle swarm optimization algorithm and genetic algorithms in beam broadening of phased array antenna," in *2010 International Symposium on Signals, Systems and Electronics*, vol. 1, pp. 1–4, Sep. 2010.

[81] X. Li and M. Yin, "Optimal synthesis of linear antenna array with composite differential evolution algorithm," *Scientia Iranica*, vol. 19, no. 6, pp. 1780 – 1787, 2012.

[82] B. Goswami and D. Mandal, "A genetic algorithm for the level control of nulls and side lobes in linear antenna arrays," *Journal of King Saud University - Computer and Information Sciences*, vol. 25, no. 2, pp. 117 – 126, 2013.

[83] S. K. Goudos, K. A. Gotsis, K. Siakavara, E. E. Vafiadis, and J. N. Sahalos, "A multi-objective approach to subarrayed linear antenna arrays design

based on memetic differential evolution," *IEEE Transactions on Antennas and Propagation*, vol. 61, pp. 3042–3052, June 2013.

[84] A. Bhargav and N. Gupta, "Multiobjective genetic optimization of nonuniform linear array with low sidelobes and beamwidth," *IEEE Antennas and Wireless Propagation Letters*, vol. 12, pp. 1547–1549, 2013.

[85] G. Ram, D. Mandal, R. Kar, and S. P. Ghoshal, "Optimized hyper beamforming of receiving linear antenna arrays using firefly algorithm," *International Journal of Microwave and Wireless Technologies*, vol. 6, no. 2, p. 181–194, 2014.

[86] A. Banookh and M. Barakati, "Optimal design of double folded stub microstrip filter by neural network modelling and particle swarm optimization," *Journal of Microwaves, Optoelectronics and Electromagnetic Applications*, vol. 11, pp. 204–213, 06 2012.

[87] A. Sharaqa and N. Dib, "Design of linear and elliptical antenna arrays using biogeography based optimization," *Arabian Journal for Science and Engineering*, vol. 39, pp. 2929–2939, 04 2013.

[88] R. Formato, "Central force optimization," 11 2015.

[89] P. Clark, "Using the cubesat paradigm for lunar orbiters," in *in Proceedings of Interplanetary Small Satellite Conference, Santa Clara, CA.*, 2015.

[90] B. C. P. Banazadeh P. Hayne and R. Stahele, "Lunar flashlight: A cubesat architecture for deep space exploration," in *Interplanetary Small Satellite Conference (ISSC), Pasadena, CA,*, 2014.

[91] L. J. A. Frick, J. Castillo-Rogez and J. Dervan, "Nea scout: A cubesat architecture for near earth easteroid (nea) exploration," in *Proceedings of Interplanetary Small Satellite Conference (ISSC), Pasadena, CA*, 2014.

[92] J. M. L. Coll, "X-band antenna for cubesat satellite," Master's thesis, Laboratory of Electromagnetics and Antennas, January 2017.

[93] S. E. Hosseininejad, N. Komjani, and A. Mohammadi, "Accurate design of planar slotted SIW array antennas," *IEEE Antennas and Wireless Propagation Letters*, vol. 14, pp. 261–264, 2015.

[94] F. H. Aguirre, "X-band electronics for the inspire cubesat deep space radio," in *2015 IEEE Aerospace Conference*, pp. 1–10, March 2015.

[95] A. Babuscia, T. Choi, J. Sauder, A. Chandra, and J. Thangavelautham, "Inflatable antenna for cubesats: Development of the x-band prototype," in *2016 IEEE Aerospace Conference*, pp. 1–11, March 2016.

[96] M. Bozzi, F. Xu, D. Deslandes, and K. Wu, "Modeling and design considerations for substrate integrated waveguide circuits and components," in *8th International Conference on Telecommunications in Modern Satellite, Cable and Broadcasting Services*, pp. P–VII–P–XVI, Sept 2007.

[97] G. Fan and J.-M. Jin, "Scattering from a cylindrically conformal slotted-waveguide array antenna," in *1996 IEEE Antennas and Propagation Society International Symposium*, vol. 2, pp. 1394–1397 vol.2, July 1996.

[98] J. Dong, Y. Wang, F. Meng, and W. Feng, "A research on airborne conformal array with high gain and low SLL," in *2014 International Conference on Computational Intelligence and Communication Networks*, pp. 334–338, Nov 2014.

[99] K. Labowski, C. Penney, and J. F. Stack Jr, "Conformal antenna array design on a missile platform," *Microwave Journal*, vol. 56, no. 1, pp. 112–113, 2013.

[100] K. Fan, Z. C. Hao, and M. He, "Cylindrical conformal array antenna with fan-shaped beam for millimeter-wave application," in *2015 International Symposium on Antennas and Propagation (ISAP)*, pp. 1–3, Nov 2015.

[101] S. W. Schneider, C. Bozada, R. Dettmer, and J. Tenbarge, "Enabling technologies for future structurally integrated conformal apertures," in *IEEE Antennas and Propagation Society International Symposium. 2001 Digest. Held*

in conjunction with: USNC/URSI National Radio Science Meeting (Cat. No.01CH37229), vol. 2, pp. 330–333 vol.2, July 2001.

[102] D. Wingert and B. Howard, "Potential impact of smart electromagnetic antennas on aircraft performance and design," in *Proceedings of the NATO Workshop on Smart Electromagnetic Antenna Structures*, pp. 1–10, 1996.

[103] D. Deslandes, "Design equations for tapered microstrip-to-substrate integrated waveguide transitions," in *2010 IEEE MTT-S International Microwave Symposium*, pp. 704–707, May 2010.

[104] D. Deslandes and K. Wu, "Integrated microstrip and rectangular waveguide in planar form," *IEEE Microwave and Wireless Components Letters*, vol. 11, pp. 68–70, Feb 2001.

[105] J. Wu, Y. J. Cheng, and Y. Fan, "A wideband high-gain high-efficiency hybrid integrated plate array antenna for V-band inter-satellite links," *IEEE Transactions on Antennas and Propagation*, vol. 63, pp. 1225–1233, April 2015.

[106] P. Chopra, M. Bhandari, and S. Saxena, "Conformal antenna using circular microstrip patches in C band," in *3rd International Conference on Signal Processing and Integrated Networks (SPIN)*, pp. 759–762, Feb 2016.

[107] R. Harrington, *Time-Harmonic Electromagnetic Fields*. IEEE Press Series on Electromagnetic Wave Theory, Wiley, 2001.

[108] H. Khalil, M. M. Ahmed, U. Rafique, Saeed-ur-Rehman, M. Latif, and W. Nazar, "Design of x-band cylindrical conformal substrate integrated waveguide slot antenna array," in *2018 21st Saudi Computer Society National Computer Conference (NCC)*, pp. 1–4, April 2018.

[109] A. Rhbanou, S. Bri, and M. Sabbane, "Analysis of substrate integrated waveguide (siw) resonator and design of miniaturized siw bandpass filter," *International Journal of Electronics and Telecommunications*, vol. 63, 01 2017.

[110] R. Vincenti Gatti, R. Rossi, and M. Dionigi, "Broadband right-angle rectangular waveguide to substrate integrated waveguide transition with distributed impedance matching network," *Applied Sciences*, vol. 9, p. 389, 01 2019.

[111] Y. Qiang, L. Guo, J. Miao, Q. Lai, and J. Wang, "A conformal low-profile cavity-backed slot antenna array," in *2016 CIE International Conference on Radar (RADAR)*, pp. 1–3, IEEE, 2016.

[112] Y. Qiang, L. Guo, M. Jing, and Q. Lai, "A design of conformal dipole array for aircraft applications," in *2016 IEEE International Conference on Microwave and Millimeter Wave Technology (ICMMT)*, vol. 1, pp. 464–466, IEEE, 2016.

[113] Y. Xia, B. Muneer, and Q. Zhu, "Design of a full solid angle scanning cylindrical-and-conical phased array antennas," *IEEE Transactions on Antennas and Propagation*, vol. 65, no. 9, pp. 4645–4655, 2017.

[114] C. L., L. Xiao, W. S. Hai, H. Wang, and X. Li, "A compact missile-borne conformal array antenna with off-axis radiation," *Microwave and Optical Technology Letters*, vol. 60, pp. 1010–1013, 08 March 2018.

[115] J.-X. Xu, W.-Q. Pan, L. Gao, and X.-L. Zhao, "Filtering power divider based on lumped elements," *Progress In Electromagnetics Research*, vol. 49, pp. 31–38, 2014.

[116] J.-X. Xu, W.-Q. Pan, L. Gao, and X.-L. Zhao, "Filtering power divider based on lumped elements," *Progress In Electromagnetics Research*, vol. 49, pp. 31–38, 2014.

[117] https://www.ansys.com/products/electronics/ansys hfss.